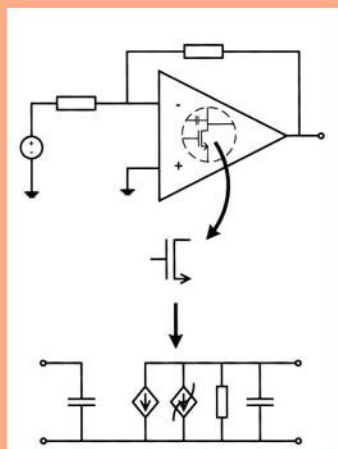


# DESIGN CRITERIA FOR LOW DISTORTION IN FEEDBACK OPAMP CIRCUITS

**Bjørnar Hernes and Trond Sæther**

**Foreword by Willy Sansen**



**Kluwer Academic Publishers**

TLFeBOOK

DESIGN CRITERIA FOR LOW DISTORTION IN  
FEEDBACK OPAMP CIRCUITS

**THE KLUWER INTERNATIONAL SERIES IN ENGINEERING AND  
COMPUTER SCIENCE**

**ANALOG CIRCUITS AND SIGNAL PROCESSING**

*Consulting Editor: Mohammed Ismail. Ohio State University*

*Related Titles:*

**CIRCUIT TECHNIQUES FOR LOW-VOLTAGE AND HIGH-SPEED A/D CONVERTERS**

Walteri

ISBN: 1-4020-7244-9

**DESIGN OF HIGH-PERFORMANCE CMOS VOLTAGE CONTROLLED OSCILLATORS**

Dai and Harjani

ISBN: 1-4020-7238-4

**CMOS CIRCUIT DESIGN FOR RF SENSORS**

Gudnason and Bruun

ISBN: 1-4020-7127-2

**ARCHITECTURES FOR RF FREQUENCY SYNTHESIZERS**

Vaucher

ISBN: 1-4020-7120-5

**THE PIEZOJUNCTION EFFECT IN SILICON INTEGRATED CIRCUITS AND SENSORS**

Fruett and Meijer

ISBN: 1-4020-7053-5

**CMOS CURRENT AMPLIFIERS; SPEED VERSUS NONLINEARITY**

Koli and Halonen

ISBN: 1-4020-7045-4

**MULTI-STANDARD CMOS WIRELESS RECEIVERS**

Li and Ismail

ISBN: 1-4020-7032-2

**A DESIGN AND SYNTHESIS ENVIRONMENT FOR ANALOG INTEGRATED CIRCUITS**

Van der Plas, Gielen and Sansen

ISBN: 0-7923-7697-8

**RF CMOS POWER AMPLIFIERS: THEORY, DESIGN AND IMPLEMENTATION**

Hella and Ismail

ISBN: 0-7923-7628-5

**DATA CONVERTERS FOR WIRELESS STANDARDS**

C. Shi and M. Ismail

ISBN: 0-7923-7623-4

**DIRECT CONVERSION RECEIVERS IN WIDE-BAND SYSTEMS**

A. Parssinen

ISBN: 0-7923-7607-2

**AUTOMATIC CALIBRATION OF MODULATED FREQUENCY SYNTHESIZERS**

D. McMahill

ISBN: 0-7923-7589-0

**MODEL ENGINEERING IN MIXED-SIGNAL CIRCUIT DESIGN**

S. Huss

ISBN: 0-7923-7598-X

**ANALOG DESIGN FOR CMOS VLSI SYSTEMS**

F. Maloberti

ISBN: 0-7923-7550-5

**CONTINUOUS-TIME SIGMA-DELTA MODULATION FOR A/D CONVERSION IN RADIO  
RECEIVERS**

L. Breems, J.H. Huijsing

ISBN: 0-7923-7492-4

**DIRECT DIGITAL SYNTHESIZERS: THEORY, DESIGN AND APPLICATIONS**

J. Vankka, K. Halonen

ISBN: 0-7923 7366-9

**SYSTEMATIC DESIGN FOR OPTIMISATION OF PIPELINED ADCs**

J. Goes, J.C. Vital, J. Franca

ISBN: 0-7923-7291-3

**OPERATIONAL AMPLIFIERS: Theory and Design**

J. Huijsing

ISBN: 0-7923-7284-0

# DESIGN CRITERIA FOR LOW DISTORTION IN FEEDBACK OPAMP CIRCUITS

*by*

**Bjørnar Hernes**

*Nordic VLSI ASA, Norway*

and

**Trond Sæther**

*Nordic VLSI ASA, Norway and  
Norwegian University of Science and Technology, Norway*

**KLUWER ACADEMIC PUBLISHERS**

NEW YORK, BOSTON, DORDRECHT, LONDON, MOSCOW

eBook ISBN: 0-306-48013-1  
Print ISBN: 1-4020-7356-9

©2003 Kluwer Academic Publishers  
New York, Boston, Dordrecht, London, Moscow

Print ©2003 Kluwer Academic Publishers  
Dordrecht

All rights reserved

No part of this eBook may be reproduced or transmitted in any form or by any means, electronic, mechanical, recording, or otherwise, without written consent from the Publisher

Created in the United States of America

Visit Kluwer Online at: <http://kluweronline.com>  
and Kluwer's eBookstore at: <http://ebooks.kluweronline.com>

# Contents

<b>List of Figures</b>	<b>ix</b>
<b>List of Tables</b>	<b>xiii</b>
<b>Symbols and Abbreviations</b>	<b>xv</b>
<b>Foreword</b>	<b>xxi</b>
<b>Preface</b>	<b>xxiii</b>
<b>Acknowledgement</b>	<b>xxv</b>
<b>Chapter 1 Introduction</b>	<b>1</b>
<b>1.1 Motivation</b>	<b>1</b>
<b>1.2 Earlier Work</b>	<b>3</b>
<b>1.3 Design Issues for Low Nonlinear Distortion</b>	<b>4</b>
<b>1.4 Outline</b>	<b>5</b>
<b>1.5 Summary</b>	<b>6</b>
<b>Chapter 2 Specification and Analysis of Nonlinear Circuits</b>	<b>9</b>
<b>2.1 Linearity Specifications</b>	<b>9</b>
2.1.1 Single-Frequency Excitation	11
2.1.2 Dual-Frequency Excitation	14
<b>2.2 Volterra Series</b>	<b>17</b>

<b>2.3 Phasor Method</b>	<b>20</b>
2.3.1 Example: Nonlinear LP-Filter	22
<b>2.4 Concluding Remarks</b>	<b>26</b>
<b>Chapter 3 Biasing and Opamp Modeling for Low Distortion</b>	<b>31</b>
<b>3.1 Biasing for Robust Linearity Performance</b>	<b>32</b>
3.1.1 Transistor Model	32
3.1.2 Biasing of Current Sources	34
3.1.3 Biasing of Signal Transistors	36
3.1.4 Biasing Guidelines for Low Distortion	38
<b>3.2 Opamp Modeling for Nonlinear Analysis</b>	<b>41</b>
3.2.1 The Opamp as a Two-Input Device	42
3.2.2 Splitting of Transfer Functions	44
3.2.3 Case: Miller Opamp	45
<b>Chapter 4 Nonlinear Analyzes of Feedback Miller Opamp</b>	<b>53</b>
<b>4.1 The Non-Inverting Configuration</b>	<b>54</b>
4.1.1 Contributions to 2 <sup>nd</sup> Harmonic	57
4.1.2 Contributions to 3 <sup>rd</sup> Harmonic	62
4.1.3 Non-Inverting: Design Considerations for Low Distortion	68
<b>4.2 The Inverting Configuration</b>	<b>70</b>
4.2.1 Contributions to 2 <sup>nd</sup> Harmonic: $H_{2v_{e\_CL}}(j\omega)$	73
4.2.2 Contributions to 3 <sup>rd</sup> Harmonic: $H_{3v_{e\_CL}}(j\omega)$	75
4.2.3 Inverting: Design Considerations for Low Distortion	78
<b>4.3 Concluding Remarks</b>	<b>81</b>
<b>Chapter 5 Opamp Circuits with High Linearity Performance</b>	<b>85</b>
<b>5.1 Measurement System</b>	<b>86</b>
<b>5.2 A 1.8V CMOS Opamp with <math>-77.5\text{dB}</math> <math>HD_2</math> and <math>HD_3</math> at 80MHz</b>	<b>90</b>
5.2.1 Design Considerations	90
5.2.2 Contributions to Nonlinear Distortion	91
5.2.3 Measurement Results	96
<b>5.3 A 3.3V CMOS Opamp with <math>-80\text{dB}</math> <math>HD_3</math> at 80 MHz</b>	<b>103</b>

5.3.1	Design Considerations	103
5.3.2	Contributions to Nonlinear Distortion	104
5.3.3	Measurement Results	108
<b>5.4</b>	<b>A 3.3V CMOS Current Opamp with <math>-63\text{dB HD}_3</math> at 100MHz</b>	<b>114</b>
5.4.1	Design Considerations	114
5.4.2	Contributions to Nonlinear Distortion	117
5.4.3	Measurement Results	121
<b>5.5</b>	<b>A 3.3V CMOS Unity-Gain Opamp with <math>-80\text{dB HD}_3</math> at 10MHz</b>	<b>126</b>
<b>5.6</b>	<b>Concluding Remarks</b>	<b>128</b>
<b>Chapter 6 Conclusions and Discussions</b>		<b>133</b>
<b>6.1</b>	<b>Opamp Topologies Versus Linearity</b>	<b>135</b>
6.1.1	One-Stage Opamp	136
6.1.2	Two-Stage Opamp	138
6.1.3	Three-Stage Opamp	139
6.1.4	Concluding Remarks	140
<b>Appendix A Transistor Model</b>		<b>141</b>
<b>Appendix B Closed Loop Opamp Transfer Functions</b>		<b>145</b>
<b>B.1</b>	<b>Non-Inverting Opamp Configuration</b>	<b>145</b>
B.1.1	First Order CL Response	146
B.1.2	Second Order CL Response	148
B.1.3	Third Order CL Response	149
<b>B.2</b>	<b>Inverting Opamp Configuration</b>	<b>150</b>
B.2.1	First, Second and Third Order CL Responses	150
<b>Appendix C Open Loop Opamp Transfer Functions</b>		<b>155</b>
<b>C.1</b>	<b>First Order Responses</b>	<b>157</b>
C.1.1	$H_{V_e}(j\omega)$	157
C.1.2	$H_{V_{cm}}(j\omega)$	158

*This page intentionally left blank*

# List of Figures

<i>Figure 1-1.</i>	Typical transfer function for a one-pole opamp.....	2
<i>Figure 2-1.</i>	Nonlinear system.....	10
<i>Figure 2-2.</i>	The output voltage versus the input voltage. $V_{out\_nonl}$ is (2-1) truncated to 5 <sup>th</sup> order and $V_{out\_ideal}$ is (2-1) truncated to 1 <sup>st</sup> order. The coefficients are: $K_1=1$ , $K_2=0.1$ , $K_3=-0.2$ , $K_4=-0.025$ and $K_5=-0.05$ . .....	11
<i>Figure 2-3.</i>	Harmonic distortion. The “_ideal”-curves are obtained by the first term in (2-4) to (2-6) and the “_nonl”-curve is (2-4) truncated to the 5 <sup>th</sup> order coefficient. ....	13
<i>Figure 2-4.</i>	Intermodulation distortion. The plots are obtained by setting the $V_{p,1}$ and $V_{p,2}$ equal. The “_ideal”-curves are obtained by the first term in (2-13) to (2-15) and the “_nonl”-curve is (2-13) truncated to the 5 <sup>th</sup> order coefficient. ....	16
<i>Figure 2-5.</i>	Two-dimensional nonlinear coefficient represented by Volterra series. ....	19
<i>Figure 2-6.</i>	Two-dimensional nonlinear coefficient represented by the phasor method. ....	22
<i>Figure 2-7.</i>	LP-filter with a voltage dependent resistor. ....	22
<i>Figure 2-8.</i>	Circuit for computation of 1 <sup>st</sup> order response.....	23
<i>Figure 2-9.</i>	Circuit for computation of 2 <sup>nd</sup> and 3 <sup>rd</sup> order responses. The parameter $x$ is 2 or 3 for 2 <sup>nd</sup> and 3 <sup>rd</sup> order analysis, respectively.....	24
<i>Figure 2-10.</i>	Plotting of 1 <sup>st</sup> to 3 <sup>rd</sup> order responses of the LP-filter. The parameters used are $g_a=10\text{mS}$ , $K2_{ga}=g_a/5$ , $K3_{ga}=-g_a/10$ and $C_L=5\text{pF}$ . The input voltage is $1V_{\text{peak}}$ and the -3dB frequency is located at 318MHz. ....	26
<i>Figure 3-1.</i>	The transistor model.....	32
<i>Figure 3-2.</i>	The transistor as a current source. $V_B$ is the gate bias voltage and $C_p$ is the parasitic capacitance when looking into the drain terminal.....	35
<i>Figure 3-3.</i>	Output conductance and 2 <sup>nd</sup> and 3 <sup>rd</sup> order nonlinear coefficients as a function of the DS-voltage of the transistor. The gate length equals $0.35\mu\text{m}$ , $V_{GS}=0.75\text{V}$ and the threshold voltage $V_T=0.58\text{V}$ (extracted by Eldo).....	35
<i>Figure 3-4.</i>	Signal transistor in common source amplifier stage. $v_{IN}$ is the voltage from the previous stage and $gd_L$ is the output conductance from a current source. ....	37

Figure 3-5. Transconductance and nonlinear coefficients for the signal transistor as a function of the GS-voltage. The gate length equals  $0.35\mu\text{m}$ ,  $V_{DS}=1.65\text{V}$  and the threshold voltage  $V_T=0.58\text{V}$  (extracted by Eldo)..... 37

Figure 3-6. Output conductance and 2<sup>nd</sup> and 3<sup>rd</sup> order nonlinear coefficients of the transistor as a function of the DS-voltage. The gate length equals  $0.18\mu\text{m}$ ,  $V_{GS}=0.686\text{V}$  and the threshold voltage  $V_T=0.51\text{V}$  (extracted by Eldo)..... 40

Figure 3-7. Transconductance and nonlinear coefficients of the transistor as a function of the GS-voltage. The gate length equals  $0.18\mu\text{m}$ ,  $V_{DS}=0.9\text{V}$  and  $V_T=0.51\text{V}$  (extracted by Eldo). .... 40

Figure 3-8. The opamp with differential and CM input voltage (a) and the model of the two-input opamp (b), where  $V_e$  and  $V_{cm}$  are the input voltages to the two-input opamp model computed from  $V^+$  and  $V^-$ .... 43

Figure 3-9. An arbitrary nonlinear current source embedded in the opamp. .... 45

Figure 3-10. Two-stage cascoded Miller opamp..... 46

Figure 3-11. Small-signal model of the opamp for use in linear and nonlinear analysis..... 47

Figure 4-1. Non-inverting opamp configuration..... 54

Figure 4-2. 2<sup>nd</sup> order responses with high CM-gain..... 59

Figure 4-3. 2<sup>nd</sup> order responses with low CM-gain..... 59

Figure 4-4. High CM-gain, the main contributing nonlinear coefficients to  $H_{V_e, V_{cm}, CL}(j\omega)$ . .... 60

Figure 4-5. Low CM-gain, the main contributing nonlinear coefficients to  $H_{V_e, V_{cm}, CL}(j\omega)$ . .... 60

Figure 4-6. “H\_Ve\_Vcm\_CL” and “H\_Ve\_Vcm\_CL\_apr” are the accurate and approximated version (given by (4-11)) of  $H_{V_e, V_{cm}, CL}(j\omega)$ , respectively. The plot is obtained using low CM-gain..... 62

Figure 4-7. Plots of the various 3<sup>rd</sup> order transfer functions using high CM-gain..... 64

Figure 4-8. Plots of the various 3<sup>rd</sup> order transfer functions using low CM-gain. . 64

Figure 4-9. High CM-gain, main contributions to  $H_{V_e, 2V_{cm}, CL}(j\omega)$ ..... 66

Figure 4-10. Low CM-gain, main contributions to  $H_{V_e, 2V_{cm}, CL}(j\omega)$ ..... 66

Figure 4-11. “H\_Ve\_2Vcm\_CL” is the accurate version of  $H_{V_e, 2V_{cm}, CL}(j\omega)$  and “H\_Ve\_2Vcm\_CL\_apr” is (4-19). Both curves are plotted with low CM-gain. .... 67

Figure 4-12. Inverting opamp configuration. .... 71

Figure 4-13. Plots of the 2<sup>nd</sup> order CL transfer functions.  $H_{2V_e, CL}(j\omega)$  is the main contribution to the total 2<sup>nd</sup> order response. .... 72

Figure 4-14. Plots of the 3<sup>rd</sup> order CL transfer functions.  $H_{3V_e, CL}(j\omega)$  is the main contribution to the total 3<sup>rd</sup> order response..... 72

<i>Figure 4-15.</i> The main contributions to $H_{2V_{e\_CL}}(j\omega)$ . The “all”-curve is $H_{2V_{e\_CL}}(j\omega)$ with all nonlinear coefficients included. The other curves is $H_{2V_{e\_CL}}(j\omega)$ with only the denoted nonlinear coefficients included.....	73
<i>Figure 4-16.</i> Equation (4-23) (labeled “H_2_CL_apr”) plotted together with the total 2 <sup>nd</sup> order response (“H_2_all_CL”).....	75
<i>Figure 4-17.</i> The major nonlinear coefficients of $H_{3V_{e\_CL}}(j\omega)$ .....	76
<i>Figure 4-18.</i> The sum of (4-26) and (4-27) (labeled “H_3_CL_apr”) and the total 3 <sup>rd</sup> order response (“H_3_all_CL”) including all 3 <sup>rd</sup> order transfer functions and nonlinear coefficients. ....	78
<i>Figure 5-1.</i> Measurement system.....	87
<i>Figure 5-2.</i> Contribution from the measurement system to $HD2$ and $HD3$ . ....	89
<i>Figure 5-3.</i> Micrograph of the test-chip fabricated in $0.18\mu\text{m}$ technology. ....	89
<i>Figure 5-4.</i> The 1.8V opamp in $0.18\mu\text{m}$ fabrication technology. ....	91
<i>Figure 5-5.</i> 2 <sup>nd</sup> order response, accurate expression (“H_2_all_CL”) and approximated expression (“H_2_CL_apr”) for the 1.8V opamp. ....	95
<i>Figure 5-6.</i> 3 <sup>rd</sup> order response, accurate expression (“H_3_all_CL”) and approximated expression (“H_3_CL_apr”) for the 1.8V opamp. ....	95
<i>Figure 5-7.</i> $HD2$ of the 1.8V opamp. The curves marked “Ch1” to “Ch3” are the measured results of three different circuit samples. The curves marked “Maple” and “Eldo” are the simulation results from Maple and Eldo, respectively. ....	97
<i>Figure 5-8.</i> $HD3$ of the 1.8V opamp. The naming of the curves follows the same “convention” as used in Figure 5-7.....	97
<i>Figure 5-9.</i> $HD2$ and $HD3$ versus output amplitude at 80MHz. The two curves named “_IDEAL” are the weakly nonlinear values of $HD2$ and $HD3$ . The assumption made is that the circuit has weakly nonlinear behavior at $0.35V_{p-p}$ output swing.....	100
<i>Figure 5-10.</i> Linearity versus CM-voltage at 80MHz.....	101
<i>Figure 5-11.</i> Linearity versus supply voltage at 80MHz.....	101
<i>Figure 5-12.</i> Linearity versus input bias current at 80MHz. ....	102
<i>Figure 5-13.</i> The 3.3V opamp in $0.18\mu\text{m}$ fabrication technology.....	103
<i>Figure 5-14.</i> 2 <sup>nd</sup> order response, accurate expression (“H_2_all_CL”) and approximated expression (“H_2_CL_apr”) for the 3.3V opamp. ....	106
<i>Figure 5-15.</i> 3 <sup>rd</sup> order response, accurate expression (“H_3_all_CL”) and approximated expression (“H_3_CL_apr”) for the 3.3V opamp. ....	106
<i>Figure 5-16.</i> $HD2$ of the 3.3V opamp. The curves marked “Ch1” to “Ch3” are the measured results of three different circuit samples. The curves marked “Maple” and “Eldo” are the simulation results from Maple and Eldo, respectively. ....	109
<i>Figure 5-17.</i> $HD3$ of the 3.3V opamp. ....	109

<i>Figure 5-18.</i> <i>HD2</i> and <i>HD3</i> versus output amplitude at 80MHz. The two curves named “_IDEAL” are the weakly nonlinear values of <i>HD2</i> and <i>HD3</i> . The assumption made is that the circuit has weakly nonlinear behavior at $0.5V_{p-p}$ output swing.....	112
<i>Figure 5-19.</i> Linearity versus CM-voltage at 80MHz.....	112
<i>Figure 5-20.</i> Linearity versus power-supply voltage at 80MHz. Here, the bias current is scaled with the power-supply voltage. ....	113
<i>Figure 5-21.</i> Linearity versus bias current at 80MHz. ....	113
<i>Figure 5-22.</i> The 3.3V COA in $0.18\mu m$ fabrication technology. ....	115
<i>Figure 5-23.</i> Model of the COA used for simulations of nonlinear responses in Maple. ....	118
<i>Figure 5-24.</i> 2 <sup>nd</sup> order response, accurate expression (“H_2_all_CL”) and approximated expression (“H_2_CL_apr”) for the 3.3V COA.....	120
<i>Figure 5-25.</i> 3 <sup>rd</sup> order response, accurate expression (“H_3_all_CL”) and approximated expression (“H_3_CL_apr”) for the 3.3V COA.....	120
<i>Figure 5-26.</i> <i>HD2</i> of the 3.3V COA. The curves marked “Ch1” to “Ch3” are the measured results of three different circuit samples. The curves marked “Maple” and “Eldo” are the simulation results from Maple and Eldo, respectively. ....	122
<i>Figure 5-27.</i> <i>HD3</i> of the 3.3V COA.....	122
<i>Figure 5-28.</i> <i>HD2</i> and <i>HD3</i> versus output amplitude at 80MHz. The two curves named “_IDEAL” are the weakly nonlinear values of <i>HD2</i> and <i>HD3</i> . The assumption made is that the circuit has weakly nonlinear behavior at $0.35V_{p-p}$ output swing.....	124
<i>Figure 5-29.</i> Linearity versus CM-voltage at 80MHz.....	124
<i>Figure 5-30.</i> Linearity versus power-supply voltage at 80MHz. The bias current is scaled with the power-supply voltage. ....	125
<i>Figure 5-31.</i> Linearity versus bias current at 80MHz. ....	125
<i>Figure 5-32.</i> Voltage buffer, to buffer the signal from the opamp to the off-chip load. ....	127
<i>Figure 5-33.</i> Comparison of harmonic <i>IP2</i> . ....	131
<i>Figure 5-34.</i> Comparison of harmonic <i>IP3</i> . ....	131
<i>Figure 6-1.</i> One-stage opamp capable to handle large output voltage swing.....	137
<i>Figure 6-2.</i> Two-stage Miller opamp.....	138
<i>Figure B-1.</i> Non-inverting opamp configuration (a) and its 1 <sup>st</sup> order model (b). .	146
<i>Figure B-2.</i> Models for derivation of CL transfer functions, 2 <sup>nd</sup> order (a) and 3 <sup>rd</sup> order (b). ....	147
<i>Figure B-3.</i> Inverting opamp configuration (a), and its 1 <sup>st</sup> order model (b). ....	151

# List of Tables

*Table 3-1.* Extracted parameters obtained from the transistor model MM9 for a 0.35 $\mu\text{m}$  fabrication technology for the opamp in Figure 3-10. The parameters will be used in simulations of nonlinear distortion in Maple, carried out in Chapter 4. .... 50

*Table 3-2.* Parameters for the opamp in Figure 3-10 obtained from the small-signal parameters in Table 3-1 and the equations for the opamp..... 51

*Table 5-1.* Estimated result for the 1.8V opamp. The estimated values are from simulations carried out in Eldo (\*) and equation given in previous chapters (\*\*). The simulations include the effects from the output pad, package and external load (see Figure 5-1). Additionally, parasitic capacitances are extracted from layout..... 92

*Table 5-2.* Extracted parameters from the transistor models for the 1.8V opamp for use in simulations of nonlinear distortion in Maple. .... 93

*Table 5-3.* Worst case *HD2* and *HD3* of three measured samples at some test frequencies. .... 99

*Table 5-4.* Estimated result for the 3.3V opamp. The estimated values are from simulations carried out in Eldo (\*) and equation given in previous chapters (\*\*). The simulations include the effects from the output pad, package and external load (see Figure 5-1). Additionally, parasitic capacitances are extracted from layout..... 104

*Table 5-5.* Extracted parameters from the transistor models for the 3.3V opamp for use in Maple simulations of nonlinear distortion. .... 105

*Table 5-6.* Comparison of the attenuation of nonlinear responses between the 1.8V and 3.3V opamps. The equations are quoted from section 4.2. . 108

*Table 5-7.* Worst case *HD2* and *HD3* of three measured samples at some test frequencies. .... 110

*Table 5-8.* Estimated results for the 3.3V COA. The estimated values are from simulations carried out in Eldo (\*) and equations given above, and in previous chapters (\*\*). The simulations include the effects from the output pad, package and external load (see Figure 5-1). Additionally, parasitic capacitances are extracted from layout..... 116

*Table 5-9.* Extracted parameters from the transistor models for the 3.3V opamp for use in Maple simulations of nonlinear distortion. .... 119

<i>Table 5-10.</i> Comparison of the attenuation of nonlinear responses between the COA and the 3.3V opamps. ....	121
<i>Table 5-11.</i> Worst case <i>HD2</i> and <i>HD3</i> of three measured samples at some test frequencies. ....	123
<i>Table 5-12.</i> Estimated result for the 3.3V unity-gain opamp. The values are from Eldo simulations, which are done with parasitic capacitances extracted from layout. ....	126
<i>Table 5-13.</i> Simulated result for the 6.5V voltage buffer. The simulations are carried out in Eldo with the effects from the output pad, external load and parasitic capacitances extracted from layout. ....	128

## Symbols and Abbreviations

$A_{CL}$	closed loop gain of the opamp circuit
ADC	Analog to Digital Converters
$\beta$	Feedback factor
BP	Band Pass
BSIM	Berkeley Short-channel IGFET Model, transistor model for MOS-transistors
$C_{DB}$	DB capacitor of the transistor
$C_{GS}$	GS capacitor of the transistor
CL	Closed Loop
CM	Common Mode
CMOS	Complementary Metal Oxide Semiconductor
COA	Current OpAmp
$C_{SB}$	SB capacitor of the transistor
DAC	Digital to Analog Converter
DB	Drain-Body of MOS transistor
DC	Direct Current, used to express zero frequency
DS	Drain-Source of MOS transistor
FFT	Fast Fourier Transform
FPBW	Full Power Bandwidth
GBW	Gain Bandwidth
GD	Gate-Drain of MOS transistor
$gd$	the drain conductance of the transistor
$gm$	the transconductance of the transistor

$GM$	Gain Margin
$gmb$	the transconductance due to the body-source voltage of the transistor
GS	Gate-Source of MOS transistor
$H_1(V_e, V_{cm}, j\omega)$	1 <sup>st</sup> order response of the two-input opamp model
$H_2(V_e, V_{cm}, j\omega)$	2 <sup>nd</sup> order response of the two-input opamp model
$H_3(V_e, V_{cm}, j\omega)$	3 <sup>rd</sup> order response of the two-input opamp model
$H_{Ve}(j\omega), H_{Ve\_CL}(j\omega)$	1 <sup>st</sup> order OL and CL transfer functions, respectively, of the two-input opamp model due to $V_e$
$H_{Vcm}(j\omega), H_{Vcm\_CL}(j\omega)$	1 <sup>st</sup> order OL and CL transfer functions, respectively, of the two-input opamp model due to $V_{cm}$
$H_{2Ve}(j\omega), H_{2Ve\_CL}(j\omega)$	2 <sup>nd</sup> order OL and CL transfer functions, respectively, of the two-input opamp model due to $V_e^2$
$H_{Ve\_Vcm}(j\omega), H_{Ve\_Vcm\_CL}(j\omega)$	2 <sup>nd</sup> order OL and CL transfer functions, respectively, of the two-input opamp model due to $V_e \cdot V_{cm}$
$H_{2Vcm}(j\omega), H_{2Vcm\_CL}(j\omega)$	2 <sup>nd</sup> order OL and CL transfer functions, respectively, of the two-input opamp model due to $V_{cm}^2$
$H_{3Ve}(j\omega), H_{3Ve\_CL}(j\omega)$	3 <sup>rd</sup> order OL and CL transfer functions, respectively, of the two-input opamp model due to $V_e^3$
$H_{2Ve\_Vcm}(j\omega), H_{2Ve\_Vcm\_CL}(j\omega)$	3 <sup>rd</sup> order OL and CL transfer functions, respectively, of the two-input opamp model due to $V_e^2 \cdot V_{cm}$
$H_{Ve\_2Vcm}(j\omega), H_{Ve\_2Vcm\_CL}(j\omega)$	3 <sup>rd</sup> order OL and CL transfer functions, respectively, of the two-input opamp model due to $V_e \cdot V_{cm}^2$
$H_{3Vcm}(j\omega), H_{3Vcm\_CL}(j\omega)$	3 <sup>rd</sup> order OL and CL transfer functions, respectively, of the two-input opamp

$H_{3,2}(\cdot), H_{3,2-CL}(\cdot)$	model due to $V_{cm}$ <sup>3</sup> 3 <sup>rd</sup> order OL and CL transfer functions, respectively, of the two-input opamp model due to mixing of 2 <sup>nd</sup> harmonic and fundamental frequency in 2 <sup>nd</sup> order transfer functions in the two-input opamp model
<i>HD2</i>	2 <sup>nd</sup> order Harmonic Distortion
<i>HD3</i>	3 <sup>rd</sup> order Harmonic Distortion
IF	Intermediate Frequency
<i>IM2</i>	InterModulation of 2 <sup>nd</sup> order
<i>IM3</i>	InterModulation of 3 <sup>rd</sup> order
<i>IP2<sub>h</sub></i>	harmonic Intercept Point of 2 <sup>nd</sup> order
<i>IP2<sub>i</sub></i>	intermodulation Intercept Point of 2 <sup>nd</sup> order
<i>IP3<sub>h</sub></i>	harmonic Intercept Point of 3 <sup>rd</sup> order
<i>IP3<sub>i</sub></i>	intermodulation Intercept Point of 3 <sup>rd</sup> order
JFET	Junction Field Effect Transistor
$K2_{CSB}, K2_{CDB}$	The 2 <sup>nd</sup> order nonlinear coefficient of the SB and DB capacitances, respectively
$K2_{gd}$	The 2 <sup>nd</sup> order nonlinear coefficient of the transistor due to the DS-voltage
$K2_{gm}$	The 2 <sup>nd</sup> order nonlinear coefficient of the transistor due to the GS-voltage
$K2_{gmb}$	The 2 <sup>nd</sup> order nonlinear coefficient of the transistor due to the BS-voltage
$K2_{gm\_gd}$	The 2 <sup>nd</sup> order nonlinear coefficient of the transistor due to the GS- and DS-voltages
$K2_{gmb\_gm}$	The 2 <sup>nd</sup> order nonlinear coefficient of the transistor due to the BS- and GS-voltages
$K2_{gmb\_gd}$	The 2 <sup>nd</sup> order nonlinear coefficient of the transistor due to the BS- and DS-voltages

$K3_{C_{SB}}$	$K3_{C_{DB}}$	The 3 <sup>rd</sup> order nonlinear coefficient of the SB and DB capacitances, respectively
$K3_{gd}$		The 3 <sup>rd</sup> order nonlinear coefficient of the transistor due to the DS-voltage
$K3_{gm}$		The 3 <sup>rd</sup> order nonlinear coefficient of the transistor due to the GS-voltage
$K3_{gmb}$		The 3 <sup>rd</sup> order nonlinear coefficient of the transistor due to the BS-voltage
$K3_{2gm\_gd}$		The 3 <sup>rd</sup> order nonlinear coefficient of the transistor due to the 2 <sup>nd</sup> order GS-voltage and DS-voltage
$K3_{gm\_2gd}$		The 3 <sup>rd</sup> order nonlinear coefficient of the transistor due to the GS-voltage and 2 <sup>nd</sup> order DS-voltage
$K3_{2gmb\_gm}$		The 3 <sup>rd</sup> order nonlinear coefficient of the transistor due to the 2 <sup>nd</sup> order BS-voltage and GS-voltage
$K3_{gmb\_2gm}$		The 3 <sup>rd</sup> order nonlinear coefficient of the transistor due to the BS-voltage and 2 <sup>nd</sup> order GS-voltage
$K3_{2gmb\_gd}$		The 3 <sup>rd</sup> order nonlinear coefficient of the transistor due to the 2 <sup>nd</sup> order BS-voltage and DS-voltage
$K3_{gmb\_2gd}$		The 3 <sup>rd</sup> order nonlinear coefficient of the transistor due to the BS-voltage and 2 <sup>nd</sup> order DS-voltage
$K3_{gm\_gmb\_gd}$		The 3 <sup>rd</sup> order nonlinear coefficient of the transistor due to the GS-, BS- and DS-voltages
LP		Low Pass
MM9		MOS Model 9, transistor model for MOS transistors
$\omega$		frequency in rad./sec.
$\omega_{GBW}$		gain-bandwidth frequency of the opamp
OL		Open Loop

PCB	Printed Circuit Board
<i>PM</i>	Phase Margin
SB	Source-Body of MOS transistor
SR	Slew-Rate
THA	Track and Hold Amplifier
<i>THD</i>	Total Harmonic Distortion
$v_{in}, v_{out}$	Signal value, disregarding the DC value
$v_{IN}, v_{OUT}$	Signal value, including the DC value
$V_{in}, V_{out}$	Phasor representation
$V_{out_1}, V_{out_2}, V_{out_3}$	Phasor representation of the output voltage at the fundamental frequency, 2 <sup>nd</sup> and 3 <sup>rd</sup> harmonics, respectively
$V_e, V_{cm}$	Phasor representation of the differential and common-mode input voltages, respectively, to the two-input opamp model
$V_{e_1}, V_{e_2}$	Phasor representation of the differential input voltage at the fundamental frequency and 2 <sup>nd</sup> harmonic, respectively
$V_{cm_1}, V_{cm_2}$	Phasor representation of the common mode input voltage at the fundamental frequency and 2 <sup>nd</sup> harmonic, respectively

*This page intentionally left blank*

# Foreword

An increasing number of analog integrated circuits suffer from distortion. It limits the signal swing, subject to the supply voltage available. Together with noise, it thus establishes the ultimate dynamic range. Distortion is a difficult topic however. Too few books and papers are devoted to it. This is why this new edition deserves our full attention.

It is even more difficult to handle distortion at high frequencies. Volterra series can be used but the phasor method is much more practical indeed. This book provides an excellent example on how to use the phasor method towards the analysis of distortion in analog circuits such as operational amplifiers. It is shown that the Miller opamp with folded-cascode at the input, is certainly one of the best contenders for high-speed and low distortion.

In a separate chapter, the non-linear coefficients are examined versus frequency. They are analyzed in much greater detail than ever before. The slopes of the distortion versus input amplitudes and versus frequencies are predicted by means of hand calculations and verified by means of simulations. Finally experimental data is added, which is of utmost importance in designs with low distortion.

It can be concluded that a new generation of low-distortion opamps has been designed and realized with distortion as one of the most important specifications. This work therefore deserves being read and studied. Since hand calculations are given, followed by simulations and experiments, it is clear that this book is of use for both novice designers and for experts, who want to deepen their knowledge and insight.

09-2002

Willy Sansen

*This page intentionally left blank*

# Preface

Broadband operational amplifiers (opamps) for multi-channel communication systems have strong demands on linearity performance. When these opamps are integrated in deep sub-micron CMOS technologies, the signal-swing has to occupy a large part of the rather low supply voltage to maintain the signal-to-noise-ratio. To obtain opamps with low distortion it is necessary to do a thorough analysis of the nonlinear behavior of such circuits. This is the main subject of this book.

The biasing of each transistor in the circuit is a major issue and is addressed in this work. It is important to bias the transistor such that the distortion is low and stable in the entire range of its terminal voltages. This will ensure high linearity and robustness against variations in circuit conditions such as power supply voltage, bias current and process variations.

Further, a general two-input weakly nonlinear model of the opamp is developed, with the differential and the common-mode voltages as the inputs. This model accounts for the effect that the input common-mode voltage has on the linearity performance. The model describes the opamp with a set of linear and nonlinear transfer functions. The linear transfer functions are the well-known differential gain and common-mode gain of the opamp. The nonlinear transfer functions depend on the two input voltages, the input frequency and the nonlinear sources embedded in the opamp.

The two-input model, applied on a folded cascode Miller opamp, is further used to explore the non-inverting and inverting opamp configurations. For each of the configurations, the strongest contributions to nonlinear distortion are found. Simplified expressions for the closed-loop nonlinear responses are presented as a function of the input frequency. From the closed loop expressions, design equations are extracted, which show how the distortion can be suppressed in the different ranges of frequency. For computation of the nonlinear transfer functions, a method based on the Volterra series is used. The method, which in this book is referred to as the phasor method, results in a subset of the Volterra series.

The analysis of the nonlinear behavior results in a design procedure for achievement of highly linear opamp circuits. The design procedure is used in design of three opamps connected in the inverting configuration. The measurements show that  $HD_2$  and  $HD_3$  are both less than  $-77.5\text{dB}$  at  $80\text{MHz}$  for an opamp with  $1.8\text{V}$  supply voltage and  $0.75\text{V}_{\text{p-p}}$  signal swing.

Additionally, a unity-gain opamp is designed, which uses a tail-current-compensation-circuit to suppress the effect of large common-mode voltage swing.

This book is based on a Ph.D. project initiated by Nordic VLSI ASA and performed at the Norwegian University of Science and Technology (NTNU), dept. of Physical Electronic, both located in Trondheim, Norway.

09-2002

Trondheim, Norway

Bjørnar Hernes

Trond Sæther

## Acknowledgement

This work had not been possible without the financial support from *Nordic VLSI ASA* and the *Norwegian Research Council* (under the project number 130946/221). In addition, I am grateful to my colleagues at Nordic VLSI ASA, dept. for Dataconverters, including Rune Kvernland.

Bjørnar Hernes

*This page intentionally left blank*

# Chapter 1

## Introduction

### 1.1 Motivation

Broadband operational amplifiers (opamp) with low nonlinear distortion are important building blocks in many applications. Examples of such applications are multi-channel communication systems, multi-channel video systems, and buffers for broadband Analog-to-Digital and Digital-to-Analog Converters (ADC and DAC). These systems are moving towards higher level of integration in low-cost technologies, such as deep sub-micron CMOS processes.

Analog design in modern CMOS technologies suffers from the low supply voltage that is required by these processes. To make the signal-to-noise ratio as high as possible the signal swing has to occupy a large part of the available supply voltage. This means that the voltage left to bias the circuit is small. This represents one of the bottlenecks in achieving low distortion for opamps implemented in deep sub-micron technologies.

When increasing the loop gain of a feedback circuit the nonlinear distortion will decrease. Thus, a well-known method to obtain low distortion in feedback circuits is to design for high loop gain. However, the loop gain is only high in a limited frequency range. For opamp circuits, the loop gain is decreasing for frequencies above the dominant pole. This is shown in Figure 1-1, where  $A_0$  is the low frequency open loop gain and  $\omega_p$  is the dominant pole of the opamp. Thus, the maximum loop gain at a specified frequency is set by the maximum Gain-Band-Width (GBW) of the opamp. The maximum GBW is a result of the opamp topology and fabrication technology.

Another challenge in the design phase of linear analog circuits is estimation of the nonlinear distortion. The harmonics and intermodulation

products depend on higher order derivatives of the drain current of the transistors. The higher order derivatives are often poorly modeled in the transistor models available in SPICE-like circuit simulators, especially for sub-micron CMOS devices [1], [2]. Further, when simulating nonlinearity in SPICE-like simulators it is not possible to get any information about the strongest contributions to nonlinear distortion and what parameters to use for minimizing it.

Facing the problems described above, it was necessary to develop a design method to achieve linear opamp circuits. The method is twofold. First, careful biasing of each transistor in the circuit such that the higher order derivatives of the drain current is on a minimum and, further, stable in the entire range of the transistor's terminal voltages. This results in high and robust linearity performance. Next, find the largest contributions to nonlinear distortion and derive symbolic expressions for these. It is then possible to optimize the circuit for low distortion even without accurate modeling of higher order derivatives.

The method sketched above is used in design of three opamps in a  $0.18\mu\text{m}$  CMOS fabrication technology, two with 3.3V supply voltage and one with 1.8V supply voltage. Additionally, a 3.3V opamp in  $0.35\mu\text{m}$  technology is designed. Measurement results from the opamps are presented in this book.

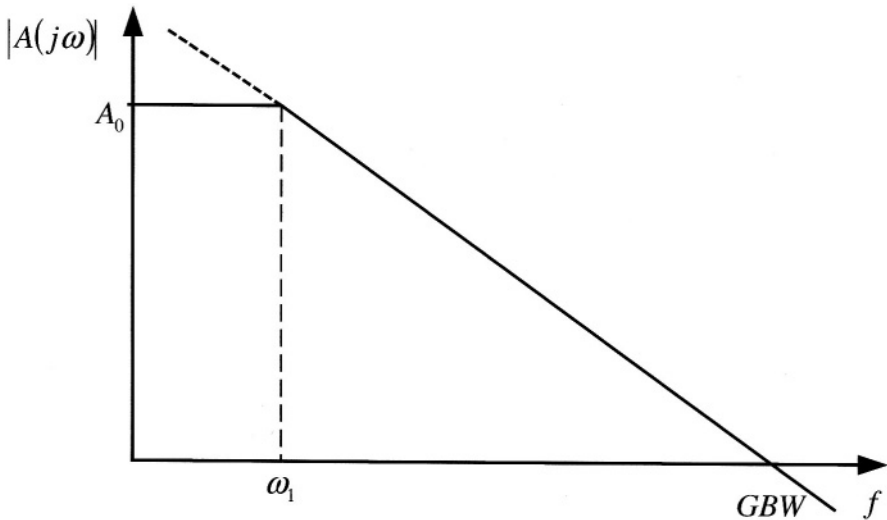


Figure 1-1. Typical transfer function for a one-pole opamp.

## 1.2 Earlier Work

To derive symbolic expressions for nonlinear distortion, a mathematical analyzing tool is needed. Since the linearity performance at frequencies above the dominant pole of the opamp is important, the requirement for the analyzing tool is to include the frequency response of the distortion. This is done by the Volterra series. The Volterra series has since 1967 been used to compute the nonlinear behavior of weakly nonlinear analog circuits as a function of frequency. In [3] and [4] Volterra series is used to model distortion in bipolar transistors and in [5] the issue is JFET-transistors. The derived models are further applied on one-transistor amplifiers.

Feedback systems are also presented in terms of Volterra series in literature. In [6] the Volterra series is applied to a feedback amplifier and the effect of the feedback is explained. Similar derivations are done in [1] and [7]. In [8] cross-modulation and intermodulation is found for a two-transistor bipolar amplifier with feedback.

Additionally, the Volterra series are used to find the nonlinear distortion in many other applications. For example, distortion in log-domain filters is described in [9] and distortion analysis of larger analog systems is addressed in [10].

Volterra series represents a general representation of the nonlinearity, but leads to complex derivations with many unnecessary kernels when the circuit is excited by only one or two frequencies or when the circuit has two inputs. In [11] a technique called the probing method is described. This method computes the terms in the Volterra series by iterative solving the same differential equations with different excitations for the circuit. In [12] a simplified version of the probing method is presented. This method exploits the fact that the circuit performance often is measured by applying one or two frequencies at the input. The method uses phasors to represent currents and voltages, and is in this book referred to as the “phasor method”.

To include the effect that the input Common-Mode (CM) voltage has on the linearity performance, the opamp is considered as a two-input device with the differential voltage and the CM-voltage as the inputs. The nonlinear responses for the two-input opamp are computed and further used to derive the nonlinear responses for the Closed-Loop (CL) circuits, the inverting and non-inverting opamp configurations. The phasor method is simpler to use for analyses of two-input devices than the Volterra series. In [13] the phasor method is described for a double-balanced mixer and in [2] for a CMOS up-conversion mixer. Further, in [2] and [14] the phasor method is applied on a CL Miller opamp and simplified expressions are shown for 2<sup>nd</sup> and 3<sup>rd</sup> harmonics, including the strongest contribution to distortion.

The book of Wambacq and Sansen [1] describes both the Volterra series and the phasor method. Additionally, it shows many useful examples on how nonlinear analysis of electrical circuits can be done. This source has been the most useful reference for the work presented in this book.

### **1.3 Design Issues for Low Nonlinear Distortion**

The approach of this work is to achieve a design method for obtaining low nonlinear distortion in feedback opamp circuits. Distortion in transistor circuits is mainly due to non-zero higher order derivatives of the transistor drain current. These higher order derivatives can be viewed as nonlinear sources in the circuit. Thus, it is important that the strength of the nonlinear sources is low and that they are attenuated as much as possible to the output of the circuit. These are the key issues of the design method, which can be summarized as follows:

1. Biasing each transistor in the circuit such that the higher order derivatives of the drain current are small and stable in the entire range of the terminal voltages.
2. Find the strongest contributions to nonlinear distortion for the CL circuit and derive symbolic expressions for these. From the symbolic expressions, design equations can be obtained.
3. Use the biasing point obtained in 1 as a starting point for the optimization for minimum nonlinear distortion of the CL circuit. The optimization is carried out in a circuit simulator with the design equations as guidelines.

How to bias the transistor is found by plotting the higher order derivatives of the transistor drain current and find at what range of the terminal voltages they are small and stable. This is done in a circuit simulator with transistor parameters given by the fabrication technology to be used. The accuracy of these derivatives is less important as long as the shapes of the curves are approximately correct.

The strongest contributions to nonlinear distortion are found by implementing the phasor method in a symbolic mathematical tool. Maple6 [15] is used in this work. The phasor method is further applied on a weakly nonlinear model of the circuit. The nonlinear behavior of this model is due to the higher order derivatives of the transistor drain current. Each of the higher order derivatives represent a source to nonlinear distortion and it is important to detect the strongest contributing sources. This is done by plotting the contribution from each source in the same plot as a function of frequency. It is then easy to compare them and pick out the most important sources.

By using a two-input model of the opamp, it is further possible to view the effect that the CM-voltage has on the linearity performance. This is especially important when the opamp has large swing in the input CM-voltage, which is the case for the non-inverting opamp configuration. Further, Maple6 can be used to derive simplified CL responses of the distortion, including the strongest contributing nonlinear sources. From these responses, it is possible to obtain design equations that show what circuit parameters to alter to suppress the distortion.

Finally, the design equations are used to optimize the circuit for minimum distortion. The optimization is carried out in a circuit simulator using the biasing obtained in point 1 above as a starting point. The equations show which parameters to use to enhance the linearity performance of the circuit.

Because that the phasor method is a series, the simulations in Maple6 and the simplified expressions for the nonlinear distortion are under the assumption that the circuit is weakly nonlinear. The phrase “weakly nonlinear” means that the nonlinear behavior is mainly determined by 2<sup>nd</sup> and 3<sup>rd</sup> order nonlinearity. This can be a good approximation in feedback opamp circuits, design for high linearity performance. However, the issue is not accurate modeling of distortion, but to provide insight and understanding of how distortion occurs and how to minimize it. The phrase “weakly nonlinear” is more thoroughly explained in Chapter 2.

## 1.4 Outline

In Chapter 2 the basic of nonlinear specification and analyses are described. First, some measurement parameters are presented for one- and two-frequency excitation of the circuit. Second, the Volterra series and phasor method are described and an example is given to show the difference between the two methods. Further, the phasor method is applied on a simple circuit example, where the nonlinear responses for 2<sup>nd</sup> and 3<sup>rd</sup> harmonics are found.

Chapter 3 presents some important issues in modeling, symbolic analysis and design of weakly nonlinear circuits. First, the nonlinear model of the transistor is presented, where the drain current and currents through the diffusion capacitances are expressed as Taylor expansions. Further, based on the transistor model, the biasing technique for obtaining low higher order derivatives of the transistor drain current is presented. Second, the opamp as a two-input device is described in general terms and further the principle of splitting of nonlinear transfer functions. At the end of Chapter 3 the cascoded Miller opamp and its model are presented. This model will further

be used to derive nonlinear responses for the CL opamp circuits in Chapter 4.

In Chapter 4 the non-inverting and inverting opamp configurations are explored regarding nonlinear behavior. The main contributions to nonlinear distortion are shown by plotting. The expressions for 2nd and 3rd harmonics are given including the strongest contributions. From these expressions, it is possible to give guidelines and design equations for obtaining low distortion in feedback opamp circuits.

The design guidelines achieved in Chapter 3 and Chapter 4 are further used in design of several opamp circuits. These are presented in Chapter 5. Here, also the measurement system is described, which is used for testing the opamp circuits. Further, the opamp with the best linearity performance, as regards the supply voltage, is compared to previous reported results and some commercial available opamps with high linearity performance.

Chapter 6 summarizes this book and gives proposal to further work. Here, also a comparison between the presented opamp circuits is carried out. These are further compared to some commercial available opamps with high linearity performance.

## **1.5 Summary**

The main contributions in this work are as follows:

- Method for biasing CMOS transistors to obtain low and stable higher order derivatives of the drain current of the transistor and thus high and robust linearity performance.
- Thoroughly description of the nonlinear behavior of feedback opamp circuits. This work is an evolution of the work presented in [2] and [16] for feedback opamp circuits. The work consist of the following parts:
  - Describing the opamp as a two-input device, one input for the differential voltage and one for the CM-voltage. This makes it possible to take into consideration the effect of swing in the CM-voltage. This swing can be damaging for the linearity performance of the circuit.
  - Exploiting the phasor method to split-up the nonlinear responses of distortion. For the CL circuit, these responses tend to be very complex. By using the iterative nature of the phasor method, in conjunction with the two-input model of the opamp, it is possible to factorize the responses in many terms. This makes it simple to do simplification on each term and to obtain surveyable expressions for the nonlinear responses as a function of frequency. This is done for both the inverting and non-inverting opamp configurations by using a folded cascode Miller opamp.

- Extracting design equations from the CL nonlinear responses. These equations show what circuit parameters that minimize the nonlinear distortion.
- Design procedure for opamps circuits to obtain low nonlinear distortion.
- Design of highly linear opamps in modern CMOS technologies:
  - A 1.8V CMOS opamp with  $-77.5\text{dB}$   $HD_2$  and  $HD_3$  at 80MHz. The input voltage swing was  $0.75V_{p-p}$  and the circuit is fabricated in a  $0.18\mu\text{m}$  process.
  - A 3.3V CMOS opamp with  $-80\text{dB}$   $HD_3$  at 80 MHz. The input voltage swing was  $1.0V_{p-p}$  and the circuit is fabricated in a  $0.18\mu\text{m}$  process.
  - A 3.3V CMOS current opamp with  $-63\text{dB}$   $HD_3$  at 100MHz. The input voltage swing was  $1.0V_{p-p}$  and the circuit is fabricated in a  $0.18\mu\text{m}$  process.
  - A 3.3V CMOS unity-gain opamp with  $-80\text{dB}$   $HD_3$  at 10MHz. The input voltage swing was  $1.0V_{p-p}$  and the circuit is fabricated in a  $0.35\mu\text{m}$  process. This circuit uses a new tail-current-compensation-circuit to suppress the effect of large CM-voltage swing [17].

## REFERENCES

- [1] P. Wambacq, W. Sansen, "Distortion Analysis of Analog Integrated Circuits," Norwell, MA: Kluwer Academic Publishers, 1998.
- [2] P. Wambacq, G. G. E. Gielen, P. R. Kinget, W. Sansen, "High-Frequency Distortion Analysis of Analog Integrated Circuits," *IEEE Tr. on Circuits and Systems—II: Analog and Digital Signal Processing*, vol. 46, no. 3, pp. 335-345, Mar. 1999.
- [3] S. Narayanan, "Transistor Distortion Analysis Using Volterra Series Representation," *The Bell System Technical Journal*, vol. 46, pp. 991-1024, May-June 1967.
- [4] S. Narayanan, H. C. Poon, "An Analysis of Distortion in Bipolar Transistors Using Integral Charge Control Model and Volterra Series," *IEEE Transaction on Circuit Theory*, vol. CT-20, no. 4, pp. 341-351, Jul. 1973.
- [5] A. M. Khadr, R. H. Johnston, "Distortion in High-Frequency FET Amplifiers," *IEEE Journal of Solid-State Circuits*, vol. SC-9, no. 4, pp. 180-189, Aug. 1974.
- [6] S. Narayanan, "Applications of Volterra Series to Intermodulation Distortion Analysis of Transistor Feedback Amplifiers," *IEEE Transaction on Circuit Theory*, vol. CT-17, no. 4, pp. 518-527, Nov. 1970.
- [7] H. Jardon, R. Gomes, O. Golovin, "Nonlinear Analysis of Amplifiers with Local and Global Negative Feedback," *IEEE International Symposium on Circuits and Systems 1997*, June 9-12 1997, pp. 965-968.
- [8] R. G. Meyer, M. J. Shensa, R. Eschenback, "Cross Modulation and Intermodulation in Amplifiers at High Frequencies," *IEEE Journal of Solid-State Circuits*, vol. SC-7, no. 1, pp. 16-23, Feb. 1972.
- [9] C. Beainy, R. A. Baki, M. N. El-Gamal, "Distortion Analysis of High-Frequency Log-Domain Filters Using Volterra Series," *IEEE International Symposium on Circuits and Systems 2001*, vol. 1, 2001, pp. 472-475.

- [10] P. Wambacq, P. Dobrovolný, S. Donnay, M. Engels, I. Bolsens, "Compact modeling of nonlinear distortion in analog communication circuits," *Proceedings of Design, Automation and Test in Europe Conference and Exhibition 2000*, pp. 350-354, 2000.
- [11] J. J. Bussgang, L. Ehrman, J. W. Graham, "Analysis of Nonlinear Systems with Multiple Inputs," *Proceedings of The IEEE*, vol. 62, no. 8, pp. 1088-1119, Aug. 1974.
- [12] P. Wambacq, G. Gielen, W. Sansen, "Symbolic Simulation of Harmonic Distortion in Analog Integrated Circuits with Weak Nonlinearities," *Proceedings of ISCAS90*, May 1990, pp. 536-539.
- [13] P. Wambacq, J. Vanthienen, G. Gielen, W. Sansen, "A Design Tool for Weakly Nonlinear Analog Integrated Circuits With Multiple Inputs (Mixers, Multipliers)," *Proceedings of the IEEE 1991 Custom Integrated Circuit Conference*, 1991, pp. 5.1/1-5.1/4.
- [14] G. Gielen, P. Wambacq, W. Sansen, "Symbolic Approximation Strategies and the Symbolic Analysis of Large and Nonlinear Circuits *IEEE International Symposium on Circuits and Systems 1991*, vol. 2, 1991, pp. 806-809, 1991.
- [15] Maple 6, See <http://www.maplesoft.com/>
- [16] F. O. Eynde, P. Wambacq, W. Sansen, "On the Relationship Between the CMRR or PSRR and the Second Harmonic Distortion of Differential Input Amplifiers," *IEEE Journal of Solid-State Circuits*, vol. 24, no. 6, pp. 1740-1744, Dec. 1989.
- [17] B. Hernes, Ø. Moldsvor, T. Sæther, "A -80dB HD3 Opamp in 3.3V CMOS Technology using Tail Current Compensation," *IEEE International Symposium on Circuits and Systems 2001*, vol. 1, 2001, pp. 216-219.

## Chapter 2

# Specification and Analysis of Nonlinear Circuits

This chapter describes some of the theoretical background for specification and analysis of nonlinear systems. First, the measurement parameters that describe the nonlinear performance of an analog circuit are addressed. An example of a nonlinear system is presented, which is further used to define the measurement parameters obtained when the circuit excitation consists of one or two frequencies. Second, the Volterra series is defined. The Volterra series is an analysis tool for obtaining symbolic expressions for weakly nonlinear analog systems. The Volterra series can also be transformed to the frequency plane in a similar way as the well-known Laplace transform (e.g. [1] and [2]). However, the Volterra series leads to cumbersome analysis and complex symbolic expressions, especially for large circuits and high order nonlinearities. Thus, a simpler method is described, which throughout this book is called the phasor method. The phasor method uses phasor representation for currents and voltages in the circuit and results in a subset of the equations obtained by the Volterra series. This method is visualized by an example, which is a simple Low-Pass (LP) filter with a nonlinear resistor. The phasor method will also be used further in this book.

Most of the definition and theory in this chapter are taken from [3]. The Volterra series are further described and used in [4] to [13]. The phasor method is applied in [14], [15] and [16].

### 2.1 Linearity Specifications

Figure 2-1 shows a nonlinear system with  $v_{IN}$  as the circuit excitation and  $v_{OUT}$  as the output variable applied to the load  $Z_L$ . Disregarding the constant term, the output variable  $v_{out}$  can be expressed by (2-1). Here, the nonlinear

system is approximated by a Taylor series [1]. The requirement for the Taylor expansion is that the series converge, which means that the terms in the series decrease with increasing order. Additionally, the series must represent  $v_{out}$  with small error in the specified range of  $v_{in}$ , which is  $v^-$  to  $v^+$ . The coefficients in (2-1) are given by (2-2). These coefficients are in general a function of frequency, but will in this section be considered constant.  $K_1$  is the desired gain of the circuit. The other coefficients cause distortion and are further called nonlinear coefficients. Figure 2-2 shows (2-1) truncated to 5<sup>th</sup> order ( $Vout\_nonl$ ) and the ideal output voltage ( $Vout\_ideal$ ) disregarding all higher order terms in (2-1). Both are plotted versus the input voltage. The value of the coefficients are  $K_1=1$ ,  $K_2=0.1$ ,  $K_3=-0.2$ ,  $K_4=-0.025$  and  $K_5=-0.05$ . The plot shows that the output voltage deviate from the ideal value at low and high input voltage, which is typical behavior for many analog circuits. The nonlinear system, with the DC-response plotted in Figure 2-2, will further be used to define and plot the various nonlinear measurement parameters.

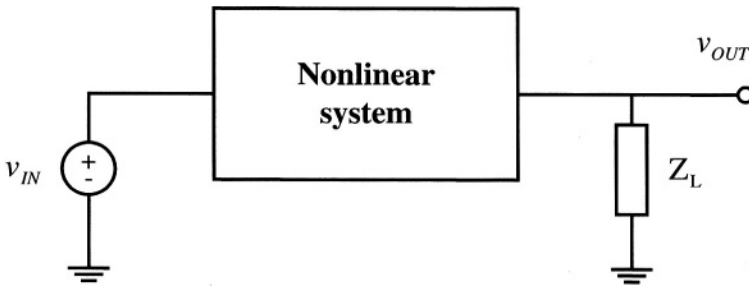


Figure 2-1. Nonlinear system.

$$v_{out} = f(v_{in}) \approx K_1 \cdot v_{in} + K_2 \cdot v_{in}^2 + K_3 \cdot v_{in}^3 + K_4 \cdot v_{in}^4 + K_5 \cdot v_{in}^5 + \dots, \quad v_{in} \in [v^-, v^+] \quad (2-1)$$

$$K_n = \left. \frac{f^{(n)}(v_{in})}{n!} \right|_{v_{in}=0} \quad (2-2)$$

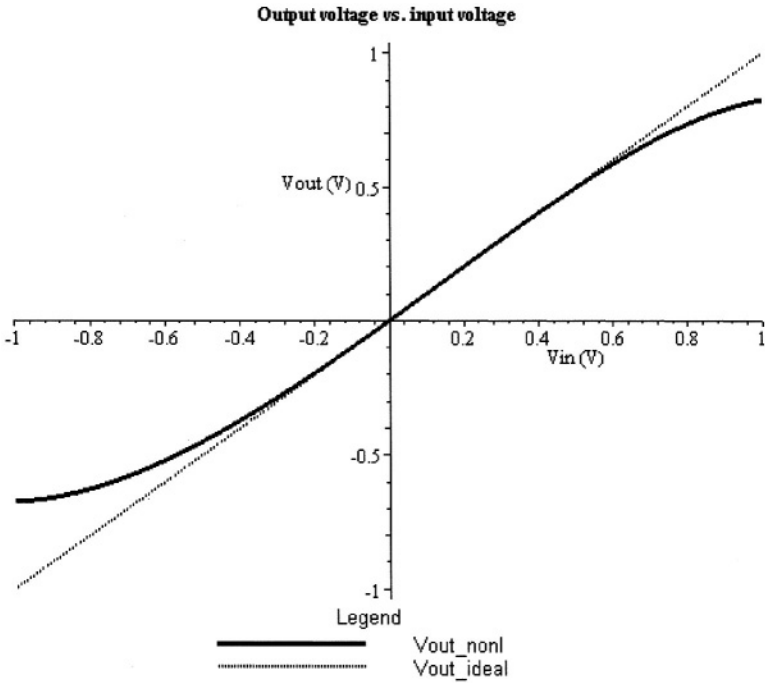


Figure 2-2. The output voltage versus the input voltage.  $V_{out\_nonl}$  is (2-1) truncated to 5<sup>th</sup> order and  $V_{out\_ideal}$  is (2-1) truncated to 1<sup>st</sup> order. The coefficients are:  $K_1=1$ ,  $K_2=0.1$ ,  $K_3=-0.2$ ,  $K_4=-0.025$  and  $K_5=-0.05$ .

### 2.1.1 Single-Frequency Excitation

The single-frequency test is carried out by applying a signal containing only one frequency component at the input of the nonlinear system. The same frequency component will occur at the output, where it is called the fundamental frequency. However, the output signal will also contain unwanted frequency components at multiples of the input frequency. These are called harmonic frequencies and are caused by the nonlinear behavior of the circuit.

In (2-3) the input voltage is shown, where  $V_{p,1}$  is the amplitude and  $\omega_{in,1}$  is the input frequency. When (2-1) represents the nonlinear system, the amplitude of the fundamental frequency on the output of the system can be expressed by (2-4). Equation (2-4) shows that this amplitude is primarily a function of the 1<sup>st</sup> order coefficients in (2-1), which is the gain of the system. Further, (2-4) is also a function of all odd order nonlinear coefficients of the system. When the input amplitude increases, the fundamental component on the output will increase or decrease, depending on the sign of the nonlinear

coefficients. If it increases it is called expansion and if it decreases it is called compression.

The equations (2-5) and (2-6) are the amplitudes of the 2<sup>nd</sup> and 3<sup>rd</sup> harmonics, respectively. The 2<sup>nd</sup> harmonic depends on all even order nonlinear coefficients, while the 3<sup>rd</sup> harmonic depends on all odd order nonlinear coefficients. The ratios between the levels of 2<sup>nd</sup> and 3<sup>rd</sup> harmonics and the level of the fundamental frequency are called *HD2* and *HD3*, respectively. *HD2* and *HD3* are widely used parameters to describe nonlinear behavior for an analog system. When the higher order terms in (2-4) to (2-6) are small, and decreases with increased order, the system is called weakly nonlinear. The phrase “weakly nonlinear” will be further and more rigorously defined in terms of Volterra series in section 2.2. When the system is weakly nonlinear, *HD2* and *HD3* can be approximated with (2-7) and (2-8) below. In (2-9) another measurement parameter is defined, the Total Harmonic Distortion (*THD*). *THD* is the square root of the ratio between the quadratic sum of the harmonic amplitudes and the amplitude of the fundamental frequency.

$$v_{in}(t) = V_{p,1} \cdot \cos(\omega_{in,1} \cdot t) \quad (2-3)$$

$$V_{out\_1} = K_1 \cdot V_{p,1} + \frac{3}{4} \cdot K_3 \cdot V_{p,1}^3 + \frac{5}{8} \cdot K_5 \cdot V_{p,1}^5 + \dots \quad (2-4)$$

$$V_{out\_2} = \frac{1}{2} \cdot K_2 \cdot V_{p,1}^2 + \frac{1}{2} \cdot K_4 \cdot V_{p,1}^4 + \dots \quad (2-5)$$

$$V_{out\_3} = \frac{1}{4} \cdot K_3 \cdot V_{p,1}^3 + \frac{5}{16} \cdot K_5 \cdot V_{p,1}^5 + \dots \quad (2-6)$$

$$HD2 \triangleq \frac{|V_{out\_2}|}{|V_{out\_1}|} \approx \frac{1}{2} \cdot \left| \frac{K_2}{K_1} \right| \cdot V_{p,1} \quad (2-7)$$

$$HD3 \triangleq \frac{|V_{out\_3}|}{|V_{out\_1}|} \approx \frac{1}{4} \cdot \left| \frac{K_3}{K_1} \right| \cdot V_{p,1}^2 \tag{2-8}$$

$$THD \triangleq \sqrt{\frac{\sum_{n=2}^{\infty} |V_{out\_n}|^2}{|V_{out\_1}|^2}} \tag{2-9}$$

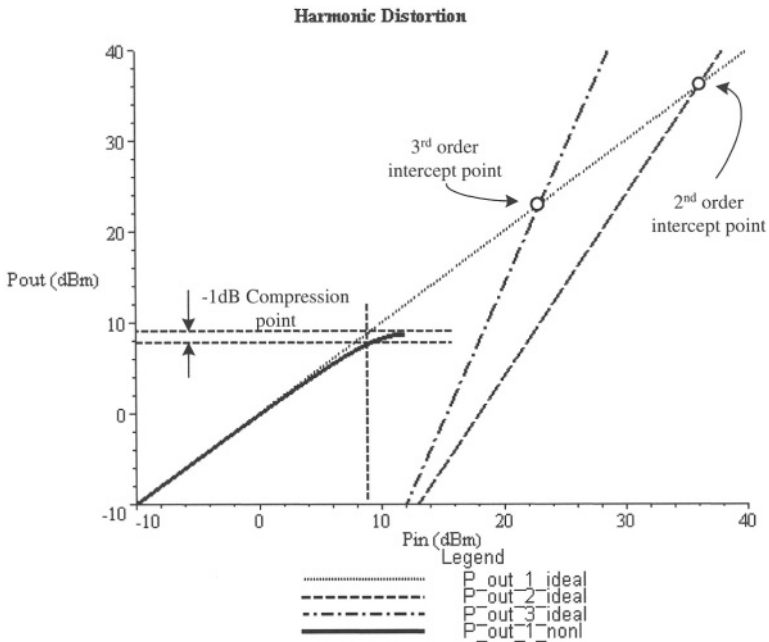


Figure 2-3. Harmonic distortion. The “\_ideal”-curves are obtained by the first term in (2-4) to (2-6) and the “\_nonl”-curve is (2-4) truncated to the 5<sup>th</sup> order coefficient.

Figure 2-3 shows the output power versus the input power for the fundamental frequency and the 2<sup>nd</sup> and 3<sup>rd</sup> harmonics. The curve  $P_{out\_1\_nonl}$  is obtained by plotting (2-4) truncated to the 5<sup>th</sup> order coefficient. At low input levels, the system has weakly nonlinear behavior. This means that the level of the fundamental frequency and the 2<sup>nd</sup> and 3<sup>rd</sup> harmonics can be expressed by the first term in (2-4) to (2-6), respectively. By extrapolating the first terms of these equations and plotting them versus

the entire input range, the curves  $P_{out\_1\_ideal}$ ,  $P_{out\_2\_ideal}$  and  $P_{out\_3\_ideal}$  are obtained. The input and output levels are in dBm, which are the levels referred to 1mW in a 50 Ohm resistor. For all curves, the coefficients are the same as for the plots in Figure 2-2.

When  $P_{in}$  is approximately 9dBm ( $V_{p,1}=0.9V$ ) the  $P_{out\_1\_nonl}$ -curve deviate from the ideal output signal power with 1dB. This is called the -1dB compression point and is shown in Figure 2-3. Further, also a -3dB compression point can be defined in the same way. The deviation from the ideal curve is caused by the nonlinear behavior of the system. There will also be compression or expansion of the 2<sup>nd</sup> and 3<sup>rd</sup> harmonics caused by the higher order terms in (2-5) and (2-6). Thus, a deviation from the extrapolated curves will occur for high input levels.

The 2<sup>nd</sup> and 3<sup>rd</sup> order intercept points are defined to be the input level that causes the extrapolated 2<sup>nd</sup> and 3<sup>rd</sup> harmonics to be equal to the level of the extrapolated level of the fundamental frequency. The harmonic intercept points are given by (2-10) and (2-11) below and visualized in Figure 2-3. By knowing the intercept points and the linear gain of the system, it is possible to compute the 2<sup>nd</sup> and 3<sup>rd</sup> harmonics for a specific input level. Further, to obtain low harmonic distortion the 2<sup>nd</sup> and 3<sup>rd</sup> order intercept points need to be as high as possible.

$$IP2_h = 2 \cdot \left| \frac{K_1}{K_2} \right| \quad (2-10)$$

$$IP3_h = 2 \cdot \sqrt{\left| \frac{K_1}{K_3} \right|} \quad (2-11)$$

Another parameter that is used to characterize analog systems is the dynamic range. In [3] the input dynamic range is defined as the ratio of the input level causing the -1 dB (or -3db) compression point and the input referred noise. This ratio is usually given in dB.

### 2.1.2 Dual-Frequency Excitation

Another test of the nonlinear behavior of an analog system can be done by applying two sinusoid signals with different frequency at the same input terminal. The total input signal can be represented as (2-12), where  $V_{p,1}$ ,  $V_{p,2}$  and  $\omega_{n,1}$ ,  $\omega_{n,2}$  are the input amplitudes and frequencies, respectively, of the sinusoids. The difference between the two frequencies is assumed small

compared to the absolute value of each of them. At the output of the nonlinear system several frequency components appear. First, both fundamental frequencies are present. The amplitude at  $\omega_{m,1}$  can be expressed as (2-13). As for the single frequency excitation, (2-13) shows that the fundamental response depends on the gain factor and the odd order nonlinear coefficients. Further, it depends on the amplitude of both input frequency components. Similar equation can be obtained for the response at  $\omega_{m,2}$  by interchanging  $V_{p,1}$  and  $V_{p,2}$  in (2-13).

Second, as for the single frequency excitation, the harmonics of the input frequencies are present at the output terminal. Further, mixing of the two signals is performed, and the sum and the difference of the various frequency components appear at the output terminal. These responses are called intermodulation products. The second order intermodulation product, shown in (2-14), is located at  $\omega_{m,1} \pm \omega_{m,2}$ . As for the 2<sup>nd</sup> harmonic, the 2<sup>nd</sup> order intermodulation product depends on all even order nonlinear coefficients. Further, it also depends on the amplitudes of both input frequencies,  $V_{p,1}$  and  $V_{p,2}$ . The 3<sup>rd</sup> order intermodulation product, located at  $2 \cdot \omega_{m,1} \pm \omega_{m,2}$ , can be expressed as (2-15). As for the 3<sup>rd</sup> harmonic, the 3<sup>rd</sup> order intermodulation product is a function of the odd order nonlinear coefficient. In addition, it also depends on the amplitude of the input frequency components. The responses at  $\omega_{m,2} \pm \omega_{m,1}$  and  $2 \cdot \omega_{m,2} \pm \omega_{m,1}$  can be obtained by interchanging  $V_{p,1}$  and  $V_{p,2}$  in (2-14) and (2-15). When assuming that the system behaves weakly nonlinear, the 2<sup>nd</sup> and 3<sup>rd</sup> order intermodulation distortion can be approximated by (2-16) and (2-17).

$$v_{in}(t) = V_{p,1} \cdot \cos(\omega_{in,1} \cdot t) + V_{p,2} \cdot \cos(\omega_{in,2} \cdot t) \quad (2-12)$$

$$V_{out_{-1,0}} = K_1 \cdot V_{p,1} + \frac{3}{4} \cdot K_3 \cdot (V_{p,1}^3 + 2 \cdot V_{p,1} \cdot V_{p,2}^2) + \frac{5}{8} \cdot K_5 \cdot (V_{p,1}^5 + 6 \cdot V_{p,1}^3 \cdot V_{p,2}^2 + 3 \cdot V_{p,1} \cdot V_{p,2}^4) + \dots \quad (2-13)$$

$$V_{out_{-1,\pm 1}} = K_2 \cdot V_{p,1} \cdot V_{p,2} + \frac{3}{2} \cdot K_4 \cdot (V_{p,1}^3 \cdot V_{p,2} + V_{p,1} \cdot V_{p,2}^3) + \dots \quad (2-14)$$

$$V_{out_{-2,\pm 1}} = \frac{3}{4} \cdot K_3 \cdot V_{p,1}^2 \cdot V_{p,2} + \frac{5}{8} \cdot K_5 \cdot (2 \cdot V_{p,1}^4 \cdot V_{p,2} + 3 \cdot V_{p,1}^2 \cdot V_{p,2}^3) + \dots \tag{2-15}$$

$$IM2 \triangleq \frac{|V_{out_{-1,\pm 1}}|}{|V_{out_{-1,0}}|} \approx \left| \frac{K_2}{K_1} \right| \cdot V_{p,2} \tag{2-16}$$

$$IM3 \triangleq \frac{|V_{out_{-2,\pm 1}}|}{|V_{out_{-1,0}}|} \approx \frac{3}{4} \cdot \left| \frac{K_3}{K_1} \right| \cdot V_{p,1} \cdot V_{p,2} \tag{2-17}$$

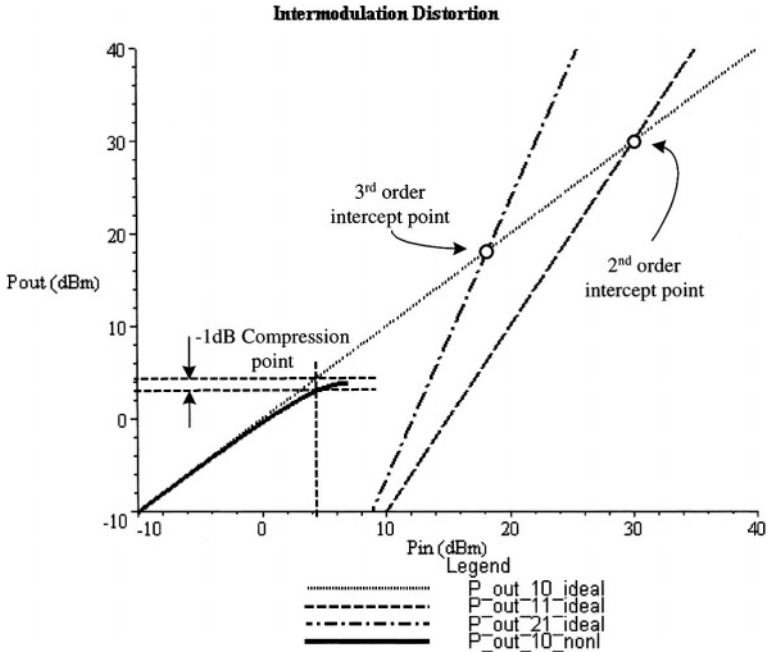


Figure 2-4. Intermodulation distortion. The plots are obtained by setting the  $V_{p,1}$  and  $V_{p,2}$  equal. The “\_ideal”-curves are obtained by the first term in (2-13) to (2-15) and the “\_nonl”-curve is (2-13) truncated to the 5<sup>th</sup> order coefficient.

In Figure 2-4 the extrapolation of the weakly nonlinear gain and 2<sup>nd</sup> and 3<sup>rd</sup> order intermodulation products are plotted. The plots of the intermodulation products are obtained by setting  $V_{p,1}$  and  $V_{p,2}$  equal. As for the single frequency excitation, a compression point can be defined and further 2<sup>nd</sup> and 3<sup>rd</sup> order intercept points. Due to larger higher order terms in the 1<sup>st</sup> order response (2-13), the -1dB compression point occur at lower level than when the system excitation is single-frequency. The intermodulation intercept points represent the input amplitude that make the extrapolated intermodulation products equal to the extrapolated 1<sup>st</sup> order response. These are defined in (2-18) and (2-19).

$$IP2_i = \left| \frac{K_1}{K_2} \right| \quad (2-18)$$

$$IP3_i = \frac{2}{\sqrt{3}} \cdot \sqrt{\left| \frac{K_1}{K_3} \right|} \quad (2-19)$$

## 2.2 Volterra Series

In (2-1) the nonlinear system is represented by a Taylor series. Taylor series can be used to approximate weakly nonlinear systems without memory. Most nonlinear systems have memory, or in other words, the response of the system depends on the frequency contents of the input signal. For describing weakly nonlinear behavior of analog systems with memory, the Volterra series can be used.

The Volterra series can be defined by (2-20), where the terms are called Volterra operators. The index numbers are the order of the operators. The Volterra operators can further be expressed as (2-21). Here,  $h_i(\cdot)$  are called Volterra kernels, where the order of the kernel is given by  $i$ . The 1<sup>st</sup> order Volterra operator in (2-21) can be recognized as the convolution integral of the impulse response of the linearized system,  $h_1(\tau_1)$ , and the input signal  $x(t)$ . The impulse response can be converted to the  $s$ -plane by doing a Laplace transform ([1], [2]). Then  $H_1(s_1)$  in (2-22) is achieved, which is the well-known  $s$ -plane representation of the linearized system. The  $s$ -plane representation is widely used in design of analog circuits. The higher order Volterra kernels in (2-21) are multidimensional impulse responses. Thus, they can also be transformed to the  $s$ -plane by using a multidimensional Laplace transform. In (2-22) the multidimensional Laplace transform is

applied to the 2<sup>nd</sup> and 3<sup>rd</sup> order Volterra kernels. The  $s$ -plane representations of the kernels are called nonlinear transfer functions. Similar transformation can be done by the Fourier transform ([1], [2]). These issues are thoroughly explained in [3].

$$y(t) = H_1[x(t)] + H_2[x(t)] + H_3[x(t)] + \dots + H_n[x(t)] + \dots \quad (2-20)$$

$$\begin{aligned} H_1[x(t)] &= \int_{-\infty}^{\infty} h_1(\tau_1) \cdot x(t - \tau_1) d\tau_1 \\ H_2[x(t)] &= \int_{-\infty}^{\infty} \int_{-\infty}^{\infty} h_2(\tau_1, \tau_2) \cdot x(t - \tau_1) \cdot x(t - \tau_2) d\tau_1 d\tau_2 \\ H_3[x(t)] &= \int_{-\infty}^{\infty} \int_{-\infty}^{\infty} \int_{-\infty}^{\infty} \left\{ h_3(\tau_1, \tau_2, \tau_3) \cdot \right. \\ &\quad \left. x(t - \tau_1) \cdot x(t - \tau_2) \cdot x(t - \tau_3) \right\} d\tau_1 d\tau_2 d\tau_3 \\ &\quad \vdots \\ H_n[x(t)] &= \int_{-\infty}^{\infty} \int_{-\infty}^{\infty} \dots \int_{-\infty}^{\infty} \left\{ h_n(\tau_1, \tau_2, \dots, \tau_n) \cdot \right. \\ &\quad \left. x(t - \tau_1) \cdot x(t - \tau_2) \cdot \right. \\ &\quad \left. \dots \cdot x(t - \tau_n) \right\} d\tau_1 d\tau_2 \dots d\tau_n \\ &\quad \vdots \end{aligned} \quad (2-21)$$

$$\begin{aligned} H_1(s_1) &= \int_{-\infty}^{\infty} h_1(\tau_1) \cdot e^{-s_1 \cdot \tau_1} d\tau_1 \\ H_2(s_1, s_2) &= \int_{-\infty}^{\infty} \int_{-\infty}^{\infty} h_2(\tau_1, \tau_2) \cdot e^{-(s_1 \cdot \tau_1 + s_2 \cdot \tau_2)} d\tau_1 d\tau_2 \\ H_3(s_1, s_2, s_3) &= \int_{-\infty}^{\infty} \int_{-\infty}^{\infty} \int_{-\infty}^{\infty} \left\{ h_3(\tau_1, \tau_2, \tau_3) \cdot \right. \\ &\quad \left. e^{-(s_1 \cdot \tau_1 + s_2 \cdot \tau_2 + s_3 \cdot \tau_3)} \right\} d\tau_1 d\tau_2 d\tau_3 \\ &\quad \vdots \end{aligned} \quad (2-22)$$

As for all series expansions, the Volterra series has limited radius of convergence. Thus, the Volterra series will diverge if the input signal become large enough. At what level of the input signal this happens, depends on the Volterra operators and thus on the nonlinear transfer functions. Another issue is how high the order of the Volterra series should be to describe the nonlinear system accurate. In this book, only weakly nonlinear systems are considered. In [3] the phrase “weakly nonlinear” is defined to be:

*“A circuit behaves weakly nonlinear if, for the applied input signal, it can be accurately described by the first three terms of its (converging) Volterra series”*

Thus, further in the book it is assumed that the circuits, in conjunction with the input signal, are weakly nonlinear as described above. The nonlinear behavior of the systems will be described in the frequency plane by the 2<sup>nd</sup> and 3<sup>rd</sup> order nonlinear transfer functions.

In the introduction of this chapter, it was mentioned that Volterra series can be cumbersome to derive and results in complex expressions. This assertion will now be visualized by an example. In Figure 2-5, a 2<sup>nd</sup> order two-dimensional nonlinear coefficient  $K2_{A\_B}$  is shown. The signals  $A$  and  $B$  have two different transfer functions from the input,  $H_A(s)$  and  $H_B(s)$ , respectively. Further,  $H_{OUT}(s)$  is the transfer function from the nonlinear coefficient to the output of the system. The 2<sup>nd</sup> order nonlinear transfer function of the entire system is given by (2-23), which cover both harmonics and intermodulation product of second order. The expression is rather large and becomes larger when inserting for the various transfer functions. For higher order, the nonlinear transfer functions contain even more terms, including all harmonic responses and intermodulation products. This is the main drawback of the Volterra series. Because of the generality, all nonlinear responses are found, which is overkill when e.g. only the harmonic responses are requested.

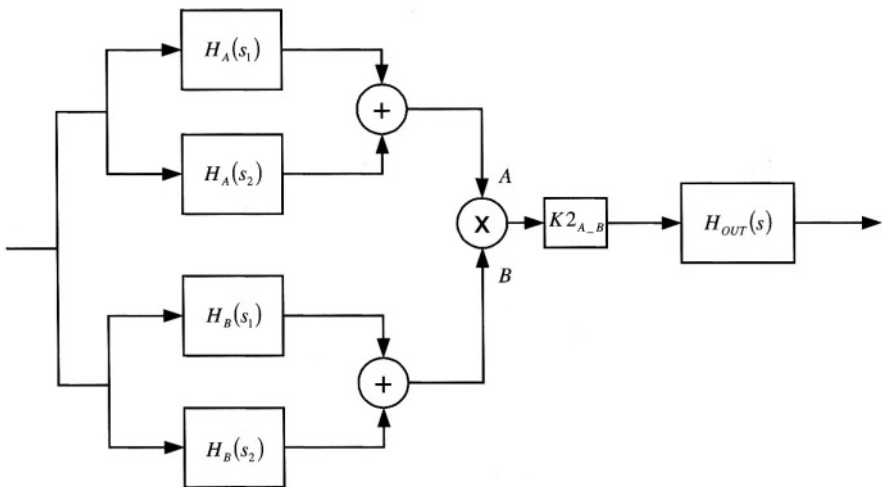


Figure 2-5. Two-dimensional nonlinear coefficient represented by Volterra series.

$$H_2(s_1, s_2) = K 2_{A-B} \cdot \left\{ \begin{array}{l} H_A(s_1) \cdot H_B(s_1) \cdot H_{OUT}(2s_1) + \\ \left[ H_A(s_1) \cdot H_B(s_2) + \right. \\ \left. H_A(s_2) \cdot H_B(s_1) \right] \cdot H_{OUT}(s_1 + s_2) + \\ \left. H_A(s_2) \cdot H_B(s_2) \cdot H_{OUT}(2s_2) \right\} \quad (2-23)$$

The phasor method described in the next section provides only the required subset of the Volterra series, e.g. the harmonic responses. Thus, the derivation and expressions for nonlinear responses will be simpler and provide more insight and understanding of the nonlinear behavior of a circuit than Volterra series does.

## 2.3 Phasor Method

When a circuit is in steady state, all currents and voltages are sinusoids. The output voltage of the system can be expressed as the input voltage with a change in amplitude and phase represented by  $|H(j\omega)|$  and  $\phi(j\omega)$ , respectively. This is shown in (2-24), where  $V_{in,p}$  and  $\omega$  is the amplitude and frequency of the input signal, respectively. Further,  $H(j\omega)$  are the 1<sup>st</sup> order transfer function of the system and  $\phi(j\omega)$  is the phase of  $H(j\omega)$ . In (2-25) the output voltage are represented in the frequency plane as a phasor [2], where  $\mathbf{P}$  represents the phasor transform. The requirement for the phasor representation is that the circuit is in steady state.

$$\begin{aligned} v_{out}(t) &= |H(j\omega)| \cdot V_{in,p} \cdot \cos(\omega \cdot t + \phi(\omega)) \\ &= \text{Re}\{H(j\omega) \cdot V_{in,p} \cdot e^{j\phi(\omega)} \cdot e^{j\omega t}\} \end{aligned} \quad (2-24)$$

$$\begin{aligned} V_{out}(j\omega) &= \mathbf{P}\left[\text{Re}\{H(j\omega) \cdot V_{in,p} \cdot e^{j\phi(\omega)} \cdot e^{j\omega t}\}\right] \\ &\hat{=} |H(j\omega)| \cdot V_{in,p} \cdot e^{j\phi(\omega)} \end{aligned} \quad (2-25)$$

The frequency components that is caused by the nonlinear behavior of the system, are also sinusoids. Thus, since the circuit is in steady state, the nonlinear responses can also be represented by phasors, with the excitation frequency equal to the frequency of the wanted harmonic or intermodulation product. The excitation of the system is now the nonlinear coefficients embedded inside the system. This is the idea of the phasor method.

The phasor method, carried out on an analog circuit, can be explained by the following procedure:

1. Find the 1<sup>st</sup> order response and all voltages/currents that control nonlinear coefficients in the circuit. These will be further used to find nonlinear responses of higher order. The circuit excitation is the input voltage to the circuit, which runs at one or more frequencies.
2. Find the desired 2<sup>nd</sup> order nonlinear response and all voltages/currents that control nonlinear coefficients in the circuit. The circuit excitation is the nonlinear coefficients of 2<sup>nd</sup> order, which depends on the 1<sup>st</sup> order voltages/currents found in 1. The excitation frequency is the frequency of the desired 2<sup>nd</sup> order nonlinear response, e.g. for the 2<sup>nd</sup> harmonic it equals  $2 \cdot \omega$ .
3. Find the desired 3<sup>rd</sup> order nonlinear response. The circuit excitation is the nonlinear coefficients of 2<sup>nd</sup> and 3<sup>rd</sup> order. Further, the nonlinear coefficients depend on voltages/currents found in both 1 and 2. The excitation frequency is the frequency for the desired 3<sup>rd</sup> order nonlinear response. E.g. for 3<sup>rd</sup> harmonic it equals  $3 \cdot \omega$ . For 3<sup>rd</sup> order intermodulation product it equals the frequency for the desired product.

The procedure shows that the  $n^{\text{th}}$  order nonlinear response depends on voltages/currents of lower order. Thus, it is necessary to begin with the 1<sup>st</sup> order response, continuing with the 2<sup>nd</sup> order and so on. The procedure can be extended to orders higher than 3, but the computation becomes complex.

The main advantage of the phasor method compared to the Volterra series is that only the necessary kernels are found. For example, when using a single-frequency test it is the 2<sup>nd</sup> and 3<sup>rd</sup> harmonic that are the desired nonlinear responses. These can be found directly by the phasor method, omitting the rest of the responses that the Volterra series provide. This can be visualized with a simple example. In Figure 2-6 the same system as described in Figure 2-5 is shown, but expressed by the phasor method. When using the procedure above the signals *A* and *B* are obtained by point 1, and the output voltage is achieved by point 2. The desired nonlinear response is the 2<sup>nd</sup> harmonic, which is expressed in (2-26). When (2-26) is compared to (2-23) it shows that (2-26) corresponds to the first term of (2-23), except for the factor  $\frac{1}{2}$ . This factor is due to the phasor representation [3]. If the 2<sup>nd</sup> order intermodulation product is to be found, it will correspond to the second term in (2-23). The nonlinear transfer functions, obtained by the phasor method, are thus a subset of the Volterra series. The phasor method provides less complex derivations and expressions at the cost of generality. Especially the harmonic nonlinear responses are simple.

Next, a simple example is shown to demonstrate how the phasor method can be used for computation of nonlinear transfer functions of electrical circuits.

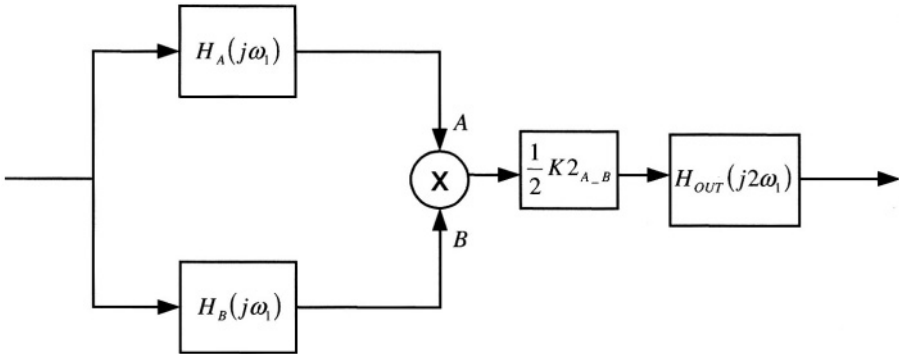


Figure 2-6. Two-dimensional nonlinear coefficient represented by the phasor method.

$$H_2(j\omega_1) = \frac{1}{2} \cdot K2_{A-B} \cdot \{H_A(j\omega_1) \cdot H_B(j\omega_1) \cdot H_{OUT}(j2\omega_1)\} \quad (2-26)$$

### 2.3.1 Example: Nonlinear LP-Filter

In Figure 2-7 a simple LP-filter is shown. The filter consists of a linear capacitor  $C_L$  and a nonlinear resistor  $R(v_a)$ .  $R(v_a)$  can for example be a simple model of a transistor used as a switch. The current through the resistor is given by (2-27), where  $g_a$  is the small-signal conductance of the resistor. Further,  $K2_{ga}$  and  $K3_{ga}$  are the 2<sup>nd</sup> and 3<sup>rd</sup> order nonlinear coefficients, respectively. The phasor method will now be applied to find the harmonic nonlinear responses for the circuit in Figure 2-7.

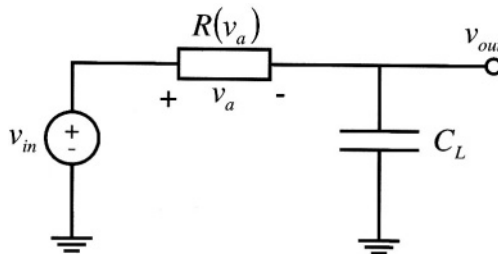


Figure 2-7. LP-filter with a voltage dependent resistor.

$$i_g \approx g_a \cdot v_a + K2_{g_a} \cdot v_a^2 + K3_{g_a} \cdot v_a^3 \quad (2-27)$$

To compute the 1<sup>st</sup> order response, the circuit in Figure 2-8 is used. Here,  $R(v_a)$  is replaced by the conductance  $g_a$ . The output response is given by (2-28) and the 1<sup>st</sup> order controlling voltage  $V_{a-1}$  for the nonlinear coefficients of  $R(v_a)$  is shown in (2-29).  $V_{a-1}$  will further be used in computation of the nonlinear responses.  $\omega_{LP}$  is the  $-3$ dB frequency of the LP-filter and is expressed in (2-30).

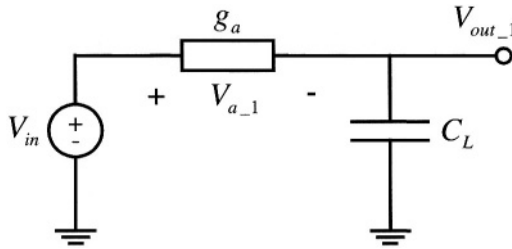


Figure 2-8. Circuit for computation of 1<sup>st</sup> order response.

$$V_{out-1} = \frac{1}{1 + j \frac{\omega}{\omega_{LP}}} \cdot V_{in} \quad (2-28)$$

$$V_{a-1} = \frac{j \frac{\omega}{\omega_{LP}}}{1 + j \frac{\omega}{\omega_{LP}}} \cdot V_{in} \quad (2-29)$$

$$\omega_{LP} = \frac{g_a}{C_L} \quad (2-30)$$

For computation of the nonlinear responses, the circuit in Figure 2-9 is used. The input voltage is shorted and the excitation for the circuit is the current  $Ix_{NL,g_a}$ . This current represents the  $x^{\text{th}}$  order nonlinear behavior of the resistance in phasor representation. Equation (2-31) shows the 2<sup>nd</sup> order

nonlinear current, which is the excitation when finding the 2<sup>nd</sup> order nonlinear response of the circuit. Because of the phasor representation, the nonlinear coefficient is preceded by the factor 1/2. The reason for this factor is shown in [3]. The 2<sup>nd</sup> order nonlinear response and controlling voltage are shown in (2-32) and (2-33), respectively.

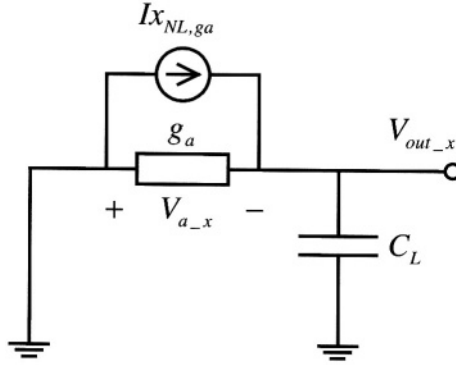


Figure 2-9. Circuit for computation of 2<sup>nd</sup> and 3<sup>rd</sup> order responses. The parameter  $x$  is 2 or 3 for 2<sup>nd</sup> and 3<sup>rd</sup> order analysis, respectively.

$$I_{2_{NL,ga}} = \frac{1}{2} \cdot K_{2_{ga}} \cdot V_{a_{-1}}^2 = \frac{1}{2} \cdot K_{2_{ga}} \cdot (V_{in} - V_{out_{-1}})^2 \quad (2-31)$$

$$V_{out_{-2}} = \frac{1}{2} \cdot \frac{K_{2_{ga}}}{g_a} \cdot \frac{\left(\frac{j\omega}{\omega_{LP}}\right)^2}{\left(1 + j\frac{\omega}{\omega_{LP}}\right)^2 \left(1 + j\frac{2 \cdot \omega}{\omega_{LP}}\right)} \cdot V_{in}^2 \quad (2-32)$$

$$V_{a_{-2}} = -V_{out_{-2}} \quad (2-33)$$

The 3<sup>rd</sup> order nonlinear response can be found by replacing  $I_{x_{NL,ga}}$  in Figure 2-9 with  $I_{3_{NL,ga}}$  of (2-34) (derivation of this current is shown in [3]). By inserting for  $V_{a_{-1}}$  and  $V_{a_{-2}}$  and further solve for the output voltage, the 3<sup>rd</sup> harmonic response is found, given by (2-35). From (2-35) it is shown that the 3<sup>rd</sup> harmonic depends on the 2<sup>nd</sup> order nonlinear coefficient, in addition to

the 3<sup>rd</sup> order nonlinear coefficient. Because of  $K2_{ga}$ , the 2<sup>nd</sup> harmonic is mixed with the fundamental frequency. The resulting frequency component is at 3<sup>rd</sup> harmonic.

$$\begin{aligned}
 I3_{NL,ga} &= K2_{ga} \cdot V_{a-1} \cdot V_{a-2} + \frac{1}{4} \cdot K3_{ga} \cdot V_{a-1}^3 \\
 &= K2_{ga} \cdot (V_{in} - V_{out-1}) \cdot (-V_{out-2}) \\
 &\quad + \frac{1}{4} \cdot K3_{ga} \cdot (V_{in} - V_{out-1})^3
 \end{aligned} \tag{2-34}$$

$$\begin{aligned}
 V_{out-3} &= \frac{1}{4} \cdot \left( \frac{K3_{ga}}{g_a} - 2 \cdot \left( \frac{K2_{ga}}{g_a} \right)^2 \cdot \frac{1}{\left( 1 + j \frac{2 \cdot \omega}{\omega_{LP}} \right)} \right) \\
 &\quad \cdot \frac{\left( \frac{j\omega}{\omega_{LP}} \right)^3}{\left( 1 + j \frac{\omega}{\omega_{LP}} \right)^3 \left( 1 + j \frac{3 \cdot \omega}{\omega_{LP}} \right)} \cdot V_{in}^3
 \end{aligned} \tag{2-35}$$

The 1<sup>st</sup> to 3<sup>rd</sup> order responses for the LP-filter are plotted in Figure 2-10. The 1<sup>st</sup> order response has the expected LP-filter shape. The 2<sup>nd</sup> and 3<sup>rd</sup> order responses are both low at low frequencies. When increasing the frequency the 2<sup>nd</sup> and 3<sup>rd</sup> harmonics increase with 40dB/decade and 60dB/decade, respectively, and reach their maximum approximately at the -3dB frequency of the filter.

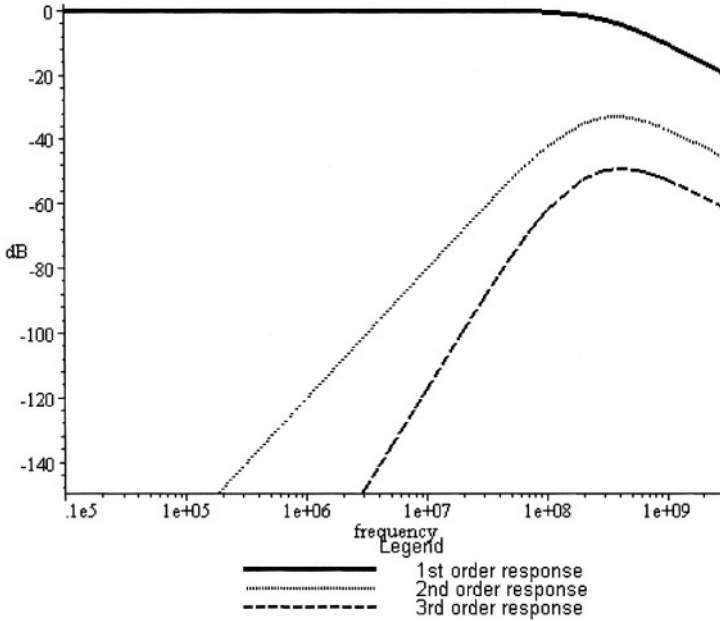


Figure 2-10. Plotting of 1<sup>st</sup> to 3<sup>rd</sup> order responses of the LP-filter. The parameters used are  $g_a=10\text{mS}$ ,  $K2_{g_a}=g_a/5$ ,  $K3_{g_a}=-g_a/10$  and  $C_l=5\text{pF}$ . The input voltage is  $1V_{\text{peak}}$  and the  $-3\text{dB}$  frequency is located at  $318\text{MHz}$ .

## 2.4 Concluding Remarks

First in this chapter, several measurement parameters were defined for both single-frequency and dual-frequency excitation of the circuit. For single-frequency excitation,  $HD2$ ,  $HD3$  and  $THD$  can be obtained. For dual-frequency excitation, it is possible to achieve  $IM2$  and  $IM3$ . For both excitations, 2<sup>nd</sup> and 3<sup>rd</sup> order intercept points can be found. From the intercept points it is possible to compute the distortion at the output of the circuit for a given excitation level on the input. Further, two tools for symbolic analysis of weakly nonlinear systems were described. The Volterra series is general, but complex. By the phasor method it is possible to find only the desired nonlinear responses. This results in simple derivations and less complex symbolic expressions.

Further in this book, the phasor method will be used for nonlinear analysis. There are two main reasons for this. First, by the phasor method it is possible to obtain only the desired nonlinear transfer functions. The derivations are more simple and the expressions are less complex than

obtained by the Volterra series. Second, in Chapter 3 and Chapter 4 the Miller opamp is considered as a two-input device. Nonlinear analysis of two-input devices is much simpler when using the phasor method than the Volterra series [3].

Further, to keep the derivaitons as simple as possible, only nonlinear transfer functions for the 2<sup>nd</sup> and 3<sup>rd</sup> harmonics will be found. Thus, intermodulation products will not be considered. However, by describing the nonlinear performance of the circuit by *HD2* and *HD3*, also information of *IM2* and *IM3* are obtained. At low frequency, and under the assumption that the circuit is weakly nonlinear, the ratios *IM2/HD2* and *IM3/HD3* equals 2 and 3, respectively. At higher frequency, the situation is somewhat different. For example, *IM2* and *HD2* are obtained in the same way. Using the phasor method, first the 1<sup>st</sup> order controlling voltages/currents to the nonlinear coefficients are obtained. For both *HD2* and *IM2*, these are derived from the 1<sup>st</sup> order circuit (as shown in Figure 2-8 for the LP-filter). For *HD2* the excitation frequency is  $\omega_{n,1}$  and for *IM2*  $\omega_{n,1}$  and  $\omega_{n,2}$ , which are close in frequency. Thus, the controlling voltages/currents are nearly equal for *HD2* and *IM2*. To find the nonlinear responses for *HD2* and *IM2* the 2<sup>nd</sup> order circuit is evaluated at two different frequencies. For *HD2* at the frequency  $2 \cdot \omega_{n,1}$ , and for *IM2* e.g. on the frequency  $\omega_{n,1} - \omega_{n,2}$ . For CL opamp circuits the nonlinear transfer functions contains zeroes well below the location of the poles. Thus, the nonlinear responses will increase with increasing frequency. Because of this, the ratio *IM2/HD2* will be less than 2 for frequency excitations higher than the locations of the zeroes of the nonlinear transfer functions. The same argument holds for *IM3/HD3*. Thus, for feedback opamp circuits, which is the main subject in this book, and for the intermodulation products at the difference of frequencies, the equations (2-36) and (2-37) are valid.

$$\frac{IM2}{HD2} \leq 2 \quad (2-36)$$

$$\frac{IM3}{HD3} \leq 3 \quad (2-37)$$

All circuits further in this book will be considered weakly nonlinear as stated in section 2.2. For feedback opamp circuits, this is an accurate description when the circuit excitation is well below the supply voltage and the biasing of the transistors in the opamp is adequate for low distortion. However, if the circuit is not weakly nonlinear, the nonlinear transfer

functions obtained by the Volterra series or the phasor method will still provide valuable information about the nonlinear behavior of the circuit and how the distortion can be minimized.

## REFERENCES

- [1] E. Kreyszig, "Advanced Engineering Mathematics," 7<sup>th</sup> edition, John Wiley & Sons, Inc., 1993.
- [2] J. W. Nilsson, "Electric Circuits," 3<sup>rd</sup> edition, Addison-Wesley Publishing Company, Inc., 1990.
- [3] P. Wambacq, W. Sansen, "Distortion Analysis of Analog Integrated Circuits," Norwell, MA: Kluwer Academic Publishers, 1998.
- [4] S. Narayanan, "Transistor Distortion Analysis Using Volterra Series Representation," *The Bell System Technical Journal*, vol. 46, pp. 991-1024, May-June 1967.
- [5] S. Narayanan, H. C. Poon, "An Analysis of Distortion in Bipolar Transistors Using Integral Charge Control Model and Volterra Series," *IEEE Transaction on Circuit Theory*, vol. CT-20, no. 4, pp. 341-351, Jul. 1973.
- [6] A. M. Khadr, R. H. Johnston, "Distortion in High-Frequency FET Amplifiers," *IEEE Journal of Solid-State Circuits*, vol. SC-9, no. 4, pp. 180-189, Aug. 1974.
- [7] S. Narayanan, "Applications of Volterra Series to Intermodulation Distortion Analysis of Transistor Feedback Amplifiers," *IEEE Transaction on Circuit Theory*, vol. CT-17, no. 4, pp. 518-527, Nov. 1970.
- [8] H. Jardon, R. Gomes, O. Golovin, "Nonlinear Analysis of Amplifiers with Local and Global Negative Feedback," *IEEE International Symposium on Circuits and Systems 1997*, June 9-12 1997, pp. 965-968.
- [9] R. G. Meyer, M. J. Shensa, R. Eschenback, "Cross Modulation and Intermodulation in Amplifiers at High Frequencies," *IEEE Journal of Solid-State Circuits*, vol. SC-7, no. 1, pp. 16-23, Feb. 1972.
- [10] C. Beainy, R. A. Baki, M. N. El-Gamal, "Distortion Analysis of High-Frequency Log-Domain Filters Using Volterra Series," *IEEE International Symposium on Circuits and Systems 2001*, vol. 1, 2001, pp. 472-475.
- [11] P. Wambacq, P. Dobrovolný, S. Donnay, M. Engels, I. Bolsens, "Compact modeling of nonlinear distortion in analog communication circuits," *Proceedings of Design, Automation and Test in Europe Conference and Exhibition 2000*, pp. 350-354, 2000.
- [12] J. J. Bussgang, L. Ehrman, J. W. Graham, "Analysis of Nonlinear Systems with Multiple Inputs," *Proceedings of The IEEE*, vol. 62, no. 8, pp. 1088-1119, Aug. 1974.
- [13] K. Gopal, M. S. Nakhla, K. Singhal, J. Vlach, "Distortion Analysis of Transistor Networks," *IEEE Tr. on Circuits and Systems*, vol. CAS-25, no. 2, pp. 99-106, Feb. 1978.
- [14] P. Wambacq, G. G. E. Gielen, P. R. Kinget, W. Sansen, "High-Frequency Distortion Analysis of Analog Integrated Circuits," *IEEE Tr. on Circuits and Systems—II: Analog and Digital Signal Processing*, vol. 46, no. 3, pp. 335-345, Mar. 1999.
- [15] P. Wambacq, G. Gielen, W. Sansen, "Symbolic Simulation of Harmonic Distortion in Analog Integrated Circuits with Weak Nonlinearities," *Proceedings of ISCAS90*, May 1990, pp. 536-539.
- [16] P. Wambacq, J. Vanthienen, G. Gielen, W. Sansen, "A Design Tool for Weakly Nonlinear Analog Integrated Circuits With Multiple Inputs (Mixers, Multipliers),"

*Proceedings of the IEEE 1991 Custom Integrated Circuit Conference*, 1991, pp. 5.1/1-5.1/4.

*This page intentionally left blank*

## Chapter 3

### **Biasing and Opamp Modeling for Low Distortion**

An important issue regarding robust design for low distortion is the biasing of each transistor in the circuit. In section 3.1, transistor biasing for high and robust linearity performance is described. First, a nonlinear model of the transistor is presented. This model is further used for arguing how to bias the transistor to achieve high and stable linearity performance. This is done by first using the transistor as current source and then as a common source amplifier. The section results in biasing guidelines to obtain low nonlinear distortion in CMOS transistor circuits.

In section 3.2 the opamp is described as a two-input device, one input for the differential voltage and one for the CM-voltage. This is done to include the effect the CM-voltage has on the linearity performance of the circuit, especially in the non-inverting opamp configuration. Section 3.2 also contains explanation of how the Open Loop (OL) and CL nonlinear transfer functions of the opamp circuit are obtained. The transfer functions are split up in different factors to make the simplifications easier and to obtain surveyable expressions for the transfer functions. This gives also valuable insight in the cause of nonlinear distortion. At the end of section 3.2 the opamp, used further in this work, and its simplified model is presented.

This chapter makes the foundation for the nonlinear transfer functions and design equations discussed in Chapter 4 and the opamp designs described in Chapter 5.

### 3.1 Biasing for Robust Linearity Performance

#### 3.1.1 Transistor Model

The transistor model is described in [1] and [2] and is shown in Figure 3-1. Here, the capacitance between gate and drain is omitted. This capacitance causes a feed forward- and feedback path when the transistor is used as an amplifier. Because of the Gate-Drain (GD) capacitance the 1<sup>st</sup> and higher order transfer functions for the total circuit (e.g. an opamp) become complex. The transistor model in Figure 3-1 will be used in the model for the opamp described in section 3.2. For this opamp, omitting the GD capacitance will only cause minor errors in the frequency responses up to GBW of the opamp.

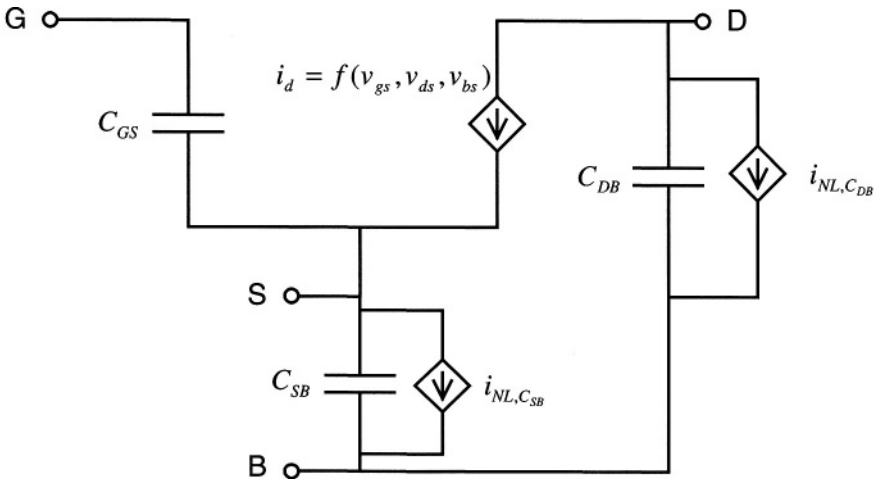


Figure 3-1. The transistor model.

The main contributions to nonlinearity for a transistor biased in strong inversion, are the nonlinear intrinsic drain current (further referred to as the drain current), the Source-Bulk (SB) capacitance and the Drain-Bulk (DB) capacitance. The D/S-B-capacitances are due to the diffusion between drain/source and bulk. The drain current is generally a three dimensional function, where the excitations are the voltages  $v_{GS}$ ,  $v_{DS}$  and  $v_{SB}$ . For weak nonlinearity, the equation for the drain current can be expressed as a series, which is evaluated around a bias point as (3-1) shows. Here,  $v_{gs}$ ,  $v_{ds}$  and  $v_{sb}$  are the terminal voltages disregarding the DC value. In (3-1)  $gm$  is the

transconductance,  $gd$  is the drain to source conductance, and  $gmb$  is the transconductance caused by the bulk modulation. These factors are the well-known small-signal parameters for a transistor, and are widely used in circuit design. The rest of the factors are because of nonlinearity in the transistor and thus called the nonlinear coefficients of the drain current. Equation (3-2) is obtained by treating the current through the diffusion capacitance in the same way. The index  $x$  is D (drain) or S (source). The definitions of the nonlinear coefficients are given in Appendix A.

$$\begin{aligned}
 i_d &= f(v_{gs}, v_{ds}, v_{bs}) \\
 &\approx gm \cdot v_{gs} + gd \cdot v_{ds} + gmb \cdot v_{bs} \\
 &+ K2_{gm} \cdot v_{gs}^2 + K3_{gm} \cdot v_{gs}^3 + K2_{gd} \cdot v_{ds}^2 + K3_{gd} \cdot v_{ds}^3 \\
 &+ K2_{gmb} \cdot v_{bs}^2 + K3_{gmb} \cdot v_{bs}^3 \\
 &+ K2_{gm\_gd} \cdot v_{gs} \cdot v_{ds} + K2_{gmb\_gm} \cdot v_{bs} \cdot v_{gs} \\
 &+ K2_{gmb\_gd} \cdot v_{bs} \cdot v_{ds} \\
 &+ K3_{2gm\_gd} \cdot v_{gs}^2 \cdot v_{ds} + K3_{gm\_2gd} \cdot v_{gs} \cdot v_{ds}^2 \\
 &+ K3_{2gmb\_gm} \cdot v_{bs}^2 \cdot v_{gs} + K3_{gmb\_2gm} \cdot v_{bs} \cdot v_{gs}^2 \\
 &+ K3_{2gmb\_gd} \cdot v_{bs}^2 \cdot v_{ds} + K3_{gmb\_2gd} \cdot v_{bs} \cdot v_{ds}^2 \\
 &+ K3_{gm\_gmb\_gd} \cdot v_{gs} \cdot v_{ds} \cdot v_{bs}
 \end{aligned} \tag{3-1}$$

$$\begin{aligned}
 i_{C_{XB}} &= C_{XB} \cdot \frac{dv_{xb}}{dt} + i_{NL, C_{XB}} \\
 &\approx C_{XB} \cdot \frac{dv_{xb}}{dt} + K2_{C_{XB}} \cdot v_{xb} \cdot \frac{dv_{xb}}{dt} + K3_{C_{XB}} \cdot v_{xb}^2 \cdot \frac{dv_{xb}}{dt}
 \end{aligned} \tag{3-2}$$

If all nonlinear coefficients in (3-1) and (3-2) are zero, the circuit is reduced to an ordinary small-signal system and does not produce any distortion. Thus, it is important to make the nonlinear coefficients and the terminal voltages as small as possible such that the higher order terms in (3-1) and (3-2) have minor contributions to the total signal current. Terminal voltage can be kept small by apply negative feedback. Small nonlinear coefficients are obtained by careful biasing of the circuit. It is also desirable that the circuit has low distortion even if the circuit conditions are changing, e.g. change in process parameters, biasing conditions, power supply voltage

etc. To make the circuit robust against these variations it is important to keep the small-signal parameters and nonlinear coefficients relatively constant in the entire range of the terminal voltages of the transistors. These topics are addressed in the next subsections.

Simulations of small-signal parameters and higher order derivatives will be shown in the next subsections. The simulations are done by the SPICE-like simulator Eldo [3] with Philips MOS Model 9 (MM9) [4] and parameter set from a 0.35 $\mu\text{m}$  CMOS technology. In [1] and [2] it is pointed out that higher order derivatives of the MOS transistor drain current often are poorly modeled in commercial available circuit simulators, especially for devices in sub-micron technologies. This is further described in [5] and [6], which show the inaccuracy of transistor models. The inaccuracy can be caused by the model itself or in conjunction with a poorly extracted parameter set. Further, the parameter sets are often worked out to obtain highly accurate first order derivatives (small signal parameters). This gives high accuracy in simulation of e.g. gain, bandwidth, gain- and phase margins of the circuit. Thus, the accuracy of higher order derivatives are often not an issue when the parameter sets are made.

In the next subsections, the higher order derivatives are viewed qualitatively and the accuracy of the absolute values is thus less important. This is done to obtain information on how to bias the transistor for low distortion. For this purpose, the shape of the curves is plotted as a function of the transistor terminal voltages and it is assumed that these shapes are approximately correct.

### 3.1.2 Biasing of Current Sources

The requirement for a current source is low output conductance and small parasitic capacitance. A simple current source can be made of one transistor as shown in Figure 3-2. Here,  $V_B$  is the bias voltage, assumed constant,  $C_p$  is the parasitic capacitance in the drain node and  $i_D$  is the drain current. When designing for high bandwidth it is often more important to keep the parasitic capacitance low, than to obtain low output conductance. By using minimum gate length, and thus keep the gate width small, the parasitic capacitance on drain will be minimum, but at the cost of higher output conductance.

When setting all voltages except  $v_d$  in (3-1) to zero, equation (3-3) is obtained. Figure 3-3 shows Eldo simulations of the coefficients in (3-3). The transistor has minimum gate length and the Gate-Source (GS) voltage is 0.75V. At low Drain-Source (DS) voltage the transistor is biased on the edge of the triode region and all nonlinear coefficients are large compared to  $gd$ . Additionally, they also have large variation with change in the DS-voltage. When the DS-voltage is increased well above the saturation voltage of the

transistor, the nonlinear coefficients become small and relatively stable. Thus, a current source with low distortion and robustness against variations in circuit conditions is obtained by biasing the transistor well above the triode region.

$$i_d \approx g_d \cdot v_{ds} + K2_{gd} \cdot v_{ds}^2 + K3_{gd} \cdot v_{ds}^3 \tag{3-3}$$

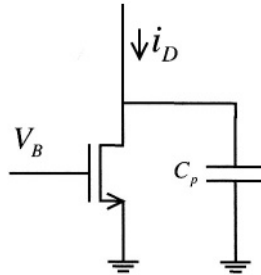


Figure 3-2. The transistor as a current source.  $V_B$  is the gate bias voltage and  $C_p$  is the parasitic capacitance when looking into the drain terminal.

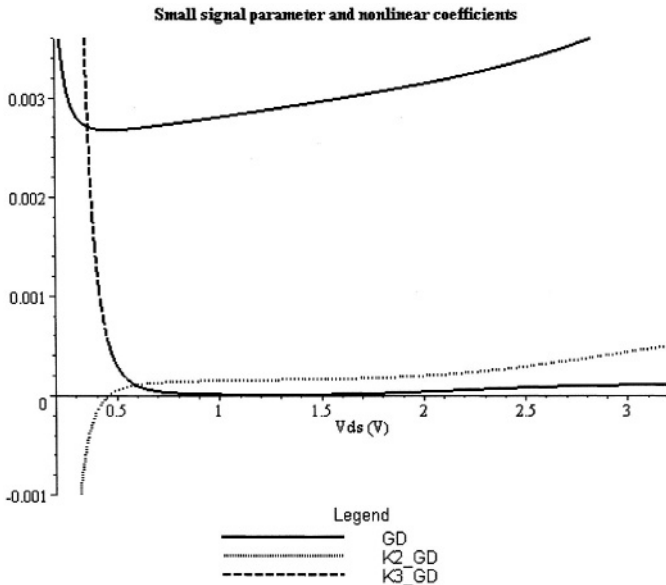


Figure 3-3. Output conductance and 2<sup>nd</sup> and 3<sup>rd</sup> order nonlinear coefficients as a function of the DS-voltage of the transistor. The gate length equals 0.35 $\mu$ m,  $V_{GS}=0.75$ V and the threshold voltage  $V_T=0.58$ V (extracted by Eldo).

It is possible to lower the saturation voltage by decreasing the GS-overdrive. This is done by making the transistor wider and/or shorter at the same drain current. However, a wider transistor gives larger  $C_p$ , which can ruin the phase- and gain-margins for the feedback circuit.

In  $C_p$  also the DB-diffusion capacitance is included. This capacitance is caused by a reverse biased pn-junction and becomes more linear as the reverse voltage increase. Thus, also for the diffusion capacitance it is important to have large DS-voltage. On the other hand, simulations show that these nonlinear coefficients contribute to distortion only in nodes with large voltage swing and only at very high frequency.

### 3.1.3 Biasing of Signal Transistors

The phrase “signal transistor” means a transistor where the signal that appears in the GS-voltage is transferred to the DS-voltage. An example of a signal transistor is shown in Figure 3-4. The transistor is used in a common source amplifier stage, where  $v_{IN}$  can be the output of the previous stage and  $gd_L$  the output conductance of a current source. Here, bulk and source are connected together through the substrate. Thus, (3-4) is obtained by setting  $v_{bs}$  in (3-1) to zero.

$$\begin{aligned}
 i_d \approx & gm \cdot v_{gs} + K2_{gm} \cdot v_{gs}^2 + K3_{gm} \cdot v_{gs}^3 \\
 & + K2_{gm\_gd} \cdot v_{gs} \cdot v_{ds} + K3_{2gm\_gd} \cdot v_{gs}^2 \cdot v_{ds} \\
 & + K3_{gm\_2gd} \cdot v_{gs} \cdot v_{ds}^2 \\
 & + gd \cdot v_{ds} + K2_{gd} \cdot v_{ds}^2 + K3_{gd} \cdot v_{ds}^3
 \end{aligned} \tag{3-4}$$

In Figure 3-5  $gm$ ,  $K2_{gm}$  and  $K3_{gm}$  are plotted versus GS-voltage with minimum gate length for the transistor and DS-voltage equal to 1.65V. The plot shows that when the GS-voltage is equal to the threshold voltage the higher order derivatives  $K2_{gm}$  and  $K3_{gm}$  have a discontinuity. The reason is the MOS model in conjunction with the parameter set used. MOS models use different equations in different biasing modes. In the transit region between two modes (e.g. between sub-threshold and above threshold) discontinuities in the higher order derivatives may occur. This is a common problem in modeling of MOS devices. To get reliable estimates of the linearity performance through simulations, it is important not to bias the transistors in the vicinity of discontinuities in the transistor models.

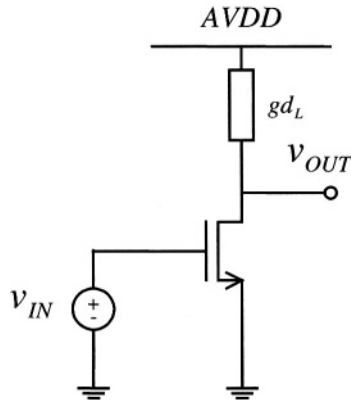


Figure 3-4. Signal transistor in common source amplifier stage.  $v_{IN}$  is the voltage from the previous stage and  $g_{dL}$  is the output conductance from a current source.

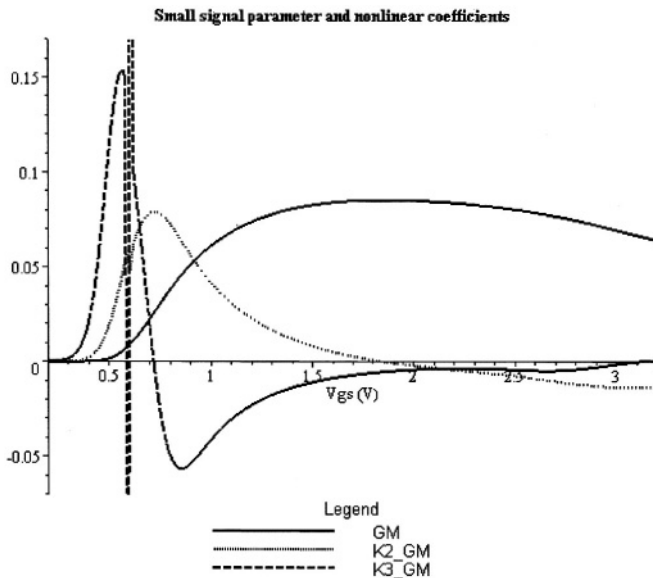


Figure 3-5. Transconductance and nonlinear coefficients for the signal transistor as a function of the GS-voltage. The gate length equals  $0.35\mu\text{m}$ ,  $V_{DS}=1.65\text{V}$  and the threshold voltage  $V_T=0.58\text{V}$  (extracted by Eldo).

Figure 3-5 shows that  $K2_{gm}$  and  $K3_{gm}$  are large compared to  $gm$  at low GS-voltages and the variations in the nonlinear coefficients are considerable. Thus, it is important to avoid biasing the transistor in this region. At higher GS-voltage, the inclination of  $gm$  rolls off and reach zero at  $1.8\text{V}$ . This is due

to a combination of velocity saturation and mobility degradation. Thus,  $K2_{gm}$  and  $K3_{gm}$  are both low compared to  $gm$  for  $v_{GS}$  in this region. On the other hand, high GS-voltage, and thus high GS-overdrive, will make the saturation voltage high and increase the nonlinear coefficients associated with the DS-terminal. This is the same situation as for the current source described in the previous subsection. Thus, a tradeoff has to be made where the optimum GS-voltage is lower than 1.8V to keep all nonlinear coefficients small and the total distortion from the transistor on a minimum.

The other nonlinear coefficients in (3-4) depend on both  $v_{gs}$  and  $v_{ds}$ . Simulations show that these coefficients are low and relatively constant with the same biasing scheme as above.

When the SB-voltage is non-zero, the nonlinear coefficients because of the bulk effect must be taken into consideration. By using the biasing scheme above, the nonlinear coefficients associated with the SB-voltage are all small and stable. Further, as long as the GS-overdrive is adequate, the effect that the biased bulk has on the other nonlinear coefficients (due to the GS- and DS-terminals) is small.

Thus, for a signal transistor the GS-voltage should be high enough to keep the nonlinear coefficient associated with the GS-voltage low and low enough to keep the transistor away from the triode region. This results in low distortion and achievement of robust linearity performance against variations in circuit conditions.

### 3.1.4 Biasing Guidelines for Low Distortion

Before starting the design process, verification of the transistor models, together with the parameter sets for the fabrication technology, should be carried out. It is important to locate discontinuities in the derivatives and to avoid bias the transistors near these points. This is to evade unreliable simulation estimates of distortion.

The selection of appropriate bias currents of the transistors is an important issue. At low frequencies, the resistive load on the transistor output consumes signal current. To avoid clipping, the equilibrium drain current has to be equal to or larger than the signal current. Further, to maintain weakly nonlinear behavior of the circuit the equilibrium drain current has to be well above the signal current. At higher frequencies, signal currents through capacitive loads come in to consideration. This will at high enough frequency result in slewing. To ensure weakly nonlinear behavior also at high frequencies, the bias current must be large enough to keep the circuit far from slewing behavior in any of its nodes, at the highest operating frequency.

For the signal transistor, it was stated in the above subsection that the GS-overdrive should not be too low because of large nonlinear coefficients in this biasing region. In feedback systems, the loop gain suppresses the distortion. It is shown in Chapter 4 that it is important to keep the transconductance of each amplifying transistor high, in order to obtain large suppression of distortion in a wide frequency range. In (3-5) a simplified equation for the transconductance is shown for a transistor in saturation. When the drain current remains constant, the only way to increase  $gm$  is to decrease the GS-overdrive by making the transistor wider. As shown in the previous subsection, the nonlinear coefficients will then increase. Thus, to obtain the lowest distortion, which means high  $gm$  and low nonlinear coefficients, the CL circuit must be optimized using a circuit simulator.

$$gm = \frac{2 \cdot I_D}{V_{GS} - V_T} \quad (3-5)$$

In Figure 5-4 in section 5.2, a 1.8V CMOS opamp manufactured in a 0.18 $\mu\text{m}$  technology is presented. This opamp is connected in inverting opamp configuration and optimized for low  $HD2$  and  $HD3$  in Eldo. The Miller transistor M4 has major contribution to the total distortion of the circuit and is thus an essential transistor when optimizing the circuit. The small-signal parameters and nonlinear coefficients of M4 after optimization are shown in Figure 3-6 and Figure 3-7. The gate length of the transistor is 0.18 $\mu\text{m}$  and the transistor model used is BSIM3 [7]. The transistor is biased with  $V_{GS}=0.686\text{V}$  and  $V_{DS}=0.9\text{V}$ . Figure 3-6 shows that the nonlinear coefficients associated with the DS-terminals are low when  $V_{DS}=0.9\text{V}$ . Further, at this bias point, the nonlinear coefficients are relatively stable in a large range of the DS-voltage. Figure 3-7 shows that at  $V_{GS}=0.686\text{V}$  both nonlinear coefficients are large, especially  $K3_{gm}$ . The reasons why the CL circuit still has minimum distortion are a combination of low saturation voltage and high transconductance obtained by low GS-overdrive as described above.

Further, the plots show no discontinuities in the higher order derivatives. Additionally, compared to the plot for the 0.35 $\mu\text{m}$  transistor,  $gm$  are more constant at high GS-voltage. The reason for this is expected to be stronger effect from velocity saturation.

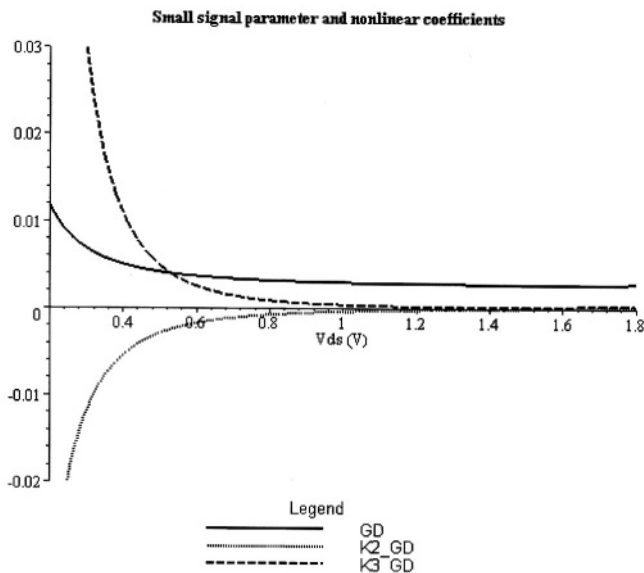


Figure 3-6. Output conductance and 2<sup>nd</sup> and 3<sup>rd</sup> order nonlinear coefficients of the transistor as a function of the DS-voltage. The gate length equals  $0.18\mu\text{m}$ ,  $V_{GS}=0.686\text{V}$  and the threshold voltage  $V_T=0.51\text{V}$  (extracted by Eldo).

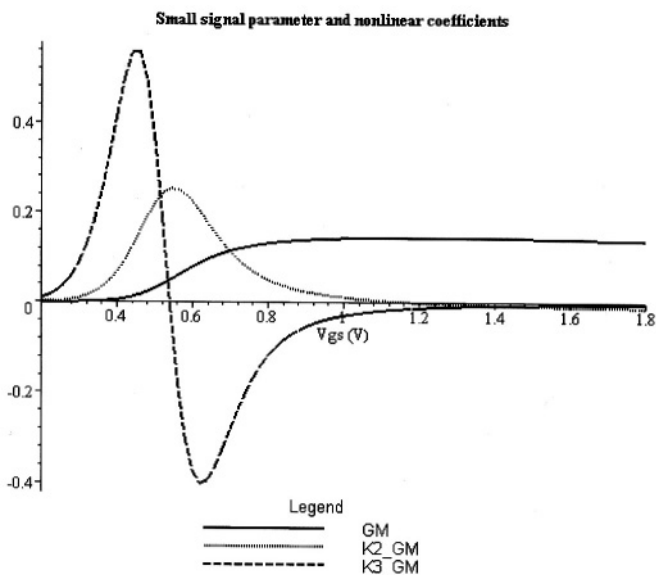


Figure 3-7. Transconductance and nonlinear coefficients of the transistor as a function of the GS-voltage. The gate length equals  $0.18\mu\text{m}$ ,  $V_{DS}=0.9\text{V}$  and  $V_T=0.51\text{V}$  (extracted by Eldo).

A set of biasing guidelines, to obtain high and robust linearity performance, can be as follows:

1. The transistor model and the parameter sets should be tested by plotting the small-signal parameters and nonlinear coefficients. It is then possible to see how the transistors should be biased to avoid discontinuities and to obtain low and stable nonlinear coefficients.
2. Choose the bias current of each transistor in the circuit such that weakly nonlinear behavior is maintained. This means that the bias currents shall be set well above the signal currents associated with each transistor. This must be satisfied in the whole frequency range of the input signal.
3. Dimensioning each transistor to set the voltage bias point such that the nonlinear coefficients are low and stable in the entire range of the transistor terminal voltages. For transistors in current sources, low GS-overdrive is important to obtain low saturation voltage. For signal transistors, the GS-overdrive has to be large enough to keep the nonlinear coefficients associated with the GS-voltage low. Further, the saturation voltage, and thus the GS-overdrive, must be low enough to achieve low nonlinear coefficients associated with the DS-voltage.
4. For feedback systems, the loop gain will attenuate the distortion. Thus, it is important to increase the transconductances for the amplifying transistors. However, when the drain current remains constant, this results in increased nonlinear coefficients. This is an optimization problem, which can be carried out in a circuit simulator to achieve the optimum biasing for low distortion. The starting point for the optimization is the biasing achieved in point 2 and 3 above.

### 3.2 Opamp Modeling for Nonlinear Analysis

In Chapter 2 the principle of weakly nonlinear circuits was explained to be a criteria for expressing the nonlinear behavior of the circuit by Volterra series and phasor method. In CL opamp circuits the higher order terms of the Volterra series is kept small by applying negative feedback in combination with careful biasing. Additionally, the circuit excitation has to be well below the supply voltage. This results in accurately analysis of the CL opamp circuits using the phasor method, even when the series is truncated to 3<sup>rd</sup> order.

To find the output responses of 1<sup>st</sup> to 3<sup>rd</sup> order of the CL circuit, the phasor method can be applied on the total circuit including the feedback network. This leads to accurate, but very complex equations that provide very little information. Instead, the phasor method can be applied only on the opamp circuit to find the 1<sup>st</sup> to 3<sup>rd</sup> order OL transfer functions. Further, the

OL transfer functions can be used to find the CL responses. By this, it is possible to obtain surveyable equations, which provides valuable insight and understanding of nonlinear behavior. The only degradation in accuracy is the loading effect on the feedback network, caused by the input terminal of the opamp. However, this effect is insignificant at frequencies below the GBW of the opamp. The pole made by the resistive feedback network and the parasitic capacitor at the opamp input terminal has to be well above the GBW of the opamp to obtain safe phase- and gain-margins.

To derive OL transfer functions for the opamp several elements have to be established. First, a general model of the opamp is described, which models the opamp as a two-input device, one for the differential input voltage and the other for the CM input voltage. Especially for the non-inverting opamp configuration, the distortion caused by the input CM-voltage is considerable. Further, it is described how the phasor method can be utilized to split-up the nonlinear transfer functions. By this, simple equations are obtained. Even more important is the insight and understanding of the nature of nonlinear distortion that can be achieved by this split-up. At the end of this section, a folded cascode Miller opamp and its simplified model are described. This opamp is further used as a case for evaluating the inverting and non-inverting opamp configurations in Chapter 4 and for some of the designs in Chapter 5.

When a circuit is in steady state it is possible to use phasor representation of node voltages and branch currents, and the phasor method can be applied. Further, in this chapter and in Chapter 4, all voltages and currents are on phasor form and written in capital letters. The indexes are written in lower case letters to indicate signals where the DC-value is disregarded.

### **3.2.1 The Opamp as a Two-Input Device**

Opamps with single ended output have differential- and CM-signal swings at the input terminals. This is illustrated in Figure 3-8(a), where  $V_e$  and  $V_{cm}$  are the differential and CM voltage swings, respectively. The CM-swing can be damaging for the linearity performance of the opamp, particularly when the swing is large. Especially the non-inverting opamp configuration suffers from large swing in the CM-voltage. Thus, when finding expressions for the harmonic responses it is important to take the effects from the CM-swing into consideration. This is the main reason why the opamp is handled as a two-input device in this work.

Figure 3-8 (b) shows a weakly nonlinear model of the opamp. The input variables to the model are  $V_e$  and  $V_{cm}$ . These voltages are computed from the terminal voltages of the opamp,  $V^+$  and  $V^-$ , as shown in the figure. The output voltage can be expressed as (3-6), when truncating the Volterra series

to 3<sup>rd</sup> order.  $H_1(\cdot)$  is representing the output response at the fundamental frequency, and  $H_2(\cdot)$  and  $H_3(\cdot)$  are the output responses for 2<sup>nd</sup> and 3<sup>rd</sup> harmonics, respectively. These transfer functions are shown in (3-7) to (3-9). In these equations  $H_{n-V_e-m-V_{cm}}(j\omega)$  are the transfer function from the input voltages indicated by the indexes  $V_e$  and  $V_{cm}$ , respectively, to the output of the opamp. The factors  $n$  and  $m$  are integers between 0 and 3, and are the exponents of  $V_e$  and  $V_{cm}$ , respectively. If  $n$  or  $m$  is zero the corresponding input voltage is also zero. The order of the transfer functions is  $n+m$ .  $H_{n-V_e-m-V_{cm}}(j\omega)$  can be found by using the phasor method on the OL opamp. The procedure for doing this is explained in Appendix C, where it is applied on the Miller opamp presented at the end of this chapter.

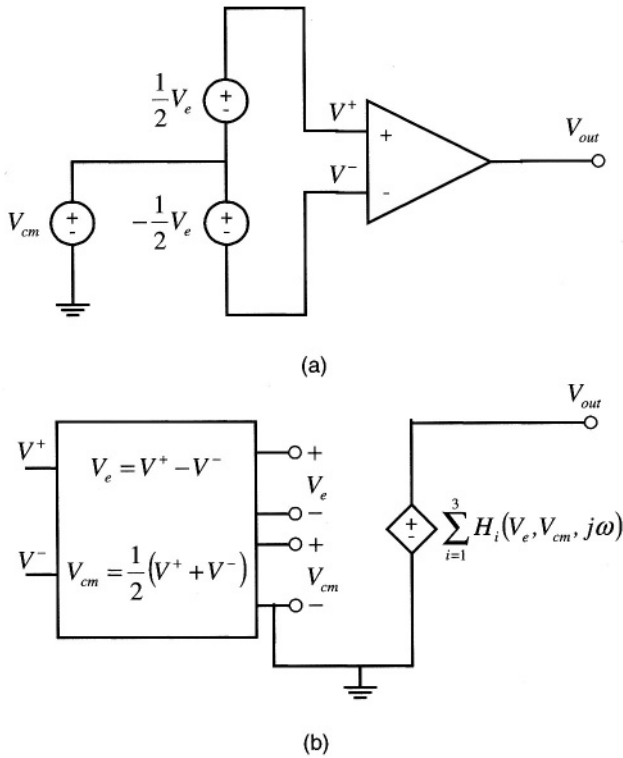


Figure 3-8. The opamp with differential and CM input voltage (a) and the model of the two-input opamp (b), where  $V_e$  and  $V_{cm}$  are the input voltages to the two-input opamp model computed from  $V^+$  and  $V^-$ .

$$V_{out} \approx H_1(V_e, V_{cm}, j\omega) + H_2(V_e, V_{cm}, j\omega) + H_3(V_e, V_{cm}, j\omega) \quad (3-6)$$

$$H_1(V_e, V_{cm}, j\omega) = H_{V_e}(j\omega) \cdot V_e + H_{V_{cm}}(j\omega) \cdot V_{cm} \quad (3-7)$$

$$H_2(V_e, V_{cm}, j\omega) = H_{2V_e}(j\omega) \cdot V_e^2 + H_{V_e \cdot V_{cm}}(j\omega) \cdot V_e \cdot V_{cm} + H_{2V_{cm}}(j\omega) \cdot V_{cm}^2 \quad (3-8)$$

$$H_3(V_e, V_{cm}, j\omega) = H_{3V_e}(j\omega) \cdot V_e^3 + H_{2V_e \cdot V_{cm}}(j\omega) \cdot V_e^2 \cdot V_{cm} + H_{V_e \cdot 2V_{cm}}(j\omega) \cdot V_e \cdot V_{cm}^2 + H_{3V_{cm}}(j\omega) \cdot V_{cm}^3 \quad (3-9)$$

The above equations represent a universal model for the two-input opamp. This model can further be used for various types of opamps connected in various configurations.

### 3.2.2 Splitting of Transfer Functions

In Figure 3-9, an arbitrary nonlinear current source in the opamp is shown with the controlling voltage  $V_c$ . The current source sees a transfer function to the output, and each of the input voltages  $V_e$  and  $V_{cm}$  experience a transfer function to the controlling voltage. The phasor method is explained in section 2.3. Carried out on the two-input opamp, it can in short be explained as follow:

1. 1<sup>st</sup> order: Derive the equation for the output voltage of the opamp (the 1<sup>st</sup> order transfer functions) as a function of the circuit excitations. Further, derive all 1<sup>st</sup> order controlling voltages (i.e. terminal voltages) for nonlinear current sources, as a function of the circuit excitations. The circuit excitations are  $V_e$  and  $V_{cm}$  and the excitation frequency is  $\omega$ .
2. 2<sup>nd</sup> order: Derive the output voltage and all 2<sup>nd</sup> order controlling voltages as a function of the circuit excitation. The circuit excitation is now all nonlinear current sources of 2<sup>nd</sup> order. Subsequently, inserting for the 1<sup>st</sup> order controlling voltages found in 1. Because of the 2<sup>nd</sup> order nonlinearity the excitation frequency is  $2\omega$ .
3. 3<sup>rd</sup> order: The same procedure as for 2<sup>nd</sup> order, but the excitations are all nonlinear current sources of 2<sup>nd</sup> and 3<sup>rd</sup> order. Insertion has to be done for 1<sup>st</sup> and 2<sup>nd</sup> order controlling voltages. The excitation frequency is  $3\omega$ .

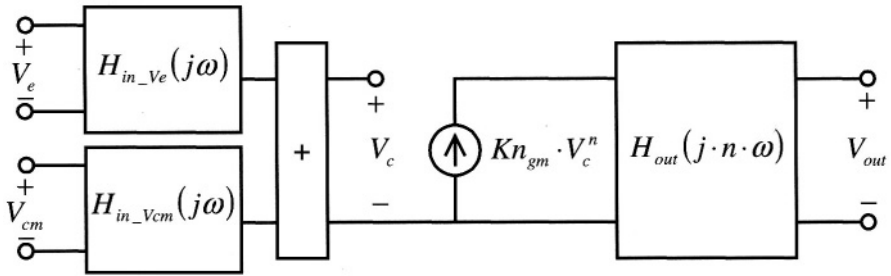


Figure 3-9. An arbitrary nonlinear current source embedded in the opamp.

It is thus possible to split the nonlinear transfer functions in two factors. One factor that represents the transfer function from the nonlinear current source to the output and one factor expressing the transfer functions from  $V_e$  and/or  $V_{cm}$  to the controlling voltage. For a multidimensional current source and for combination of 1<sup>st</sup> and 2<sup>nd</sup> order controlling voltages there are several transfer functions from  $V_e$  and/or  $V_{cm}$  to the nonlinear current source.

Further, if the opamp is viewed as a two-dimensional nonlinear element, with  $H_{n,ve,vm,vcm}(j\omega)$  as the nonlinear “coefficients”, it is possible to obtain the CL nonlinear transfer functions by using the same procedure as above on the opamp with the feedback network included. This is shown in Appendix B, and the obtained CL transfer functions are further used in Chapter 4.

This method makes it possible to split the total transfer function in many different factors. Each of these factors is easy to simplify and analyze. It also gives valuable insight in the cause and behavior of distortion. Further, the method makes it possible to isolate poles and zeros and find which design parameters that improve the linearity performance of the circuit. This technique is used to obtain simplified nonlinear CL transfer functions for non-inverting and inverting opamp configurations, which is described in section 4.1 and 4.2, respectively.

### 3.2.3 Case: Miller Opamp

A folded cascode Miller opamp [8] is shown in Figure 3-10. This opamp is chosen as an opamp case for further use in Chapter 4 and Chapter 5. The input differential pair is implemented by M1 and M2, and M3 is the tail current source. M6 to M13 make the folded cascode and the output stage is made by a common source transistor M4 with M5 as the output current source. The Miller capacitance  $C_c$  is connected between the output and the source of M1. The zero in the right half plane is moved to high frequencies and the stability problems caused by the zero is omitted. The bias currents are chosen such that the drain current of each transistor is well above the

signal current. As described in section 3.1.4, this ensures weakly nonlinear behavior of the circuit even at high frequencies.

The small-signal equivalent of the opamp is shown in Figure 3-11. The folded cascode is replaced with a linear resistor equal to the resistance seen into the drains of M9 and M11. This simplification was necessary to avoid high complexity in the expressions for  $H_{n-vc\_m-vc}(j\omega)$ . The main contributions to distortion are expected to come from the transistors that are exposed for the highest signal swing. Since the folded cascode does not have large voltage swing at any of its nodes, the estimated distortion will still be relatively accurate. The effect of the approximation will be visualized in Chapter 5 where the simulation results obtained with Maple and Eldo will be compared.

The transfer functions given in (3-7) to (3-9) will be found using the small-signal model in Figure 3-11. The procedure used is explained in Appendix C, where it is carried out to obtain the transfer functions of 1<sup>st</sup> order. Because of the large complexity the higher order transfer functions are carried out in Maple and not shown in Appendix C. The derivation of the nonlinear transfer functions of the opamp is similar to the derivation for the LP-filter carried out in section 2.3.1.

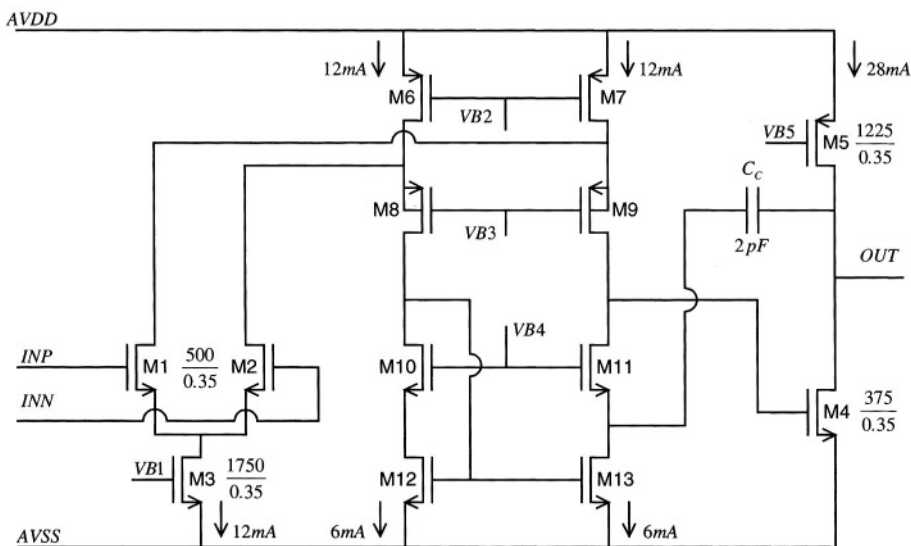


Figure 3-10. Two-stage cascoded Miller opamp.

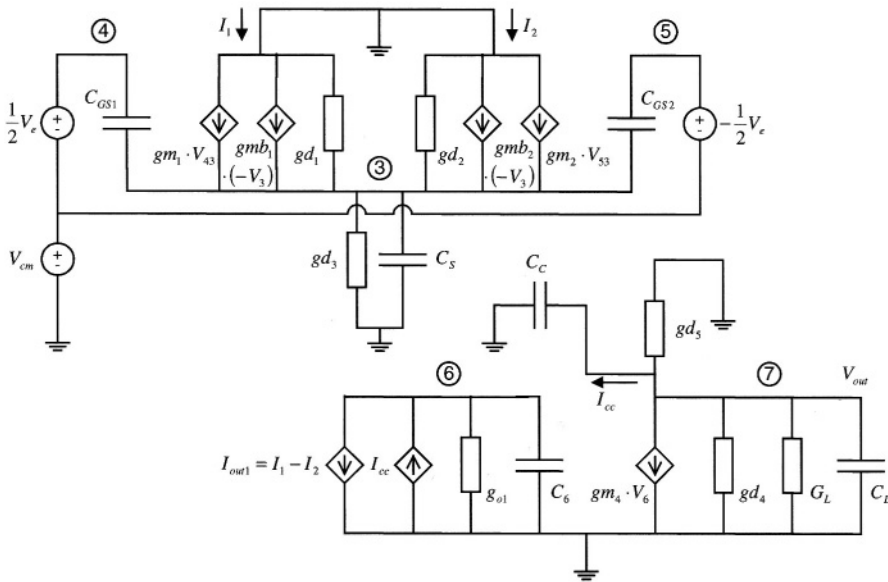


Figure 3-11. Small-signal model of the opamp for use in linear and nonlinear analysis.

Further in this book, small-signal parameters and nonlinear coefficients will have indexes according to the number of the belonging transistor. However, M1 and M2 are designed to be equal. Thus, these transistors are represented with the same small-signal parameters and nonlinear coefficients, which are without integer indexes. Differences between M1 and M2 are expressed by using a mismatch factor for each of the transistor parameters.

Simplified expressions of the first order transfer functions, disregarding poles and zeroes at high frequency, are quoted in (3-10) and (3-11). Here,  $D$  is given by (3-12), where  $d_{gm}$ ,  $d_{gmb}$  and  $d_{gd}$  are the mismatch in the small-signal parameters of M1 and M2.  $A_1$ ,  $A_2$ , poles and zeroes are given in (3-13) to (3-16) and the GBW of the opamp is given in (3-17). More accurate versions of the 1<sup>st</sup> order transfer functions are shown in Appendix C.

In the sections 4.1 and 4.2 numerical simulations of the CL responses will be carried out to find the main contributions to nonlinear distortion. The simulations are done in Maple. Thus, it is necessary to extract small-signal parameters and nonlinear coefficients for the transistors M1 to M5 of the opamp. The extractions are done individually for each transistor at their bias points, which are chosen according to the bias recommendations in section 3.1. This is carried out with Eldo and Philips MM9 MOS model with parameters from the same 0.35 $\mu$ m process that is used in section 3.1. The extracted values are given in Table 3-1 (p. 50), where all small-signal

parameters (named 1<sup>st</sup> order) are according to Figure 3-11. The capacitances due to the DB-diffusions to M4 and M5 are included in  $C_L$ , and all diffusion capacitances in the common source node of M1 and M2 are included in  $C_S$ .

Mismatch between M1 and M2 are only considered for  $gm$  and is denoted  $d_{gm}$ . In Table 3-1 the  $5\cdot\sigma$ -value for  $d_{gm}$  is given, derived from the mismatch data for the fabrication technology and the sizes of the transistors. For the rest of the small-signal parameters and nonlinear coefficients of M1 and M2, the mismatch is assumed to be zero unless stated otherwise. For the CM-gain, this can be considered as worst case. Equation (3-12) shows that setting  $d_{gmb}$  and  $d_{gd}$  to zero gives the highest  $D$  and thus the highest CM-gain, assuming that non-zero  $d_{gmb}$  and  $d_{gd}$  leads to attenuation in (3-12). Additionally, the distortion is expected to be larger when the mismatches in the nonlinear coefficients are included.

The opamp in Figure 3-10 is only used as a test case for exploring the inverting and non-inverting opamp configurations in Chapter 4. Thus, the circuit is not optimized for low distortion in a circuit simulator. However, the test case represent a realistic behavior of distortion and the contributions to nonlinearity is mainly the same as the fabricated opamps presented in Chapter 5. Table 3-2 (p. 51) shows some characteristic parameters for the test opamp, obtained with the equations below.

$$H_{ve}(j\omega) \approx \frac{A_1 \cdot A_2}{\left(1 + j \frac{\omega}{\omega_1}\right)} \quad (3-10)$$

$$H_{vcm}(j\omega) \approx \frac{-D \cdot A_1 \cdot A_2}{gd_3 + 2gm + 2gd + 2gmb} \cdot \frac{\left(1 + j \frac{\omega}{\omega_{z,cm}}\right)}{\left(1 + j \frac{\omega}{\omega_1}\right)} \quad (3-11)$$

$$D = 2 \cdot gmb \cdot (d_{gm} - d_{gmb}) + 2 \cdot gd \cdot (d_{gm} - d_{gd}) + gd_3 \cdot d_{gm} \quad (3-12)$$

$$A_1 = \frac{gm}{g_{o1}} \quad (3-13)$$

$$A_2 = \frac{gm_4}{gd_4 + gd_5 + G_L} \quad (3-14)$$

$$\omega_1 = \frac{g_{o1} \cdot (gd_4 + gd_5 + G_L)}{C_6 G_L + C_C gm_4} \quad (3-15)$$

$$\omega_{z,cm} = \frac{gd_3}{C_S - 2 \cdot \left( \frac{gd + gmb}{gm} \right) \cdot C_{GS}} \quad (3-16)$$

$$\omega_{GBW} = \frac{gm \cdot gm_4}{C_6 G_L + C_C gm_4} \quad (3-17)$$

M1 and M2 (W/L=500/0.35 (μm))					
1 <sup>st</sup> order		2 <sup>nd</sup> order		3 <sup>rd</sup> order	
$g_m$	49.5mS	$K2_{gm}$	100m	$K3_{gm}$	-70.0m
$g_d$	1.5mS	$K2_{gd}$	0.100m	$K3_{gd}$	20.0μ
$g_{mb}$	6.5mS	$K2_{gmb}$	2.70m	$K3_{gmb}$	0.350m
$C_{GS}$	0.60pF	$K2_{gm\_gd}$	6.00m	$K3_{2gm\_gd}$	-60.0m
$d_{gm}$	2%	$K2_{gmb\_gm}$	26.0m	$K3_{gm\_2gd}$	-0.220m
		$K2_{gmb\_gd}$	0.330m	$K3_{2gmb\_gm}$	0.800m
				$K3_{gmb\_2gm}$	-25.0m
				$K3_{2gmb\_gd}$	-0.270m
				$K3_{gmb\_2gd}$	-0.100m
				$K3_{gm\_gmb\_gd}$	-2.50m
M3 (W/L=1750/0.35 (μm))					
1 <sup>st</sup> order		2 <sup>nd</sup> order		3 <sup>rd</sup> order	
$gd_3$	2.7mS	$K2_{gd3}$	0.160m	$K3_{gd3}$	2.00m
$C_S$	2.4pF	$K2_{CS}$	220f	$K3_{CS}$	60.0f
M4 (W/L=375/0.35 (μm))					
1 <sup>st</sup> order		2 <sup>nd</sup> order		3 <sup>rd</sup> order	
$gm_4$	49.1mS	$K2_{gm4}$	17.5m	$K3_{gm4}$	-1.60m
$gd_4$	1.2mS	$K2_{gd4}$	-0.200m	$K3_{gd4}$	0.400m
		$K2_{gm\_gd4}$	1.30m	$K3_{2gm\_gd4}$	-1.00m
		$K2_{CDB4}$	-19.0f	$K3_{gm\_2gd4}$	-0.300m
				$K3_{CDB4}$	3.00f
M5 (W/L=1225/0.35 (μm))					
1 <sup>st</sup> order		2 <sup>nd</sup> order		3 <sup>rd</sup> order	
$gd_5$	1.80mS	$K2_{gd5}$	0.600m	$K3_{gd5}$	0.800m
		$K2_{CDB5}$	80.0f	$K3_{CDB5}$	15.0f
Other parameters					
$g_{o1}$	1/10kΩ	$C_6$	0.70pF	$R_L$	200Ω
$C_L$	4pF	$C_C$	2.0pF		

Table 3-1. Extracted parameters obtained from the transistor model MM9 for a 0.35μm fabrication technology for the opamp in Figure 3-10. The parameters will be used in simulations of nonlinear distortion in Maple, carried out in Chapter 4.

Case: 3.3V CMOS Opamp $AV_{DD}=3.3V$ , $V_{CM}=1.65V$ (input CM-voltage)		
Parameter	Values (typ.)	Unit
$A_0$ DC OL-Gain	69.7	dB
$A_1$ DC-gain in 1 <sup>st</sup> stage	495	V/V
$A_2$ DC-gain in 2 <sup>nd</sup> stage	6.1	V/V
$f_1$ Dominant pole	1.25	MHz
GBW	3.8	GHz

Table 3-2. Parameters for the opamp in Figure 3-10 obtained from the small-signal parameters in Table 3-1 and the equations for the opamp.

## REFERENCES

- [1] P. Wambacq, W. Sansen, "Distortion Analysis of Analog Integrated Circuits," Norwell, MA: Kluwer Academic Publishers, 1998.
- [2] P. Wambacq, G. G. E. Gielen, P. R. Kinget, W. Sansen, "High-Frequency Distortion Analysis of Analog Integrated Circuits," *IEEE Tr. on Circuits and Systems—II: Analog and Digital Signal Processing*, vol. 46, no. 3, pp. 335-345, Mar. 1999.
- [3] Eldo, See <http://www.mentorg.com/eldo/overview.html>
- [4] Philips MOS Model 9, MM9, See [http://www.semiconductors.philips.com/Philips\\_Models/introduction/mosmodel9/](http://www.semiconductors.philips.com/Philips_Models/introduction/mosmodel9/)
- [5] D. Foty, Tutorial: "A Circuit Designers's Guide to MOS Modeling," *IEEE International Symposium on Circuits and Systems 2001*, Geneva, Switherland, May 2001.
- [6] D. Foty, "MOSFET Modeling with SPICE: Principles and Practice," Prentice Hall, 1997.
- [7] Y. Cheng, M. Chan, K. Hui, M. Jeng, Z. Liu, J. Huang, K. Chen, J. Chen, R. Tu, P. K. To, C. Hu, "BSIM3v3 Manual (final version)," Dep. of Electrical Engineering and Computer Sciences, University of California, Berkeley, 1995.
- [8] R. Hogervorst, J. H. Huijsing, "Design of Low-Voltage, Low-Power Operational Amplifier Cells," Norwell, MA: Kluwer Academic Publishers, 1996.

*This page intentionally left blank*

## Chapter 4

### **Nonlinear Analyses of Feedback Miller Opamp**

Nonlinear analysis of feedback systems is reported in several scientific papers. In [1] and [2] Volterra series is used to find the nonlinear CL expressions as a function of the 1<sup>st</sup> to 3<sup>rd</sup> orders OL kernels of the one-input amplifier. In [3] the effect that Miller compensation has on linearity performance is investigated and in [1] and [4] the most important nonlinear coefficients of *HD2* is plotted for a two-stage Miller opamp connected in inverting configuration. The obtained results are similar to the results obtained in section 4.2 below. In [5] a comparison regarding linearity performance between the inverting and non-inverting opamp configuration is carried out. The measurements show large degradation at low frequencies when the opamp is connected in the non-inverting configuration.

In this chapter, the non-inverting and inverting opamp configurations are analyzed using the phasor method, considering the opamp as a two-input device. The 1<sup>st</sup> to 3<sup>rd</sup> order CL responses will be presented as a function of the OL transfer functions of the opamp, given in (3-7) to (3-9) (p. 44). By this, it is possible to see what influence the feedback has on linearity performance. As a case, the opamp presented in section 3.2.3 is used. For this opamp, simplified equations for distortion as a function of frequency are shown. This is done first for the opamp connected in non-inverting configuration and further in inverting configuration. These equations include the strongest nonlinear sources to distortion. The feedback network is assumed linear, which is a good approximation while using highly linear resistors. Further, design criteria for low distortion in feedback opamp circuits are given. The thoroughly analysis done in this chapter is a further evolution of the work presented in [1], [4] and [5] regarding feedback opamp circuits.

## 4.1 The Non-Inverting Configuration

In Figure 4-1 the non-inverting opamp configuration is shown. The closed loop responses for 1<sup>st</sup>, 2<sup>nd</sup> and 3<sup>rd</sup> order are given in (4-1) to (4-3), respectively. Derivations of these are done in Appendix B. The OL transfer functions of the opamp,  $H_{n-ve\_m-vcn}(j\omega)$ , are explained in section 3.2.1.  $H_{3\_2}(\cdot)$  is the transfer function because of mixing of the 2<sup>nd</sup> harmonic and the input frequency in the 2<sup>nd</sup> order nonlinear transfer functions of the opamp. The 2<sup>nd</sup> harmonic is fed from the output terminal to the inputs of the opamp through the feedback network. The input variables to  $H_{3\_2}(\cdot)$ ,  $V_{e\_1}$ ,  $V_{e\_2}$ ,  $V_{cm\_1}$  and  $V_{cm\_2}$  are the differential and CM input voltages of 1<sup>st</sup> and 2<sup>nd</sup> order. Further,  $\beta$  is the feedback factor.

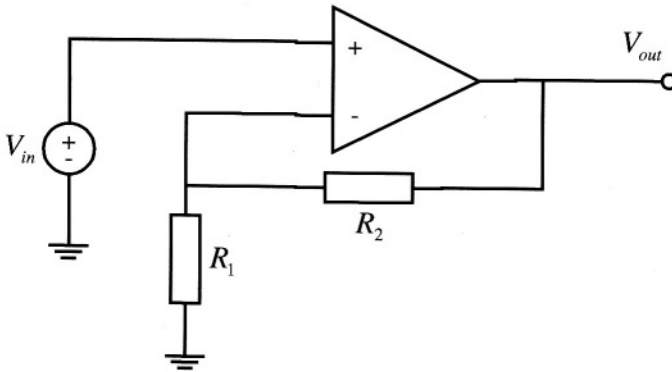


Figure 4-1. Non-inverting opamp configuration.

$$\begin{aligned}
 V_{out\_1} &= \frac{H_{ve}(j\omega) + \frac{1}{2}H_{vcn}(j\omega)}{1 + \beta \cdot \left( H_{ve}(j\omega) - \frac{1}{2}H_{vcn}(j\omega) \right)} \cdot V_{in} \\
 &\approx \frac{H_{ve}(j\omega)}{1 + \beta \cdot H_{ve}(j\omega)} \cdot V_{in} \approx \frac{1}{\beta} \cdot V_{in} = \left( 1 + \frac{R_2}{R_1} \right) \cdot V_{in}
 \end{aligned} \tag{4-1}$$

$$V_{out\_2} \approx \frac{1}{1 + \beta \cdot H_{ve}(j2\omega)} \cdot \left\{ \begin{array}{l} \frac{[1 - \beta \cdot H_{vcm}(j\omega)]^2}{[1 + \beta \cdot H_{ve}(j\omega)]^2} \cdot H_{2ve}(j\omega) + \\ \frac{1 - \beta \cdot H_{vcm}(j\omega)}{1 + \beta \cdot H_{ve}(j\omega)} \cdot H_{ve\_vcm}(j\omega) + \\ H_{2vcm}(j\omega) \end{array} \right\} \cdot V_{in}^2 \quad (4-2)$$

$$V_{out\_3} \approx \frac{1}{1 + \beta \cdot H_{ve}(j3\omega)} \cdot \left\{ \begin{array}{l} \frac{[1 - \beta \cdot H_{vcm}(j\omega)]^3}{[1 + \beta \cdot H_{ve}(j\omega)]^3} \cdot H_{3ve}(j\omega) + \\ \frac{[1 - \beta \cdot H_{vcm}(j\omega)]^2}{[1 + \beta \cdot H_{ve}(j\omega)]^2} \cdot H_{2ve\_vcm}(j\omega) + \\ \frac{1 - \beta \cdot H_{vcm}(j\omega)}{1 + \beta \cdot H_{ve}(j\omega)} \cdot H_{ve\_2vcm}(j\omega) + \\ H_{3vcm}(j\omega) + H_{3\_2} \left( \begin{array}{l} V_{e\_1}, V_{e\_2}, V_{cm\_1}, \\ V_{cm\_2}, j\omega, j2\omega \end{array} \right) \end{array} \right\} \cdot V_{in}^3 \quad (4-3)$$

The main drawback of the non-inverting configuration regarding nonlinearity is the large CM voltage swing at the input terminals of the opamp. This is reflected in the 2<sup>nd</sup> and 3<sup>rd</sup> order responses given by (4-2) and (4-3). The equations show that the OL transfer functions of the opamp that have  $m > n$  (in  $H_{n,ve,m,vcm}(j\omega)$ ), are less suppressed by the loop gain,  $\beta \cdot H_{ve}(j\omega)$ , than the transfer functions which have  $m < n$ . For instance, in (4-2)  $H_{2ve}(j\omega)$  is suppressed by the cubic loop gain while  $H_{2vcm}(j\omega)$  is only suppressed by the loop gain.

As will be shown further in this section, it is important that the CM-gain is low to obtain low distortion. The CM-gain is expressed by  $H_{vcm}(j\omega)$  given by (3-11) (p. 48). There are two reasons for keeping the CM-gain low. First, the term  $|\beta \cdot H_{vcm}(j\omega)|$  in (4-2) and (4-3) should be smaller than 1 to not increase the distortion. Further, high CM-gain causes the output transistors

to experience large voltage swing due to the CM-voltage. Thus, the distortion from the output transistors becomes dominant. Both these effects occur at low frequencies. At frequencies above the dominant pole of the opamp  $H_{vcm}(j\omega)$  rolls off and the problem disappears.

In the next subsections, the nonlinear transfer functions that have the strongest contributions to 2<sup>nd</sup> and 3<sup>rd</sup> harmonics will be found. For each of these, the major nonlinear coefficients will be detected by plotting. Further, it will be shown approximate equations for the strongest transfer functions including the major nonlinear coefficients.

The effect from the CM-gain will also be visualized. The CL nonlinear transfer functions will be plotted for both high and low CM-gain. To do this it is necessary to describe how high and low CM-gain is achieved. The CM-gain is proportional to  $D$  given by (3-12) and quoted in (4-4). The high CM-gain is obtained by setting  $d_{gmb} = d_{gd} = 0$ .  $D_{high}$  is expressed in (4-5). Low CM-gain occur when setting  $d_{gmb} = d_{gd} = d_{gm}$  and reduce  $gd_3$  to 1/5 of the value given in Table 3-1 (p. 50).  $D_{low}$  is given by (4-6). The reduction of  $gd_3$  can be achieved by e.g. a tail current compensation circuit, which is described in [6]. Thus, at low frequencies  $H_{vcm}(j\omega)$  becomes 20dB (high) and -6dB (low) when the parameters are set according to Table 3-1.

$$D = 2 \cdot gmb \cdot (d_{gm} - d_{gmb}) + 2 \cdot gd \cdot (d_{gm} - d_{gd}) + gd_3 \cdot d_{gm} \quad (4-4)$$

$$D_{high} = (2 \cdot gmb + 2 \cdot gd + gd_3) \cdot d_{gm} \quad (4-5)$$

$$D_{low} = gd_3 \cdot d_{gm} \quad (4-6)$$

All considerations and plots in this section are done with the CL-gain equal to 1, which means that the opamp is connected in unity gain configuration. This gives the highest input CM-swing and results in worst case regarding nonlinear distortion. The input voltage is  $1V_{peak}$ , and the circuit parameters are shown in Table 3-1 (p. 50). The mismatch in the differential pair is only considered through mismatch in the small-signal parameters  $gm$ ,  $gmb$  and  $gd$ , as explained above. All nonlinear coefficients because of M1 and M2 are assumed equal for the two transistors.

### 4.1.1 Contributions to 2<sup>nd</sup> Harmonic

Equation (4-2) can be expressed as (4-7) where the terms are given in (4-8) to (4-10).

$$V_{out\_2} = [H_{2V_{e\_CL}}(j\omega) + H_{V_{e\_V_{cm\_CL}}}(j\omega) + H_{2V_{cm\_CL}}(j\omega)] \cdot V_{in}^2 \quad (4-7)$$

$$H_{2V_{e\_CL}}(j\omega) \approx \frac{[1 - \beta \cdot H_{V_{cm}}(j\omega)]^2 \cdot H_{2V_{e}}(j\omega)}{[1 + \beta \cdot H_{V_{e}}(j2\omega)] \cdot [1 + \beta \cdot H_{V_{e}}(j\omega)]^2} \quad (4-8)$$

$$H_{V_{e\_V_{cm\_CL}}}(j\omega) \approx \frac{[1 - \beta \cdot H_{V_{cm}}(j\omega)] \cdot H_{V_{e\_V_{cm}}}(j\omega)}{[1 + \beta \cdot H_{V_{e}}(j2\omega)] \cdot [1 + \beta \cdot H_{V_{e}}(j\omega)]} \quad (4-9)$$

$$H_{2V_{cm\_CL}}(j\omega) \approx \frac{H_{2V_{cm}}(j\omega)}{[1 + \beta \cdot H_{V_{e}}(j2\omega)]} \quad (4-10)$$

In Figure 4-2 the accurate versions of (4-7) (labeled “H\_2\_all\_CL”) to (4-10) are plotted with high CM-gain. The plot shows that at frequencies below 10MHz, all transfer functions are large and have approximately the same contribution to the total distortion. Because of different signs, the sum of the transfer functions is lower than each of them. The reason for the large 2<sup>nd</sup> order transfer functions at low frequency is the high CM-gain. For  $H_{2V_{e\_CL}}(j\omega)$  in (4-8), the term  $(1 - \beta \cdot H_{V_{cm}}(j\omega))^2$  is the cause for the increased contribution. For  $H_{V_{e\_V_{cm\_CL}}}(j\omega)$  in (4-9), the  $(1 - \beta \cdot H_{V_{cm}}(j\omega))$ -term does some of the contribution. Additionally, because of large CM-gain, the output transistors experience large voltages and thus contribute more than the input transistors. This is also the reason why  $H_{2V_{cm\_CL}}(j\omega)$  in (4-10) are large at low frequencies. All these transfer functions rolls off when  $H_{V_{cm}}(j\omega)$  rolls off, which is at the dominant pole of the opamp. Thus, above 10MHz the input transistors have the strongest contributions to  $H_{V_{e\_V_{cm\_CL}}}(j\omega)$  and  $H_{2V_{cm\_CL}}(j\omega)$ .

Figure 4-3 shows the same transfer functions as Figure 4-2, but with low CM-gain. Here, the CL transfer functions that depend most on the CM-voltage are the largest contributions to distortion. At low frequencies, the dominant transfer function is  $H_{2V_{cm\_CL}}(j\omega)$ . Further, the overall 2<sup>nd</sup> order response is lower than when the CM-gain is large. Thus, it is important to

keep the CM-gain low to obtain small 2<sup>nd</sup> harmonic at frequencies below the dominant pole of the opamp.

At frequencies above 10MHz  $H_{V_{e\_vcm\_CL}}(j\omega)$  is the strongest contribution to 2<sup>nd</sup> harmonic regardless of the CM-gain. In the next subsection it will be shown symbolic expression for  $H_{V_{e\_vcm\_CL}}(j\omega)$ . This expression takes into consideration the major nonlinear coefficients. Since  $H_{V_{e\_vcm\_CL}}(j\omega)$  is independent of mismatch in the nonlinear coefficients, the expression will be accurate even without a mismatch model for the nonlinear coefficients of M1 and M2.

#### 4.1.1.1 $H_{V_{e\_vcm\_CL}}(j\omega)$

The curves labeled “all” in Figure 4-4 and Figure 4-5 show  $H_{V_{e\_vcm\_CL}}(j\omega)$  including all 2<sup>nd</sup> order nonlinear coefficients of the transistors M1 to M5 in the opamp. When all of the nonlinear coefficients are set to zero except for  $K2_{gm}$ , the curves denoted “K2\_gm” is obtained. The same is done for  $K2_{gmb\_gm}$  and  $K2_{gm\_gd}$ . The curve “M4 and M5” is the contributions from all 2<sup>nd</sup> order nonlinear coefficients of M4 and M5. The sum of the contributions above is plotted in the curve called “K2\_gm, K2\_gmb\_gm, K2\_gm\_gd, M4, M5”. This last curve shows close fitting to the “all”-curve in both figures. Thus, the main contributions to  $H_{V_{e\_vcm\_CL}}(j\omega)$  are covered in these plots.

Figure 4-4 shows  $H_{V_{e\_vcm\_CL}}(j\omega)$  when the CM-gain is high. At low frequencies, the transfer function is high due to the nonlinear coefficients of the output transistors, M4 and M5. These contributions rolls off with the CM-gain and above 10MHz  $H_{V_{e\_vcm\_CL}}(j\omega)$  is decided by the input transistors only. In Figure 4-5, the CM-gain is low and the output transistors contribute at a level that is 50dB lower than in Figure 4-4. This shows that much can be earned by keeping the CM-gain low.

Figure 4-5 shows that the strongest contributions above 10MHz are (in declining order)  $K2_{gm}$ ,  $K2_{gm\_gd}$  and  $K2_{gmb\_gm}$ . Because of canceling effects between the contributions,  $H_{V_{e\_vcm\_CL}}(j\omega)$  are smaller than each of them. This canceling effect is also shown by the expression for  $H_{V_{e\_vcm\_CL}}(j\omega)$ , which is given in (4-11). This equation is obtained using the technique for splitting of transfer functions described in section 3.2.2.  $\omega_1$  is the dominant pole of the opamp,  $A_1$  and  $A_2$  are the gain of input stage and output stage, all given in section 3.2.3. Poles and zeros located at high frequencies are disregarded. Because of different signs of the terms in (4-11), canceling occur between  $K2_{gm}$  and the sum of  $K2_{gm\_gd}$  and  $K2_{gmb\_gm}$ . This effect can be reliable since all nonlinear coefficients are due to the same transistor. However, because of poor modeling of higher order derivatives of the transistor current, it can be difficult to utilize this effect in the design phase.

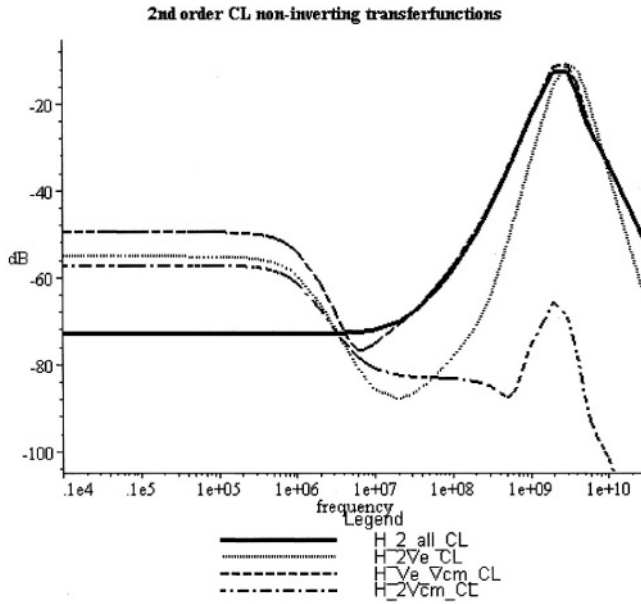


Figure 4-2. 2<sup>nd</sup> order responses with high CM-gain.

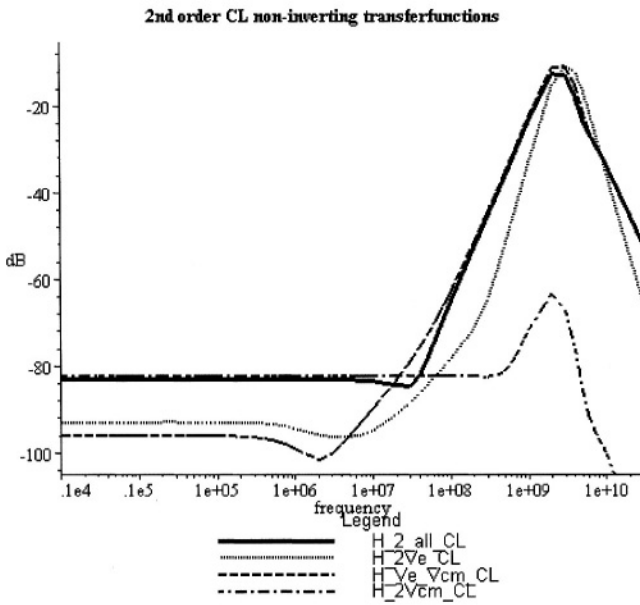


Figure 4-3. 2<sup>nd</sup> order responses with low CM-gain.

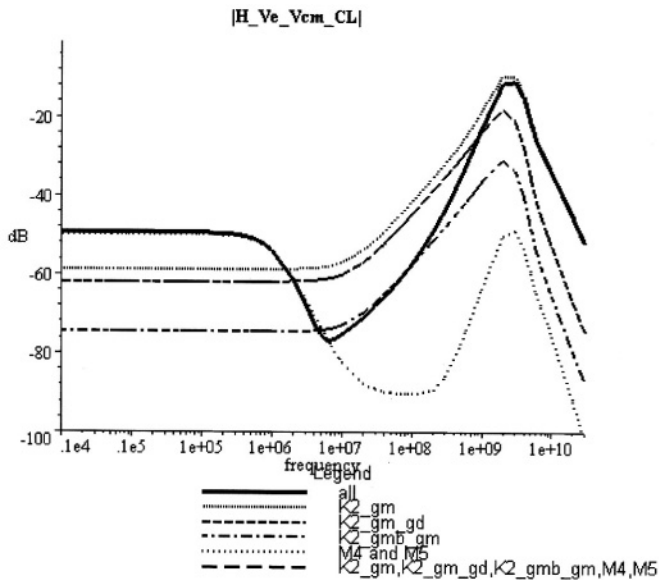


Figure 4-4. High CM-gain, the main contributing nonlinear coefficients to  $H_{Ve\_Vcm\_CL}(j\omega)$ .

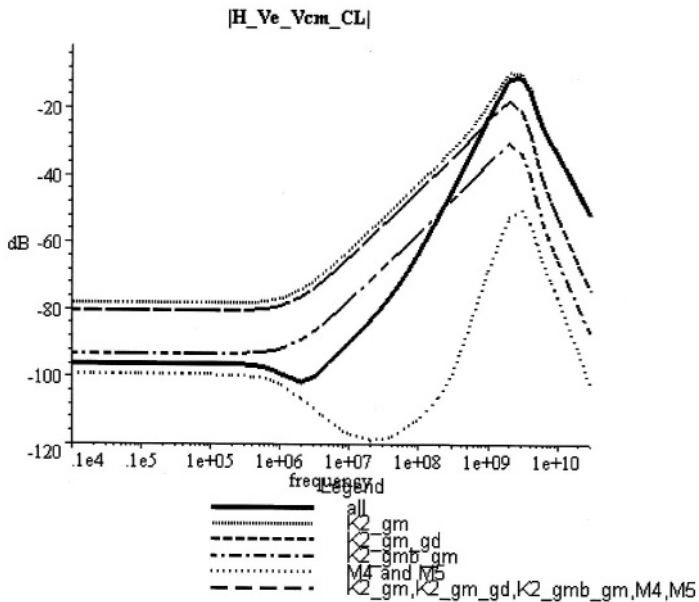


Figure 4-5. Low CM-gain, the main contributing nonlinear coefficients to  $H_{Ve\_Vcm\_CL}(j\omega)$ .

The canceling effect is also the reason for the larger inclination in the “all”-curve above approximately 50MHz compared to its contributions. Because of poles and zeros at high frequencies, the contribution from  $K2_{gm}$  starts to increase at 50MHz. This results in poorer canceling between nonlinear coefficients and the total 2<sup>nd</sup> order distortion increase. This is not included in (4-11) because poles and zeros at high frequencies are disregarded.

Equation (4-11) shows that the contributions from the nonlinear coefficients increase with 20dB/dec above the zero located at the dominant pole of the opamp  $\omega_l$ . This can also be seen in Figure 4-5. Further, for frequencies above  $\omega_l$ ,  $H_{vcm}(j\omega)$  will roll of and (4-11) can be expressed as (4-12). (4-12) shows that it is possible to lower the asymptote of  $H_{ve\_vcm\_cl}(j\omega)$ , and thus lower 2<sup>nd</sup> harmonic in this frequency range, by increasing the GBW of the opamp. The maximum GBW is limited by the stability criteria for the opamp. It can be shown that all contributions from the input stage that depends on the input differential voltage,  $V_e$ , have the same dependence of GBW. Thus, this is a secure way to lower the distortion caused by the input stage.

In Figure 4-6, equation (4-11) and the accurate version of  $H_{ve\_vcm\_cl}(j\omega)$  are plotted, denoted “H\_Ve\_Vcm\_CL\_apr” and “H\_Ve\_Vcm\_CL”, respectively. Since (4-11) does not include the contributions from the output transistors, there is some deviation at low frequencies. Further, at high frequencies, the gap between the curves is caused of high frequency poles and zeroes not included in (4-11).

$$H_{ve\_vcm\_cl}(j\omega) \stackrel{\omega \ll \omega_{GBW}}{\approx} \left( \begin{array}{c} K2_{gm} \frac{2gd + gd_3 + 2gmb}{gm} \\ -K2_{gmb\_gm} - K2_{gm\_gd} \end{array} \right) \cdot \frac{(1 - \beta \cdot H_{vcm}(j\omega)) \cdot \left( 1 + j \frac{\omega}{\omega_l} \right)}{\beta^2 \cdot A_1 \cdot A_2 \cdot (gd_3 + 2gd + 2gmb + 2gm)} \quad (4-11)$$

$$H_{ve\_vcm\_cl}(j\omega) \stackrel{\omega_l < \omega \ll \omega_{GBW}}{\approx} \left( \begin{array}{c} K2_{gm} \frac{gd_3 + 2gd + 2gmb}{gm} - K2_{gmb\_gm} - K2_{gm\_gd} \end{array} \right) \cdot \frac{j\omega}{\beta^2 (gd_3 + 2gd + 2gmb + 2gm) \omega_{GBW}} \quad (4-12)$$

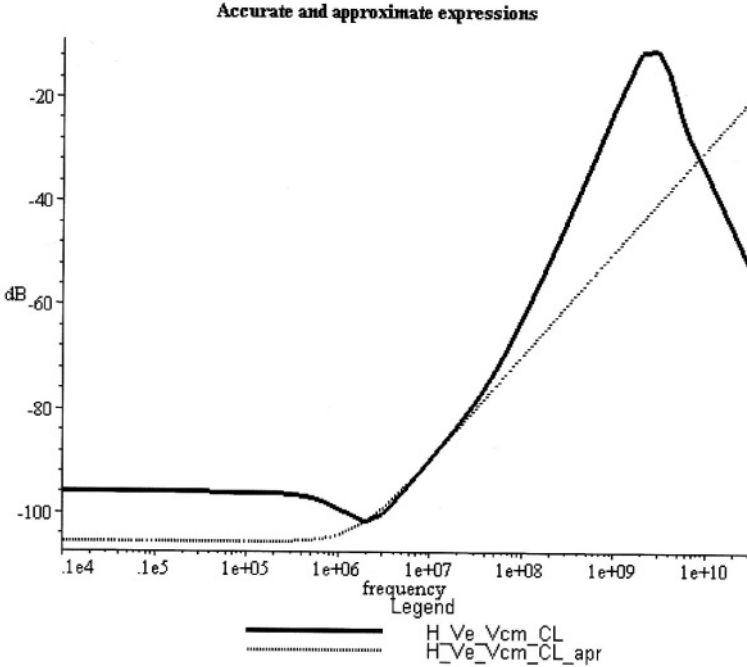


Figure 4-6. “H\_Ve\_Vcm\_CL” and “H\_Ve\_Vcm\_CL\_apr” are the accurate and approximated version (given by (4-11)) of  $H_{Ve\_Vcm\_CL}(j\omega)$ , respectively. The plot is obtained using low CM-gain.

#### 4.1.2 Contributions to 3<sup>rd</sup> Harmonic

The 3<sup>rd</sup> harmonic for the non-inverting opamp configuration is expressed in (4-3), and can be written as (4-13). The terms are shown in (4-14) to (4-18). The equations are similar to the 2<sup>nd</sup> order transfer functions and the effects are also expected to be the same.

$$V_{out\_3} = \begin{bmatrix} H_{3Ve\_CL}(j\omega) + H_{2Ve\_Vcm\_CL}(j\omega) \\ + H_{Ve\_2Vcm\_CL}(j\omega) \\ + H_{3Vcm\_CL}(j\omega) + H_{3\_2\_CL}(j\omega) \end{bmatrix} \cdot V_{in}^3 \quad (4-13)$$

$$H_{3Ve\_CL}(j\omega) \approx \frac{[1 - \beta \cdot H_{Vcm}(j\omega)]^3 \cdot H_{3Ve}(j\omega)}{[1 + \beta \cdot H_{Ve}(j3\omega)] \cdot [1 + \beta \cdot H_{Ve}(j\omega)]^3} \quad (4-14)$$

$$H_{2V_e\_V_{cm\_CL}}(j\omega) \approx \frac{[1 - \beta \cdot H_{V_{cm}}(j\omega)]^2 \cdot H_{2V_e\_V_{cm}}(j\omega)}{[1 + \beta \cdot H_{V_e}(j3\omega)] \cdot [1 + \beta \cdot H_{V_e}(j\omega)]^2} \quad (4-15)$$

$$H_{V_e\_2V_{cm\_CL}}(j\omega) \approx \frac{[1 - \beta \cdot H_{V_{cm}}(j\omega)] \cdot H_{V_e\_2V_{cm}}(j\omega)}{[1 + \beta \cdot H_{V_e}(j3\omega)] \cdot [1 + \beta \cdot H_{V_e}(j\omega)]} \quad (4-16)$$

$$H_{3V_{cm\_CL}}(j\omega) \approx \frac{H_{3V_{cm}}(j\omega)}{[1 + \beta \cdot H_{V_e}(j3\omega)]} \quad (4-17)$$

$$H_{3\_2\_CL}(j\omega) \approx \frac{H_{3\_2}(V_{e\_1}, V_{e\_2}, V_{cm\_1}, V_{cm\_2}, j\omega, j2\omega)}{[1 + \beta \cdot H_{V_e}(j3\omega)]} \quad (4-18)$$

Figure 4-7 and Figure 4-8 show the plots of the accurate versions of (4-13) to (4-18), using high and low CM-gain, respectively. The plots visualize the same effects as for the 2<sup>nd</sup> order transfer functions. For high CM-gain and low frequencies the nonlinear transfer functions are large and roll off above the dominant pole of the opamp. The total 3<sup>rd</sup> order response (denoted “H\_3\_all\_CL”) are also affected of this, in contrast to the 2<sup>nd</sup> order response. Thus, at low frequency and high CM-gain the 3<sup>rd</sup> harmonic will be unacceptably high.

For low CM-gain, the CL nonlinear transfer functions that have the strongest dependence on the CM-voltage, contribute most to 3<sup>rd</sup> harmonic. For low frequencies  $H_{3V_{cm\_CL}}(j\omega)$  are largest and  $H_{V_e\_2V_{cm\_CL}}(j\omega)$  takes over above approximately 1MHz. Next, the strongest contributions to  $H_{V_e\_2V_{cm\_CL}}(j\omega)$  will be found and a simplified expression will be shown.

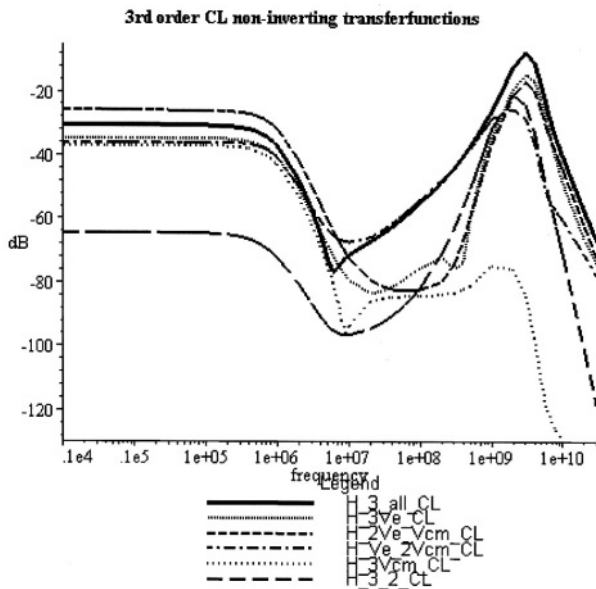


Figure 4-7. Plots of the various 3<sup>rd</sup> order transfer functions using high CM-gain.

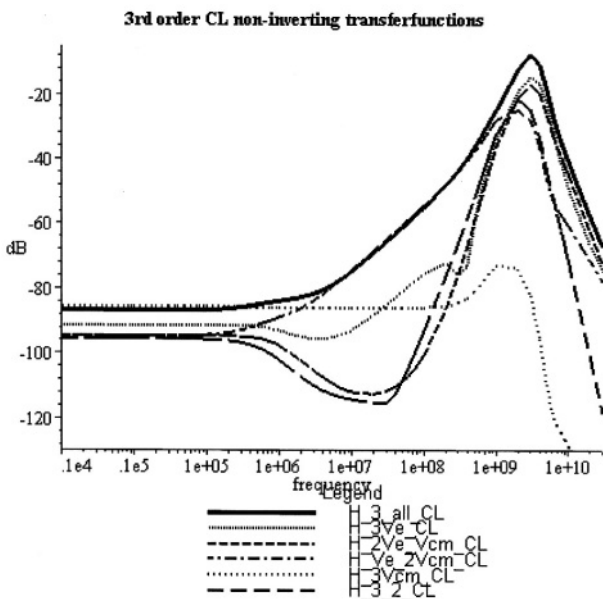


Figure 4-8. Plots of the various 3<sup>rd</sup> order transfer functions using low CM-gain.

#### 4.1.2.1 $H_{V_{e\_2V_{cm\_CL}}}(j\omega)$

Figure 4-9 and Figure 4-10 shows the main contributing nonlinear coefficients to  $H_{V_{e\_2V_{cm\_CL}}}(j\omega)$  with high and low CM-gain, respectively. The plots are obtained in the same way as for  $H_{V_{e\_V_{cm\_CL}}}(j\omega)$  and the labels of the curves have the same structure. For high CM-gain and low frequencies, the output transistors are the strongest contributors. This is seen from that the “all”-curve is decided of the “M4 and M5”-curve in this frequency range. For higher frequencies, the input transistors take over. When the CM-gain is low, the input transistors are the strongest contributors in the whole frequency range. The strongest nonlinear coefficients are (in declining order)  $K_{3_{2gm\_gd}}$ ,  $K_{2_{gm}}$ ,  $K_{3_{gm}}$ , and  $K_{2_{gmb\_gm}}$ . The curve that includes these nonlinear coefficients in addition to M4 and M5 fits the “all”-curve well for frequencies above the dominant pole of the opamp. It is in this frequency range that  $H_{V_{e\_2V_{cm\_CL}}}(j\omega)$  contribute alone to 3<sup>rd</sup> harmonic. The simplified equation for  $H_{V_{e\_2V_{cm\_CL}}}(j\omega)$  is given in (4-19) including the main nonlinear coefficients. The 2<sup>nd</sup> order coefficients  $K_{2_{gm}}$  and  $K_{2_{gmb\_gm}}$  contribute because of mixing between 2<sup>nd</sup> harmonic and the fundamental frequency. As for  $H_{V_{e\_V_{cm\_CL}}}(j\omega)$  there is a zero at  $\omega_i$ , which gives a slope equal to 20dB/dec for the nonlinear transfer function above this zero. It is possible to lower the 3<sup>rd</sup> harmonic at frequencies above  $\omega_i$  by making the GBW of the opamp as high as possible. It is also important to keep the nonlinear coefficients low and the transconductance  $gm$  high. Because of different signs of the nonlinear coefficients, some canceling effects are expected.

The accurate version of  $H_{V_{e\_2V_{cm\_CL}}}(j\omega)$  and (4-19) are plotted in Figure 4-11. The match between the two curves is close for frequencies above the dominant pole of the opamp and up to approximately 200MHz. The deviation between the curves at low frequencies is due to nonlinear coefficients not included in (4-19). Because of canceling effects the accurate curve is lower than the approximated curve. Above 200MHz the deviation is caused by omission of poles and zeroes at high frequencies.

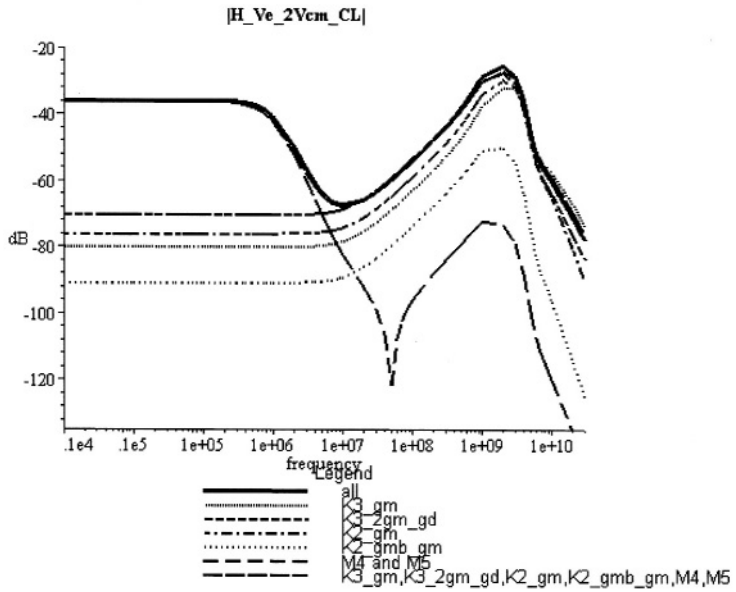


Figure 4-9. High CM-gain, main contributions to  $H_{Ve\_2Vcm\_CL}(j\omega)$ .

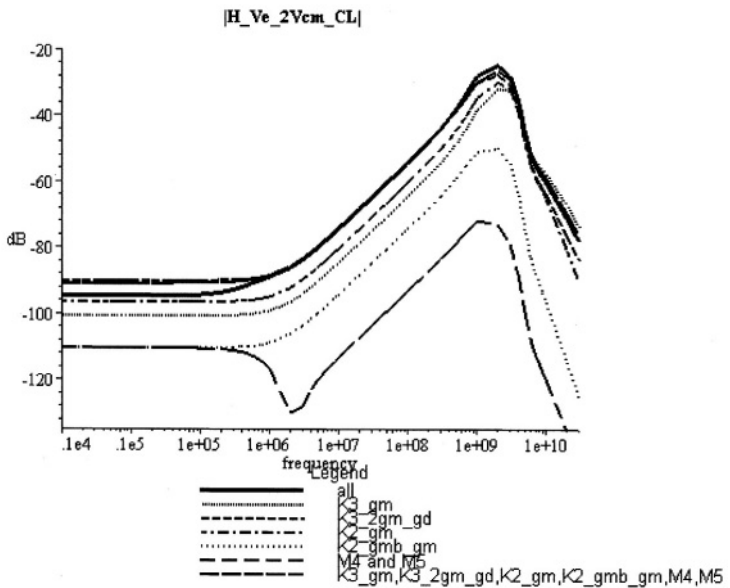


Figure 4-10. Low CM-gain, main contributions to  $H_{Ve\_2Vcm\_CL}(j\omega)$ .

$$H_{V_{e\_2V_{cm\_CL}}}(j\omega) \stackrel{\omega \ll \omega_{GBW}}{\approx} \left( \begin{array}{l} \frac{3}{4} \cdot K3_{gm} \cdot \frac{gd_3 + 2gd + 2gmb}{gm} - \\ K3_{2gm\_gd} + \left( 2 \frac{K2_{gm}}{gm} + \frac{K2_{gmb\_gm}}{gm} \right) \\ \left( K2_{gmb\_gm} \cdot gm - \right. \\ \left. \frac{K2_{gm}}{2} \cdot (gd_3 + 2gd + 2gmb) \right) \\ 1 \\ \left. \frac{1}{gd_3 + 2gd + 2gmb + 2gm} \right) \quad (4-19)$$

$$\cdot \frac{(1 - \beta \cdot H_{V_{cm}}(j\omega))}{\beta^2 \cdot A_1 \cdot A_2} \cdot \frac{gd_3 + 2gd + 2gmb}{(gd_3 + 2gd + 2gmb + 2gm)^2} \cdot \left( 1 + j \frac{\omega}{\omega_1} \right)$$

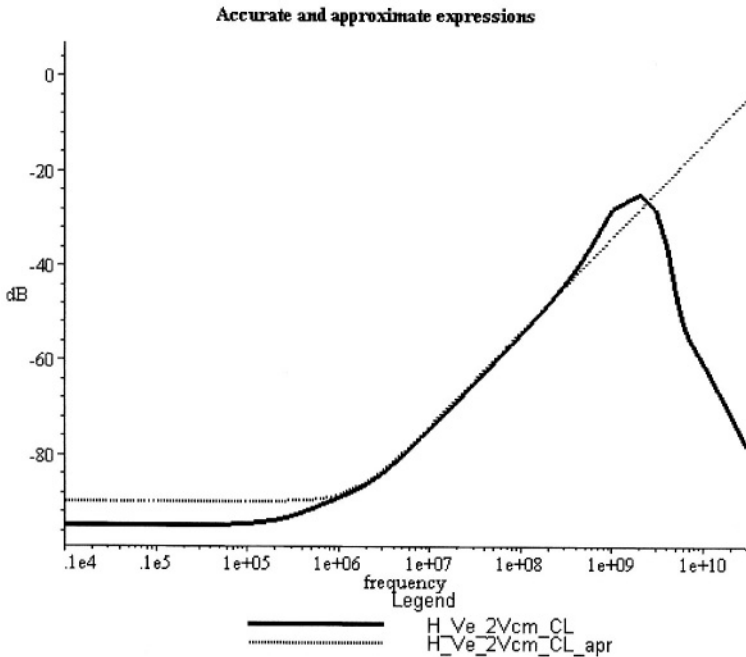


Figure 4-11. “H\_Ve\_2Vcm\_CL” is the accurate version of  $H_{V_{e\_2V_{cm\_CL}}}(j\omega)$  and “H\_Ve\_2Vcm\_CL\_apr” is (4-19). Both curves are plotted with low CM-gain.

### 4.1.3 Non-Inverting: Design Considerations for Low Distortion

In this section, the non-inverting opamp configuration with low CL gain is analyzed with respect to nonlinear behavior. The main drawback of this configuration is the high CM-voltage swing at the input terminals of the opamp. This swing is destructive for the linearity performance of the circuit. This is also reported in [5]. Thus, to achieve high linearity performance for the non-inverting opamp configuration the challenge will be design of the input stage.

The above analysis shows that low CM-gain is an important design issue. This can be obtained by close matching between the input transistors, by avoiding the bulk modulation and by making the conductance of the tail current source M3 as low as possible. According to [7] and [8], the matching of the gain factors, the threshold voltages and the body factors are all inversely proportional to the square root of the area of the transistors. Thus, close matching is achieved by using large area for the input transistors. The bulk modulation is omitted by using PMOS transistors. These are placed in N-wells in modern fabrication technologies. It is then possible to connect bulk to source and by this shorten the BS-terminal of the transistor. Low conductance in the tail current source can be attained by using a cascode. The cascode has higher saturation voltage than a one-transistor current source. This can be a problem when the input CM-swing is large compared to the supply voltage. Another possibility is to use the tail current compensation circuit described in [6]. By this solution, low output conductance is obtained at the same time as low saturation voltage.

If the CM-gain is low and  $|\beta \cdot H_{V_{cm}}(j\omega)| \ll 1$ , the strongest contributions to nonlinear distortion are the input transistors. The nonlinear coefficients of these transistors contribute through the nonlinear transfer functions that have the largest dependence on the CM-voltage. For low frequency,  $H_{x \cdot V_{cm\_CL}}(j\omega)$  (where  $x$  is 2 or 3) is the dominant transfer functions. It can be shown that  $H_{x \cdot V_{cm\_CL}}(j\omega)$  depends on the mismatch in the differential pair, M1 and M2. Thus, better matching gives lower distortion at low frequency. For higher frequency,  $H_{Ve\_y \cdot V_{cm\_CL}}(j\omega)$  (where  $y$  is 1 or 2) takes over, even if the CM-gain is large. The distortion in this frequency range can be lowered by increasing the GBW of the opamp. Additionally, the expressions (4-11) and (4-19) (p. 61 and 67, respectively) show that  $H_{Ve\_y \cdot V_{cm\_CL}}(j\omega)$  do not depend on mismatch between M1 and M2 when  $|\beta \cdot H_{V_{cm}}(j\omega)| \ll 1$ . When  $|\beta \cdot H_{V_{cm}}(j\omega)| > 1$   $H_{Ve\_y \cdot V_{cm\_CL}}(j\omega)$  will depend on mismatch through  $H_{V_{cm}}(j\omega)$ .

Both (4-11) and (4-19) are lowered by increasing the transconductance of the input transistors. This is also the case for  $H_{x \cdot V_{cm\_CL}}(j\omega)$ . Thus, it is important that the  $gm$  of M1 and M2 is as high as possible. On the other hand, when increasing  $gm$  by increasing the aspect ratio of the transistors

(W/L) and at the same time keeping the bias current constant, the GS-overdrive will decrease. In section 3.1 it is shown that biasing the transistor with low GS-overdrive results in high values for the nonlinear coefficients associated with the GS-terminal. The compromise between high transconductances and low nonlinear coefficients can be optimized in a circuit simulator to obtain low nonlinear distortion.

The linearity can also be improved by matching different nonlinear coefficients with opposite sign. For opamps in non-inverting configuration, the input differential pair has large contributions to distortion. Since the nonlinear coefficients with opposite sign are due to the same transistor, it is possible to utilize this to enhance the linearity performance. Accurately modeling of higher order derivatives of the transistor current is an important issue here.

The design guidelines for achievement of highly linear opamps for the non-inverting configuration can be summarized as follows:

- For low frequencies:
  - Obtain low CM-gain by close matching of the input differential pair, by omitting the bulk modulation and by obtaining high output resistance of the tail current source.
- For high frequencies (well above the dominant pole of the opamp):
  - High GBW of the opamp.
- Generally, in the entire frequency range:
  - Set the equilibrium currents well above the signal currents in the whole frequency range. Further, dimension the transistors to set the voltage bias point such that the nonlinear coefficients are low and stable in the entire range of the terminal voltages of the transistors. Use this as a starting point for optimization.
  - Optimizing: high transconductance versus low nonlinear coefficients.
  - Utilize canceling between nonlinear coefficients.

When the CL-gain of the circuit is increased, the CM-voltage on the inputs decrease and the contributing transfer functions shifts towards  $H_{2ve\_CL}(j\omega)$  and  $H_{3ve\_CL}(j\omega)$ . The output stage has the main contribution in these transfer functions, and it is a similar situation as for the inverting opamp configuration described in the next section.

## 4.2 The Inverting Configuration

The inverting opamp configuration is shown in Figure 4-12. The 1<sup>st</sup> to 3<sup>rd</sup> order CL responses, derived in Appendix B, are quoted in (4-20) to (4-22).  $A_{CL}$  is the ideal CL-gain equal to  $-R_2/R_1$ .

For the non-inverting opamp configuration, described in the previous section, the swing in the CM-voltage is high and not suppressed by the feedback loop. The nonlinear transfer functions, which have the strongest dependence on the input CM-voltage, are the strongest contributors to the total distortion. The large advantage of the inverting opamp configuration is the low CM-swing, which is  $V_{cm} = -V_e/2$ . Thus, for the inverting configuration all OL nonlinear transfer functions are suppressed by the same order of the loop gain ( $\beta \cdot H_{ve}(j\omega)$ ), as shown in (4-21) and (4-22). In Figure 4-13 and Figure 4-14 the CL nonlinear transfer functions are plotted. The CL transfer functions are obtained by expanding (4-21) and (4-22). The naming convention is the same as for the non-inverting configuration. For the inverting configuration the major contributors to the total CL responses are those nonlinear transfer functions that have the strongest dependence on the differential input voltage. These are  $H_{2ve\_CL}(j\omega)$  and  $H_{3ve\_CL}(j\omega)$  for 2<sup>nd</sup> and 3<sup>rd</sup> order distortion, respectively.

In the next subsections, the nonlinear coefficients with the highest contributions to  $H_{2ve\_CL}(j\omega)$  and  $H_{3ve\_CL}(j\omega)$  will be found by plotting. Further, it will be given approximate equations for these transfer functions, which also are the simplified expressions for the total 2<sup>nd</sup> and 3<sup>rd</sup> order responses. From these results some design criteria will be drawn. As for the non-inverting configuration, all parameters are according to Table 3-1 (p. 50). The input voltage is  $1V_{peak}$  and the closed loop gain is  $-1$ , which means that the feedback factor is  $\beta = 1/2$ . The mismatch between M1 and M2 are only considered through mismatch in the transconductance  $gm$ .

$$\begin{aligned}
 V_{out\_1} &= A_{CL} \cdot \frac{\beta \cdot \left( H_{ve}(j\omega) - \frac{1}{2} H_{vcm}(j\omega) \right)}{1 + \beta \cdot \left( H_{ve}(j\omega) - \frac{1}{2} H_{vcm}(j\omega) \right)} \cdot V_{in} \\
 &\approx A_{CL} \cdot \frac{\beta \cdot H_{ve}(j\omega)}{1 + \beta \cdot H_{ve}(j\omega)} \cdot V_{in} \stackrel{|\beta \cdot H_{ve}(j\omega)| \gg 1}{\approx} -\frac{R_2}{R_1} \cdot V_{in}
 \end{aligned} \tag{4-20}$$

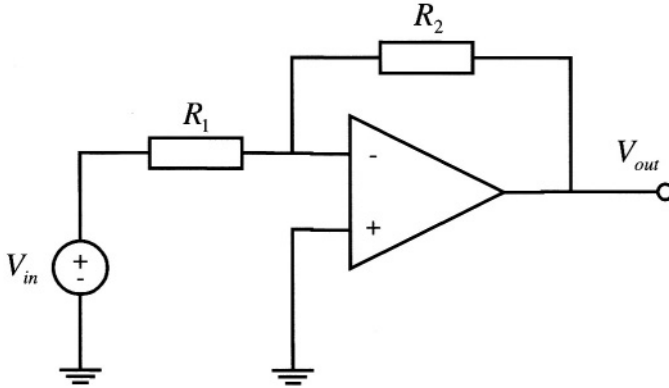


Figure 4-12. Inverting opamp configuration.

$$V_{out\_2} \approx A_{CL}^2 \cdot \frac{\beta^2}{[1 + \beta \cdot H_{ve}(j2\omega)] \cdot [1 + \beta \cdot H_{ve}(j\omega)]^2} \cdot \left\{ H_{2ve}(j\omega) - \frac{1}{2} H_{ve\_vcm}(j\omega) + \frac{1}{4} H_{2vcm}(j\omega) \right\} \cdot V_{in}^2 \quad (4-21)$$

$$V_{out\_3} \approx A_{CL}^3 \cdot \frac{\beta^3}{[1 + \beta \cdot H_{ve}(j3\omega)] \cdot [1 + \beta \cdot H_{ve}(j\omega)]^3} \cdot \left\{ H_{3ve}(j\omega) - \frac{1}{2} H_{2ve\_vcm}(j\omega) + \frac{1}{4} H_{ve\_2vcm}(j\omega) - \frac{1}{8} H_{3vcm}(j\omega) \right\} \cdot V_{in}^3 \quad (4-22)$$

$$+ \frac{H_{3\_2}(V_{e\_1}, V_{e\_2}, V_{cm\_1}, V_{cm\_2}, j\omega, j2\omega)}{[1 + \beta \cdot H_{ve}(j3\omega)]} \cdot V_{in}^3$$

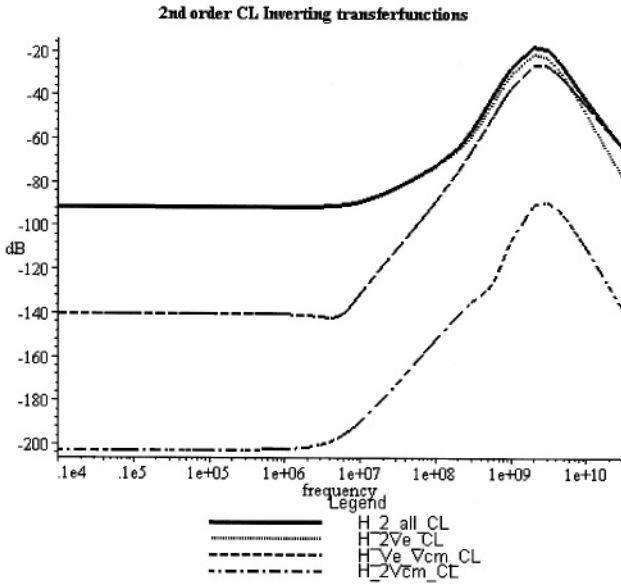


Figure 4-13. Plots of the 2<sup>nd</sup> order CL transfer functions.  $H_{2Ve\_cl}(j\omega)$  is the main contribution to the total 2<sup>nd</sup> order response.

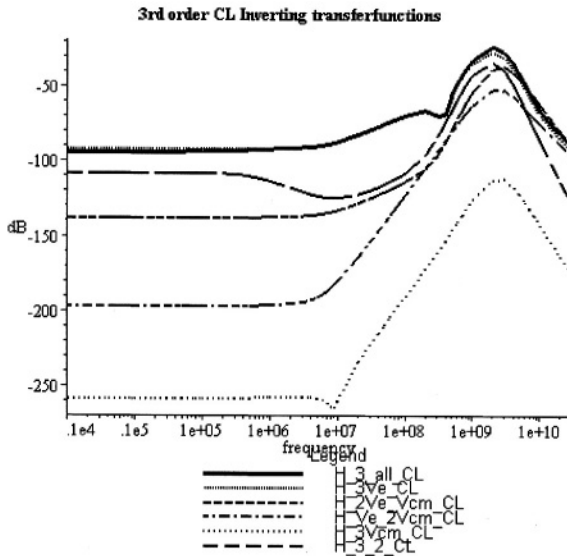


Figure 4-14. Plots of the 3<sup>rd</sup> order CL transfer functions.  $H_{3Ve\_cl}(j\omega)$  is the main contribution to the total 3<sup>rd</sup> order response.

### 4.2.1 Contributions to 2<sup>nd</sup> Harmonic: $H_{2ve\_CL}(j\omega)$

Figure 4-15 shows  $H_{2ve\_CL}(j\omega)$  with the most important nonlinear coefficients. These are  $K2_{gm4}$ ,  $K2_{gm\_gd4}$ ,  $K2_{gd4}$  and  $K2_{gd5}$ . The curve that plots the sum of these coefficients (denoted “K2\_gm4, K2\_gm\_gd4,...”) shows close fitting to the “all”-curve (seem to be identical in the plot). This shows that the major 2<sup>nd</sup> order nonlinear coefficients are included.

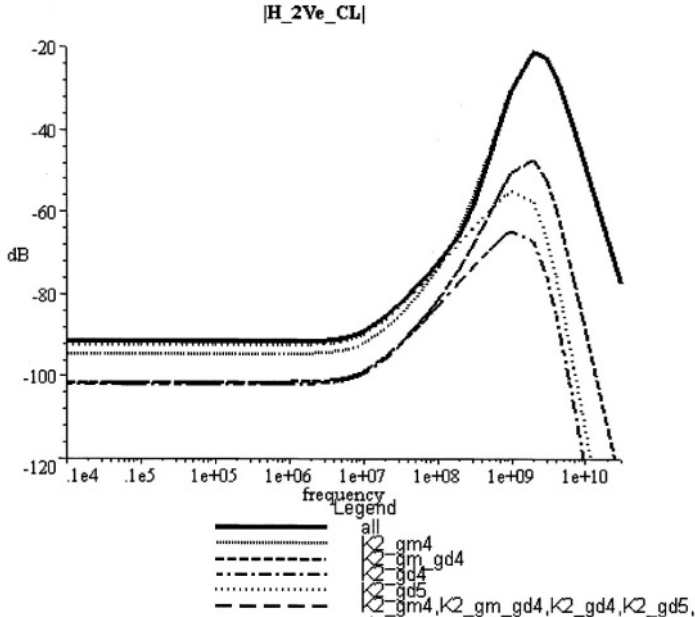


Figure 4-15. The main contributions to  $H_{2ve\_CL}(j\omega)$ . The “all”-curve is  $H_{2ve\_CL}(j\omega)$  with all nonlinear coefficients included. The other curves is  $H_{2ve\_CL}(j\omega)$  with only the denoted nonlinear coefficients included.

Equation (4-23) shows  $H_{2ve\_CL}(j\omega)$  including the nonlinear coefficients plotted in Figure 4-15. Here,  $\omega_k$  is the pole in the output node of the folded cascode when disregarding the Miller feedback capacitance.  $\omega_7$  is the pole caused by the output node of the opamp with the Miller capacitance connected to ground. These are given in (4-24) and (4-25) and appear as zeros in both  $H_{2ve\_CL}(j\omega)$  and  $H_{3ve\_CL}(j\omega)$ .  $H_{3ve\_CL}(j\omega)$  is described in the next section. The poles and zeros at high frequency are disregarded. Using (4-24) and (4-25), and the parameters from Table 3-1 (p. 50), it is possible to locate  $\omega_k$  at 23MHz and  $\omega_7$  at 212MHz. This can also be seen in Figure 4-15.

Figure 4-15 shows that at low frequency all nonlinear coefficients contribute almost at the same level. (4-23) shows that the contribution from the nonlinear coefficients increase with 20dB/dec for frequencies above  $\omega_6/2$ . Further, above  $\omega_7$   $K2_{gm\_gd4}$  and  $K2_{gm4}$  increase with 40dB/dec and 60dB/dec, respectively, due to the 1<sup>st</sup> and 2<sup>nd</sup> order zero at  $\omega_7$ . Because of the 60dB/dec slope,  $K2_{gm4}$  takes over as the strongest contribution to 2<sup>nd</sup> harmonic at frequencies above 100MHz. Similar results are presented in [1] and [4], where  $K2_{gm4}$  appears as the strongest contribution in the entire frequency range.

The total 2<sup>nd</sup> order response and (4-23) are plotted in Figure 4-16. The total 2<sup>nd</sup> order response includes all 2<sup>nd</sup> order transfer functions and all nonlinear coefficients. The plot shows close match between the curves for frequencies below 1GHz. Thus, the 2<sup>nd</sup> harmonic of the inverting opamp configuration is well approximated by (4-23).

$$H_{2ve\_CL}(j\omega) \stackrel{\omega \ll \omega_{GBW}}{\approx} \frac{1}{2} \cdot \frac{\left(\frac{R_2}{R_1}\right)^2}{gm_4 \cdot \beta \cdot A_1} \cdot \left(1 + j \frac{2\omega}{\omega_6}\right) \cdot \left[ \begin{array}{l} -\frac{K2_{gm4}}{A_2^2} \cdot \left(1 + j \frac{\omega}{\omega_7}\right)^2 \\ + \frac{K2_{gm\_gd4}}{A_2} \cdot \left(1 + j \frac{\omega}{\omega_7}\right) \\ - K2_{gd4} - K2_{gd5} \end{array} \right] \quad (4-23)$$

$$\omega_6 = \frac{g_{o1}}{C_6} \quad (4-24)$$

$$\omega_7 = \frac{gd_4 + gd_5 + G_L}{C_L + C_C} \quad (4-25)$$

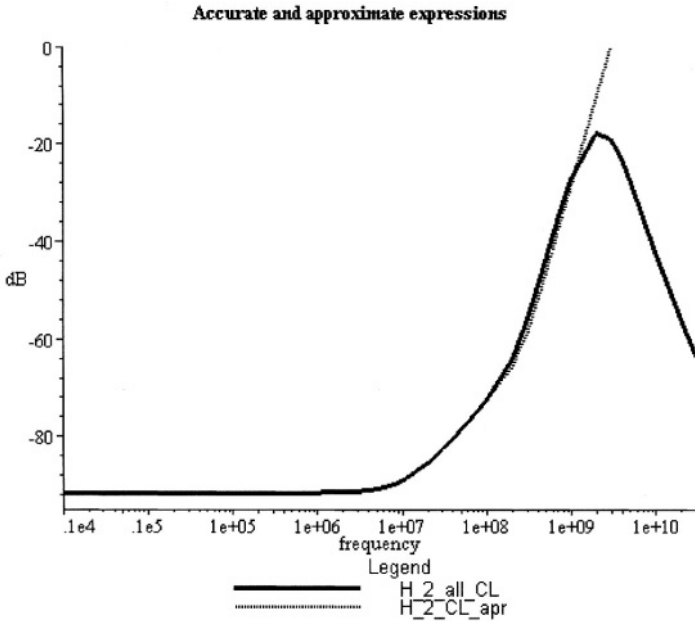


Figure 4-16. Equation (4-23) (labeled “H<sub>2</sub>\_CL\_apr”) plotted together with the total 2<sup>nd</sup> order response (“H<sub>2</sub>\_all\_CL”).

#### 4.2.2 Contributions to 3<sup>rd</sup> Harmonic: $H_{3ve\_CL}(j\omega)$

The major nonlinear coefficients contributing to  $H_{3ve\_CL}(j\omega)$  are plotted in Figure 4-17. For frequencies below 100MHz, the sum of  $K3_{gd4}$  and  $K3_{gd5}$  contributes well above the other coefficients. For high frequencies, the nonlinear coefficients with higher order zeroes take over. Especially  $K2_{gm}$  and  $K2_{gm4}$  are strong. Because of different signs between  $K2_{gm}$  and the sum of  $K3_{gd4}$  and  $K3_{gd5}$ , an optimum occurs at approximately 200MHz. The curve that covers all the major nonlinear coefficients shows close match to the “all”-curve in the entire frequency range. This shows that that the most important nonlinear coefficients are considered in Figure 4-17.

The sum of the expressions (4-26) and (4-27) makes the approximated  $H_{3ve\_CL}(j\omega)$ . (4-26) includes the 3<sup>rd</sup> order nonlinear coefficients and (4-27) the 2<sup>nd</sup> order nonlinear coefficients. (4-26) has a similar structure as  $H_{2ve\_CL}(j\omega)$  given by (4-23). All nonlinear coefficients have a zero at  $\omega/3$ , which cause a 20dB/dec slope for frequencies above this zero. Further,  $K3_{gm\_2gd4}$ ,  $K3_{2gm\_gd4}$  and  $K3_{gm4}$  have 1<sup>st</sup> to 3<sup>rd</sup> order zeroes, respectively, at  $\omega_7$ . These zeroes cause the slopes of  $K3_{gm\_2gd4}$ ,  $K3_{2gm\_gd4}$  and  $K3_{gm4}$  to be 40dB/dec, 60dB/dec and 80dB/dec, respectively, above  $\omega_7$ . (4-27) shows that

the 2<sup>nd</sup> order nonlinear coefficients have a slightly different structure. The contributions from the 2<sup>nd</sup> order coefficients are caused by mixing of 2<sup>nd</sup> harmonic and the fundamental frequency. The contribution from  $K2_{gm4}$  has a slope of 20dB/dec for frequencies below  $\omega_1/2$ , 0dB/dec between  $\omega_1/2$  and  $\omega_6$ , 20dB/dec above  $\omega_6$  and 80dB/dec above  $\omega_7$ .  $K2_{gm}$  is due to the input stage and has 60dB/dec slope above the dominant pole  $\omega_1$ . The slopes described above are also viewable in Figure 4-17.

The total 3<sup>rd</sup> order response (“H\_3\_all\_CL”) and the sum of (4-26) and (4-27) (“H\_3\_CL\_apr”) are plotted in Figure 4-18. The two curves show close fitting for frequencies below 1GHz. Thus, (4-26) and (4-27) are accurate estimation for the 3<sup>rd</sup> order response of the inverting opamp configuration.

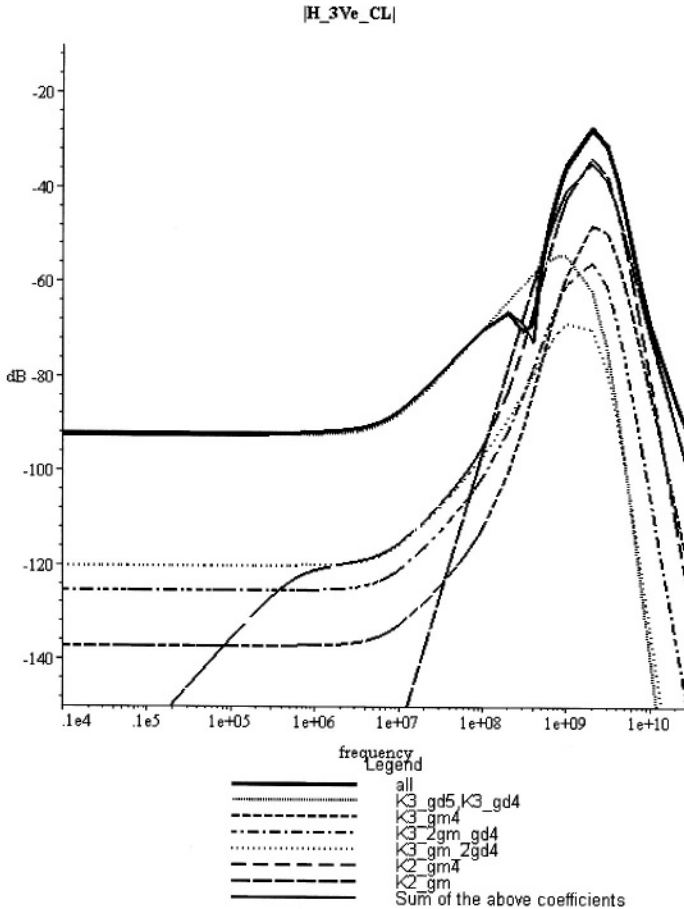


Figure 4-17. The major nonlinear coefficients of  $H_{3Ve\_CL}(j\omega)$ .

$$\begin{aligned}
 H_{3Ve\_CL}^{K3}(j\omega) \stackrel{\omega \ll \omega_{GBW}}{\approx} & \frac{1}{4} \cdot \frac{\left(\frac{R_2}{R_1}\right)^3}{gm_4 \cdot \beta \cdot A_1} \cdot \left(1 + j \frac{3\omega}{\omega_6}\right) \\
 & \cdot \left\{ -\frac{K3_{gm4}}{A_2^3} \cdot \left(1 + j \frac{\omega}{\omega_7}\right)^3 + \frac{K3_{2gm\_gd4}}{A_2^2} \cdot \left(1 + j \frac{\omega}{\omega_7}\right)^2 \right. \\
 & \left. - \frac{K3_{gm\_2gd4}}{A_2} \cdot \left(1 + j \frac{\omega}{\omega_7}\right) + K3_{gd4} + K3_{gd5} \right\} \quad (4-26)
 \end{aligned}$$

$$\begin{aligned}
 H_{3Ve\_CL}^{K2}(j\omega) \stackrel{\omega \ll \omega_{GBW}}{\approx} & \frac{\left(\frac{R_2}{R_1}\right)^3 \cdot \frac{K2_{gm4}^2}{gm_4^2} \cdot j\omega \cdot C_c \cdot \left(1 + j \frac{3\omega}{\omega_6}\right) \left(1 + j \frac{\omega}{\omega_7}\right)^3}{\beta \cdot g\omega_1 \cdot A_1 \cdot A_2^2 \cdot \left(1 + \frac{2s}{\omega_1}\right)} \quad (4-27) \\
 & + \frac{1}{4} \cdot \frac{\left(\frac{R_2}{R_1}\right)^3 \cdot K2_{gm}^2}{g\omega_1 \cdot \beta \cdot A_1^4 \cdot A_2^3} \cdot \frac{\left(1 + j \frac{\omega}{\omega_1}\right)^3}{(gd_3 + 2gd + 2gmb + 2gm)}
 \end{aligned}$$

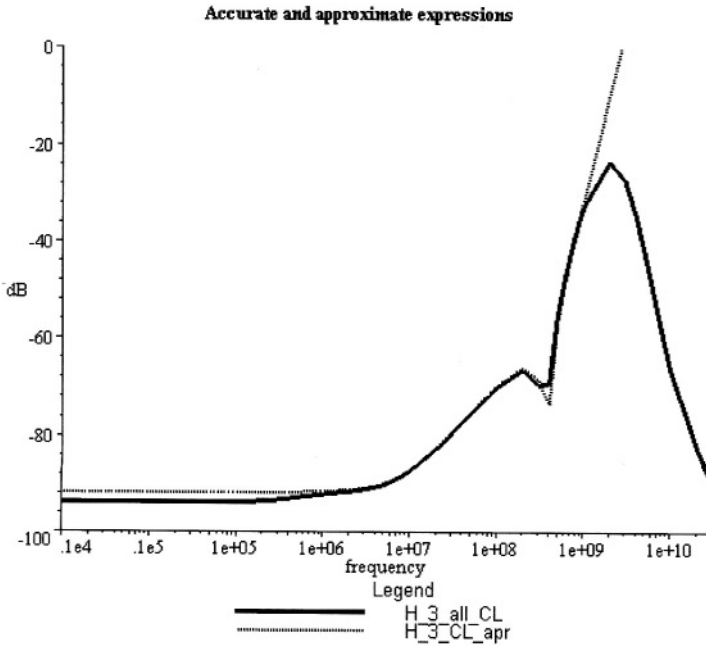


Figure 4-18. The sum of (4-26) and (4-27) (labeled “H\_3\_CL\_apr”) and the total 3<sup>rd</sup> order response (“H\_3\_all\_CL”) including all 3<sup>rd</sup> order transfer functions and nonlinear coefficients.

### 4.2.3 Inverting: Design Considerations for Low Distortion

The inverting opamp configuration has been described in this section. The main advantage of this configuration, compared to the non-inverting, is the low CM-voltage swing on the input terminals of the opamp. Because of this, the main contributions to distortion come from the output stage. The contribution from the input stage does not become considerable except at high frequencies. This also makes the analysis simpler and the derived expressions more accurate.

The strongest CL nonlinear transfer functions are  $H_{2v_{e\_CL}}(j\omega)$  and  $H_{3v_{e\_CL}}(j\omega)$  for 2<sup>nd</sup> and 3<sup>rd</sup> order responses, respectively.  $H_{2v_{e\_CL}}(j\omega)$  is well approximated by (4-23) and  $H_{3v_{e\_CL}}(j\omega)$  by the sum of (4-26) and (4-27). These transfer functions can be described by asymptotes in the various ranges of frequency. Each of the asymptotes can be lowered by the factors shown in (4-28) to (4-31). These factors can be used as design equations to obtain high linearity performance of the folded cascode Miller opamp connected in inverting configuration.

For frequencies below  $f_6 = \omega_6 / 2\pi$  both 2<sup>nd</sup> and 3<sup>rd</sup> harmonic is suppressed by (4-28). (4-28) shows that it is important to obtain high gain in the input stage and high transconductance in the output stage to achieve low distortion below  $f_6$ . In the frequency range between  $f_6$  and  $f_7 = \omega_7 / 2\pi$  the attenuation is proportional to (4-29). In this frequency range the transconductances of both the input and output stages should be as high as possible and, at the same time,  $C_6$  should be small. For frequencies above  $f_7$ , (4-30) shows that it is even more important to increase  $gm_4$ . Further, in addition to  $C_6$  the capacitances  $C_C$  and  $C_L$  should also be small.

The last section showed that at high frequencies the contribution from the input differential pair due to  $K2_{gm}$  can be considerable. This and other contributions from the input transistors M1 and M2 are suppressed by (4-31). Here, both  $gm$  and the GBW of the opamp need to be high.

$$\beta \cdot A_1 \cdot gm_4, \quad f < f_6 \quad (4-28)$$

$$\beta \cdot A_1 \cdot gm_4 \cdot \omega_6 = \beta \cdot \frac{gm \cdot gm_4}{C_6}, \quad f_6 < f < f_7 \quad (4-29)$$

$$\beta \cdot A_1 \cdot gm_4 \cdot \omega_6 \cdot A_2 \cdot \omega_7 = \beta \cdot \frac{gm \cdot gm_4^2}{C_6 \cdot (C_C + C_L)}, \quad f > f_7 \quad (4-30)$$

$$\beta \cdot gm^2 \cdot \omega_{GBW}^3, \quad f > f_1 \quad (4-31)$$

Common factors in (4-28) to (4-31) are the transconductances of the amplifying transistors. The transconductances  $gm$  and  $gm_4$  needs both to be large to obtain large attenuation of the asymptotes that describes the nonlinear transfer functions. However, increasing the transconductances has some side effects. For example, in (4-29)  $C_6$  is mainly determined by the GS capacitance of M4. Thus, increasing  $gm_4$  by making M4 wider will also increase  $C_6$ . Additionally, the nonlinear coefficients will increase due to lower GS-overdrive of M4, as explained in section 3.1. Another possibility is to increase  $gm$  of the input stage. However, this will increase the nonlinear coefficients of the input transistors, which can be damaging for the 3<sup>rd</sup> harmonic at high frequency. Thus, a trade off between these contradictions has to be done to obtain low distortion.

Using the biasing guidelines of section 3.1.4 and the design equations (4-28) to (4-31) it is possible to make qualified decisions on how to optimize the linearity performance of a folded cascode Miller opamp connected in inverting configuration. Because that the various parameters are interfering with each other, and the nonlinear coefficients will be altered when changing the small-signal parameters, the circuit has to be optimized in a circuit simulator. Using the biasing guidelines (given by 1 to 3 in section 3.1.4) as the starting point for the optimization, the equations (4-28) to (4-31) describes how to enhance the linearity performance in the different frequency ranges. Guidelines for obtaining low distortion can thus be summarized as follows:

- Generally:
  - Biasing such that the equilibrium currents are well above the signal currents in the whole frequency range.
  - Dimensioning each transistor in the circuit to set the voltage bias point such that the nonlinear coefficients are low and stable in the entire range of the terminal voltages of the transistors. Use this as a starting point for optimization.
  - Optimizing: high transconductance versus low nonlinear coefficients.
  - Utilize canceling between nonlinear coefficients.
- For low frequencies ( $f < f_6$ ):
  - High OL DC-gain in the opamp.
  - High transconductance in M4.
- For high frequencies ( $f > f_6$ ):
  - High transconductance in M4.
  - High transconductance in the input differential pair M1 and M2.
  - Make  $C_6$  and  $C_C + C_L$  as small as possible.
  - Make the GBW of the opamp as high as possible to suppress the contributions from the input differential pair.

The nonlinear coefficients in (4-23), (4-26) and (4-27), are the strongest contributions to nonlinear distortion for the opamp used. In Chapter 5 three folded cascode Miller opamps are presented, all connected in inverting configuration. These are optimized for low distortion using the biasing guidelines of section 3.1.4 and the design equations above. For these opamp circuits the contributions to distortion come from the same nonlinear coefficients as described above and the linearity performance is accurately described by (4-23), (4-26) and (4-27). This will be further described in Chapter 5. Thus, the expressions and design equations obtained in this

section contain the most important nonlinear contributions while the opamp is biased properly.

When increasing the CL-gain  $A_{CL}$  of the inverting configuration the output responses due to  $H_{2V_{e\_CL}}(j\omega)$  and  $H_{3V_{e\_CL}}(j\omega)$  will increase with  $1/\beta$ , where  $\beta$  is given by (4-32). This is under the assumption that the input voltage is lowered by the CL-gain, such that the swing in the output voltage remains the same. This assumption also results in that the input CM-voltage is independent of the CL-gain. Thus, the nonlinear transferfunctions that depends on the input CM-voltage will still not contribute to the distortion. The conclusion is that by increasing the CL-gain the distortion will increase with  $1/\beta$  in the frequency range from DC to  $\beta \cdot \omega_{GBW}$ . The approximate expressions (4-23), (4-26) and (4-27) are still valid.

$$\beta = \frac{1}{1 + \frac{R_2}{R_1}} = \frac{1}{1 + |A_{CL}|} \quad (4-32)$$

### 4.3 Concluding Remarks

In section 3.1 it was pointed out that if the nonlinear coefficients and the swing in the terminal voltages of the transistors are small the distortion will be low. In feedback circuits, only a few nodes are exposed to large voltage swing. In this chapter, the non-inverting and inverting opamp configurations have been described regarding nonlinear behavior. Both configurations have large voltage swing at the output node of the opamp. The non-inverting configuration has in addition large CM-voltage swing at the input terminals.

The analysis of the non-inverting configuration showed that high linearity performance at low frequencies can be obtained by keeping the CM-gain of the opamp low. Further, even with low CM-gain, the input differential pair has the main contribution to nonlinear distortion in the entire frequency range and contributes well above the output stage. For large CL-gain, the non-inverting configuration becomes more similar to the inverting configuration. The reason for this is that the input CM-swing decreases and the strongest transfer functions shift towards  $H_{2V_{e\_CL}}(j\omega)$  and  $H_{3V_{e\_CL}}(j\omega)$ . However, low CM-gain is still required.

For the inverting configuration, only the output node of the opamp has large voltage swing and the output transistors are thus the main contributors to distortion. This simplifies the analysis of the nonlinear behavior and makes the optimization for low distortion less complicated. Because of these features, it is possible to obtain better linearity performance for the inverting

than for the non-inverting configuration. This is also shown when comparing the plots for 2<sup>nd</sup> and 3<sup>rd</sup> order responses for the two configurations. The inverting configuration should thus be the preferred choice when low distortion is important.

Nonlinearity because of voltage coefficients in the resistors in the feedback network is very harmful for the linearity performance of the CL-circuit. The distortion produced of this network will not be suppressed at the circuit output. In addition, the feedback network is connected to nodes with large voltage swing. Thus, it is important to use linear resistors for the feedback circuit. Linear resistors can be obtained on-chip by implementing the resistors in metal. The drawback of metal resistors is large area, especially for high resistance. However, for circuits with large bandwidth the resistance has to be small because of the parasitic pole on the inverting input of the opamp. This pole appears in the loop gain of the circuit and will cause stability problems if not located well above the GBW of the OL circuit. Metal resistors are then the best alternative.

In the next chapter, three opamps connected in the inverting opamp configuration are presented. These opamps are designed using the design equations obtained in section 4.2 and the biasing guidelines of section 3.1.

## REFERENCES

- [1] S. Narayanan, "Applications of Volterra Series to Intermodulation Distortion Analysis of Transistor Feedback Amplifiers," *IEEE Transaction on Circuit Theory*, vol. CT-17, no. 4, pp. 518-527, Nov. 1970.
- [2] H. Jardon, R. Gomes, O. Golovin, "Nonlinear Analysis of Amplifiers with Local and Global Negative Feedback," *IEEE International Symposium on Circuits and Systems 1997*, June 9-12 1997, pp. 965-968.
- [3] F. O. Eynde, P. F. M. Ampe, L. Verdeyen, W. Sansen, "A CMOS Large-Swing Low-Distortion Three-Stage Class AB Power Amplifier," *IEEE Journal of Solid-State Circuits*, vol. 25, no. 1, pp. 265-273, Feb. 1990.
- [4] P. Wambacq, G. G. E. Gielen, P. R. Kinget, W. Sansen, "High-Frequency Distortion Analysis of Analog Integrated Circuits," *IEEE Tr. on Circuits and Systems—II: Analog and Digital Signal Processing*, vol. 46, no. 3, pp. 335-345, Mar. 1999.
- [5] F. O. Eynde, P. Wambacq, W. Sansen, "On the Relationship Between the CMRR or PSRR and the Second Harmonic Distortion of Differential Input Amplifiers," *IEEE Journal of Solid-State Circuits*, vol. 24, no. 6, pp. 1740-1744, Dec. 1989.
- [6] B. Hernes, Ø. Moldsvor, T. Sæther, "A -80dB HD3 Opamp in 3.3V CMOS Technology using Tail Current Compensation," *IEEE International Symposium on Circuits and Systems 2001*, vol. 1, 2001, pp. 216-219.
- [7] M. J. Pelgrom, A. C. Duijnmaijer, A. P. Welbers, "Matching Properties of MOS Transistors," *IEEE Journal of Solid-State Circuits*, vol. 24, no. 5, pp. 1433-1440, Oct. 1989.

- [8] K. R. Laker, W. Sansen, “Design of Analog Integrated Circuits and Systems,” McGraw-Hill, Inc., 1994.

*This page intentionally left blank*

## Chapter 5

### Opamp Circuits with High Linearity Performance

In this chapter four opamp circuits are presented, all designed for high linearity performance. Three of the opamps are using the inverting opamp configuration with the CL gain equal to  $-1$ . These are designed using the biasing guidelines of section 3.1 and the design equations obtained in section 4.2. The circuits are fabricated in a  $0.18\mu\text{m}$  CMOS technology. The last opamp is connected in unity gain. It uses a tail current compensation circuit to linearize the input differential pair because of the large input CM-voltage swing. The circuit is fabricated in a  $0.35\mu\text{m}$  CMOS technology with 3.3V supply voltage.

To perform measurements of low nonlinear distortion, several precautions must be taken. Thus, the measurement system, used for the opamps connected in inverting configuration, is introduced. Further, the various opamp circuits are presented, one by one, beginning with a 1.8V cascoded Miller opamp. The design procedure used to achieve low nonlinear distortion is described and the strongest contributions to nonlinear distortion are found, using the Maple model applied in section 4.2 for the opamp. Further, the measurement results are presented and compared to simulations. A 3.3V cascoded Miller opamp and a 3.3V Current OpAmp (COA) are described in the same way. The unity gain opamp and its measurement system is described in [1] and only a brief description is included in this chapter with some supplementary characteristics obtained from simulations. At the end of the chapter, some concluding remarks are written and a comparison, regarding low distortion, is done against state of the art circuits.

## 5.1 Measurement System

The measurement system shown in Figure 5-1 is used for characterization of the opamp circuits described in the next three subsections. The opamps are connected in inverting configuration with the CL gain equal to  $-1$ . To prevent stability problems, due to the parasitic pole on the inverting input terminal of the opamp, the values of the resistors in the feedback network are chosen small. The parasitic pole, formed by the parallel connection of the two resistors and the input capacitance of the opamp, will then be well above the unity gain frequency of the OL circuit. The opamps are all intended to be used in on-chip applications. Thus, a 50 Ohms resistor ( $R_{OUT}$ ) is connected between the output of the opamp and the pad. This will isolate the opamp from the rather large capacitive and inductive load due to pad, bond wire, package and off-chip PCB (Printed Circuit Board) loading effects. To prevent any distortion caused by voltage coefficients, all resistors are implemented using metal. The input CM-voltage,  $V_{CM}$ , is typically set to half the supply voltage, but may also be adjusted externally. Each opamp has a bias circuitry, which generate bias voltages and thus set up the bias currents in the opamp. To maintain simplicity, this circuitry will not be shown in the schematic of the opamps. The bias circuitry is supplied by an external current of  $250\mu\text{A}$  (typ.). This current is referred to as the opamp bias current in the following subsections. Additionally, the protection diodes in the signal carrying pads were removed due to their expected contribution to nonlinear distortion.

The signal generator is a SML 03 from Rohde & Schwarz [2]. The signal generator is followed by high-order Chebyshev Band-Pass (BP) filters from TTE [3], one for each test frequency. The BP-filter is necessary to suppress the harmonics generated by the signal generator. On the output of the test-chip, the signal is applied to a voltage divider for conversion to the 50 Ohm load of the spectrum analyzer. The spectrum analyzer consists of two parts. HP89441A [4] is a mixer that converts the radio frequency to a base-band. The base-band is then applied to the low frequency part HP89410A [5] that does the signal processing and shows the frequency spectrum on a screen.

The measurements of nonlinear distortion is carried out as follows:

1. Compute the output level of the measurement system (on the input of the spectrum analyzer in Figure 5-1) referred to the desired voltage swing on the output of the opamp.
2. For each of the test frequencies, insert the BP-filter and adjust signal generator such that the measured level is equal to the level computed in 1 above.

3. Measure  $HD_2$  and  $HD_3$  by finding the difference between the level of the fundamental frequency and  $2^{\text{nd}}$  and  $3^{\text{rd}}$  harmonic, respectively.

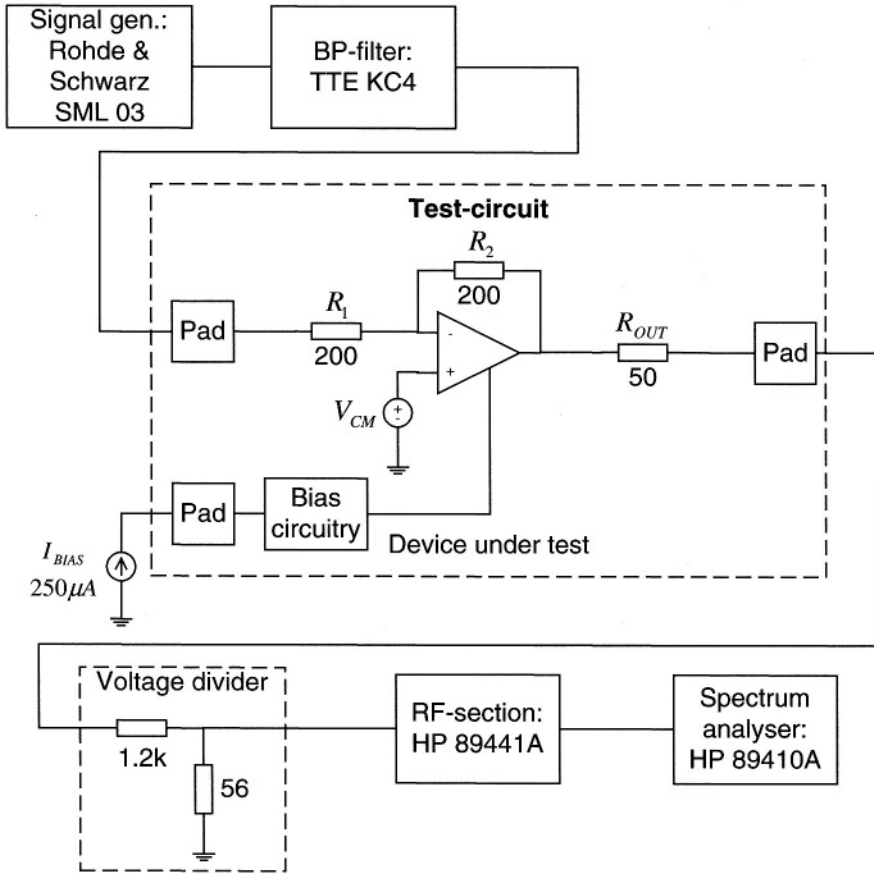


Figure 5-1. Measurement system.

The levels of the harmonics measured by the spectrum analyzer were very low. Thus, it was necessary to use the internal filtering function of the spectrum analyzer with very narrow bandwidth to keep the noise floor low enough. The filter function was set such that the error in the measured level was less than 0.01dB. The measurement was carried out by first measuring the signal level at the fundamental frequency with low filtering bandwidth, and with the range of the instrument well above the input signal. Next, the  $2^{\text{nd}}$  harmonic was measured, then  $3^{\text{rd}}$  harmonic and, for computation of  $THD$ ,  $4^{\text{th}}$  and  $5^{\text{th}}$  harmonics. The same range and filtering bandwidth was used for the harmonics as for the fundamental frequency.

The opamp circuits presented in this chapter are intended for use in a Track and Hold Amplifier (THA) preceding an ADC. Examples on such ADC's can be [6] and [7], which have 1.8V and 3.3V power supply voltage, respectively. The maximum differential voltage swings on the input of these ADC's are  $1.5V_{p-p}$  and  $2V_{p-p}$ , respectively. This is the reason why the single ended voltage swing is chosen to be  $0.75V_{p-p}$  for the opamp with 1.8V supply voltage and  $1V_{p-p}$  for the opamps with 3.3V supply voltage. Further, the THA is to be used in multi-channel IF systems. Such systems have strong demands on linearity performance in the frequency range from 10MHz to 200MHz. Thus, the opamps are optimized and tested for low distortion at these frequencies.

A reference measurement was done to measure how much the measurement system contributes to the nonlinear distortion. The test-chip was removed and the input and output pads on the PCB was connected by a strap. The results from these measurements are shown in Figure 5-2. The figure shows that below 10MHz the measurement system contributes to distortion at the same level as the opamps described in the next subsections. Above 10MHz  $HD2$  and  $HD3$  of the system is below  $-100\text{dB}$  and at some frequencies below the noise floor, which is at approximately  $-110\text{dB}$ . In this frequency range the contribution from the measurement system is well below the nonlinear distortion from the opamp circuits.

The micrograph of the test-chip is shown in Figure 5-3, containing the three opamps connected in inverting configuration. The fabrication technology is a  $0.18\mu\text{m}$  CMOS process.

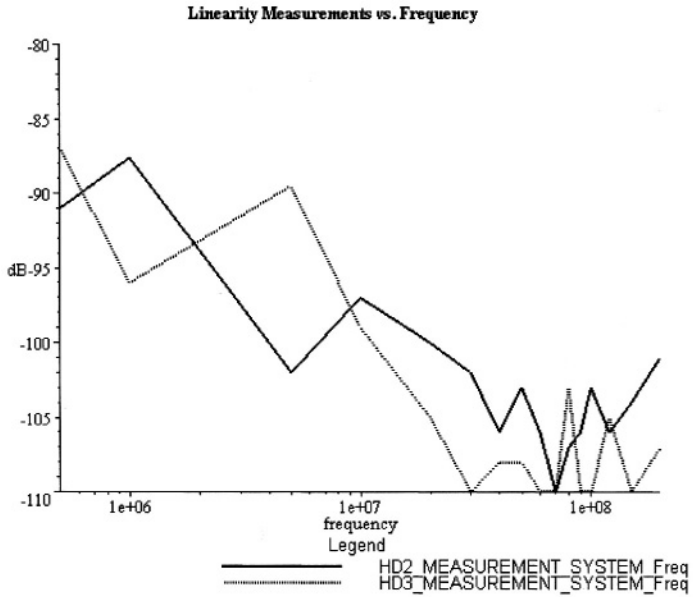


Figure 5-2. Contribution from the measurement system to HD2 and HD3.

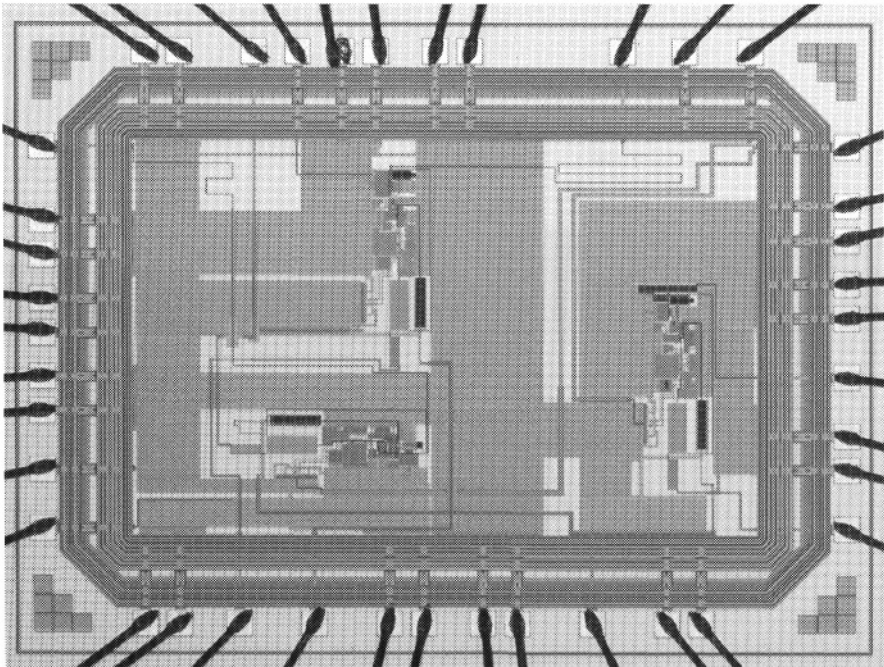


Figure 5-3. Micrograph of the test-chip fabricated in 0.18µm technology.

## 5.2 A 1.8V CMOS Opamp with $-77.5\text{dB}$ $HD_2$ and $HD_3$ at 80MHz

In this section a CMOS opamp fabricated in a  $0.18\mu\text{m}$  fabrication technology is presented. The opamp has 1.8V power supply voltage and the OL-gain is 66dB (typ.). When connected in inverting configuration with CL-gain equal to 1, the bandwidth is 2.9GHz. The opamp is optimized for low nonlinear distortion using the design criteria described in Chapter 3 and Chapter 4. Measurements show that  $HD_2$  and  $HD_3$  are less than  $-90.5\text{dB}$  at 20MHz and less than  $-77.5\text{dB}$  at 80MHz, with the output voltage swing of the opamp equal to  $0.75V_{\text{p-p}}$ .

### 5.2.1 Design Considerations

In section 4.2 design criteria for low nonlinear distortion were found for the cascoded Miller opamp used in inverting configuration. For the opamps presented in this chapter the main design specification was low nonlinear distortion at high signal frequencies. The circuits were optimized for low  $HD_2$  and/or  $HD_3$  in the frequency range 10MHz to 100MHz. For high frequencies it is important that the value of the design equations (4-28) to (4-31) (p. 79) are as large as possible. At the same time, the nonlinear coefficients should be as small as possible. As mentioned in section 4.2 this is a contradiction and a circuit simulator has to be used to find the optimum sizes and biasing of the transistors.

The folded cascode Miller opamp [8] described in section 3.2 was used. To achieve high linearity performance the following design procedure was applied:

1. Choose the bias current of the transistors to be well above the associate signal current. This was done by finding the Slew-Rate (SR) specification of the opamp output node and of the folded cascode output (see Figure 5-4). Further, the bias currents are chosen such that the circuit is far from slewing at the highest signal frequency. In other words, the Full Power Bandwidth (FPBW) of the CL circuit has to be well above the highest signal frequency. These choices of bias currents are also well above the maximum resistive signal currents.
2. Dimension each transistor in the circuit to set the voltage bias point such that the nonlinear coefficients are low and stable in the entire range of the terminal voltages, as described in section 3.1. This gives low nonlinear coefficients and robustness against variations in circuit conditions (power supply, bias current etc.) and is a starting point for the optimization, which will be carried out in 4.

- Simulation of OL-gain of the opamp and the feedback circuit together. The simulation is done with the circuit simulator Eldo [9]. Through these simulations a minimum Miller compensation capacitance is found, which give safe gain- and phase margins and at the same time the largest GBW.
- Optimize the CL circuit for low  $HD_2$  and  $HD_3$  at high frequencies. The CL responses given by (4-23), (4-26) and (4-27) and the design equations (4-28) to (4-31) are used as optimization guidelines. All equations are given in section 4.2.

Some iteration of the points above was necessary to obtain low nonlinear distortion and safe phase- and gain margins. The resulting opamp is shown in Figure 5-4 and some important simulated and estimated parameter values are shown in Table 5-1. The simulations are done with capacitive, inductive and resistive loading effects due to output pad, package pin and external load. The estimated values are computed with equations given in section 3.2.3 and Chapter 4.

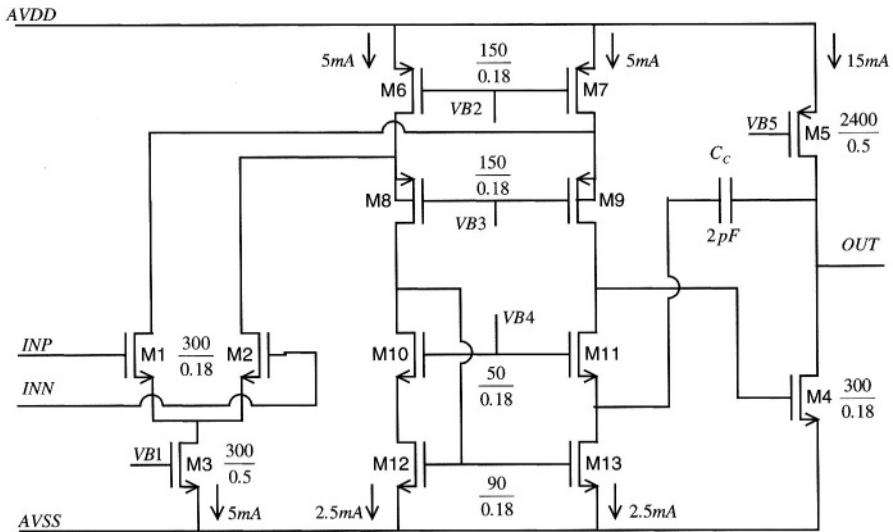


Figure 5-4. The 1.8V opamp in 0.18 $\mu\text{m}$  fabrication technology.

## 5.2.2 Contributions to Nonlinear Distortion

For implementation in Maple6 [10], the opamp model described in section 3.2 was applied on the opamp in Figure 5-4. For the transistors M1 to M5, the terminal voltages were found from a CL DC simulation, and were subsequently used to extract small-signal parameters and nonlinear

coefficients for each of the transistors. All simulations were done using Eldo and the transistor model BSIM3v3 [11]. The model parameters were given by the fabrication technology. The output conductance of the folded cascode,  $g_{o1}$ , and the Miller capacitance,  $C_C$ , were adjusted in the opamp model of section 3.2. This was done such that the low frequency loop gain and the dominant pole were equal to the values obtained by the Eldo simulation. In addition, parasitic capacitances were extracted from the opamp layout and included in the model. All parameters are given in Table 5-2, and are used for simulation of nonlinear responses in Maple.

<b>1.8V CMOS Opamp</b>		
$AVDD=1.8V, I_{BIAS}=250\mu A, V_{CM}=0.9V$ (input CM-voltage)		
Parameter	Values (typ.)	Unit
$A_0$ DC OL-Gain	66.0*	dB
$A_1$ ((3-13) on p. 48) DC-gain in 1 <sup>st</sup> stage	182**	V/V
$A_2$ ((3-14) on p. 49) DC-gain in 2 <sup>nd</sup> stage	11**	V/V
$f_l$ Dominant pole	1.26*	MHz
$f_6$ ((4-24) on p. 74)	52.5**	MHz
$f_7$ ((4-25) on p. 74)	144**	MHz
$f_T$ Unity gain bandwidth of the opamp + feedback network	1.13*	GHz
$PM$ Phase Margin for opamp + feedback network	57.8*	degrees
$GM$ Gain Margin for opamp + feedback network	9.3*	dB
$f_{-3dB,CL}$ -3 dB bandwidth of the CL circuit, at the output of the opamp	2.88*	GHz
$f_{FPBW} = SR/(2\pi V_{peak}), V_{peak} = 0.375V$ Full Power Bandwidth	373*	MHz

Table 5-1. Estimated result for the 1.8V opamp. The estimated values are from simulations carried out in Eldo (\*) and equation given in previous chapters (\*\*). The simulations include the effects from the output pad, package and external load (see Figure 5-1). Additionally, parasitic capacitances are extracted from layout.

M1 and M2 (W/L=300/0.18 (μm))					
1 <sup>st</sup> order		2 <sup>nd</sup> order		3 <sup>rd</sup> order	
$g_m$	39.6mS	$K2_{gm}$	243m	$K3_{gm}$	242m
$g_d$	1.02mS	$K2_{gd}$	6.98μ	$K3_{gd}$	55.8μ
$g_{mb}$	9.11mS	$K2_{gmb}$	15.5m	$K3_{gmb}$	13.3m
$C_{GS}$	0.11pF	$K2_{gm\_gd}$	6.00m	$K3_{2gm\_gd}$	35.5m
$d_{gm}$	0.75%	$K2_{gmb\_gm}$	108m	$K3_{gm\_2gd}$	-0.777m
		$K2_{gmb\_gd}$	2.46m	$K3_{2gmb\_gm}$	89.5m
				$K3_{gmb\_2gm}$	195m
				$K3_{2gmb\_gd}$	1.74m
				$K3_{gmb\_2gd}$	-3.14m
				$K3_{gm\_gmb\_gd}$	-2.00m
M3 (W/L=300/0.5 (μm))					
1 <sup>st</sup> order		2 <sup>nd</sup> order		3 <sup>rd</sup> order	
$gd_3$	1.67mS	$K2_{gd3}$	-6.23m	$K3_{gd3}$	28.1m
$C_S$	0.69pF	$K2_{CS}$	-136f	$K3_{CS}$	96.6f
M4 (W/L=300/0.18 (μm))					
1 <sup>st</sup> order		2 <sup>nd</sup> order		3 <sup>rd</sup> order	
$gm_4$	108mS	$K2_{gm4}$	135m	$K3_{gm4}$	-344m
$gd_4$	3.06mS	$K2_{gd4}$	-0.566m	$K3_{gd4}$	0.632m
		$K2_{gm\_gd4}$	14.2m	$K3_{2gm\_gd4}$	-6.95m
		$K2_{CDB4}$	-17.6f	$K3_{gm\_2gd4}$	-5.66m
				$K3_{CDB4}$	5.10f
M5 (W/L=2400/0.5 (μm))					
1 <sup>st</sup> order		2 <sup>nd</sup> order		3 <sup>rd</sup> order	
$gd_5$	1.05mS	$K2_{gd5}$	0.431m	$K3_{gd5}$	0.514m
		$K2_{CDB5}$	16.1f	$K3_{CDB5}$	42.5f
Other parameters					
$g_{o1}$	1/4.6kΩ	$C_6$	0.66pF	$R_L$	173Ω
$C_L$	8.5pF	$C_C$	2.46pF	$\beta$	½
$V_{OUT}$	0.75V <sub>P-P</sub>				

Table 5-2. Extracted parameters from the transistor models for the 1.8V opamp for use in simulations of nonlinear distortion in Maple.

As for the inverting opamp configuration described in section 4.2, the contributing transfer functions are  $H_{2ve\_CL}(j\omega)$  for the 2<sup>nd</sup> harmonic and

$H_{3ve\_CL}(j\omega)$  for the 3<sup>rd</sup> harmonic. At low frequency the strongest contributions to  $H_{2ve\_CL}(j\omega)$  are (in descending order)  $K2_{gm\_gd4}$ ,  $K2_{gm4}$ ,  $K2_{gd5}$ , and  $K2_{gd4}$ . For frequencies above 70MHz only  $K2_{gm\_gd4}$  and  $K2_{gm4}$  contribute and, due to higher order zeros,  $K2_{gm4}$  contributes alone at high frequencies. The total 2<sup>nd</sup> order response, including all 2<sup>nd</sup> order transfer functions and nonlinear coefficients, are plotted in Figure 5-5 together with (4-23) (section 4.2). The plot shows that (4-23) approximates the 2<sup>nd</sup> order response well.

The total 3<sup>rd</sup> order response and the sum of (4-26) and (4-27) (section 4.2) are plotted in Figure 5-6. This plot also shows good matching between the accurate and approximated equations. The curves show an optimum in 3<sup>rd</sup> order distortion at 70MHz. The reason for this optimum can be explained as follows. At low frequencies  $K3_{gd4}$ ,  $K3_{gd5}$ , and  $K3_{gm\_2gd4}$  are the strongest contributions to 3<sup>rd</sup> harmonic. At higher frequencies  $K2_{gm}$ ,  $K2_{gm4}$  and  $K3_{gm4}$  take over due to the higher order zeroes. The contributions from the 2<sup>nd</sup> order coefficients are caused by mixing of the fundamental frequency and the 2<sup>nd</sup> harmonic, both present at the transistors terminals. At approximately 70MHz the sum of  $K3_{gd4}$ ,  $K3_{gd5}$ , and  $K3_{gm\_2gd4}$  has the same magnitude as  $K2_{gm}$ , but the signs are opposite (+j and -j, respectively). Thus, a cancellation is achieved and a minimum in the 3<sup>rd</sup> order response occurs.  $K2_{gm4}$  and  $K3_{gm4}$  make the cancellation less ideal.

As explained in Chapter 3 several sources to nonlinear distortion are omitted in the Maple simulation. The equation for the drain current is a series truncated to 3<sup>rd</sup> order, which means that the nonlinear analysis only is valid for relatively small-signal amplitudes. Especially for the opamp output transistors this can be an inaccurate simplification due to the large voltage swing at the output node. However, because of careful biasing of the transistors the nonlinear coefficients are relatively constant in the entire range of the terminal voltages. Both simulations and measurements show that the opamp circuits presented in this chapter have near weakly nonlinear behavior at the signal swing used. Further, the folded cascode (M6 to M13 in Figure 5-4) is replaced by a linear resistor equal to the output resistance of the cascode. For the 2<sup>nd</sup> order response this is a fair approximation since nonlinearity due to M1, M2 and M6 to M9 is attenuated because of the differential nature of these transistors. The main contribution from the folded cascode to 2<sup>nd</sup> harmonic thus comes from M10 to M13. On the other hand, the contribution from the cascode to the 3<sup>rd</sup> harmonic is larger since the 3<sup>rd</sup> order signal currents are not differentiated.

Because that the folded cascode is omitted, it will be a gap between the simulation done in Maple and the simulation done in Eldo. It is also a risk that the Eldo simulations does not give accurate estimates of the nonlinear behavior due to inaccurate modeling of higher order derivatives of the drain current of the transistors. These topics will be described in the next sub-

section where the measurements are presented and compared to the simulated results from Maple and Eldo.

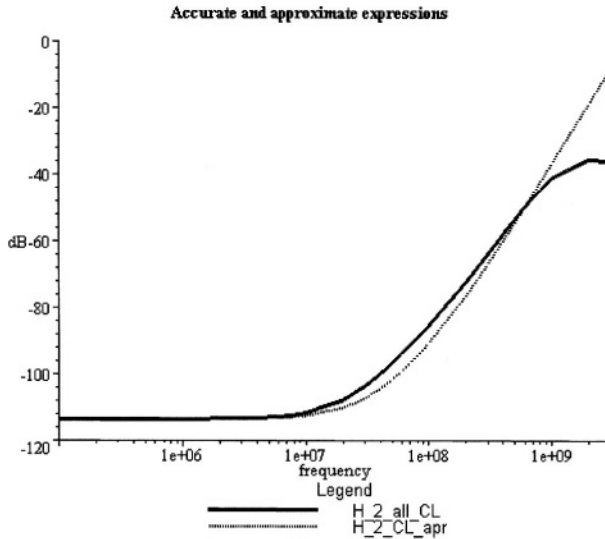


Figure 5-5. 2<sup>nd</sup> order response, accurate expression (“H\_2\_all\_CL”) and approximated expression (“H\_2\_CL\_apr”) for the 1.8V opamp.

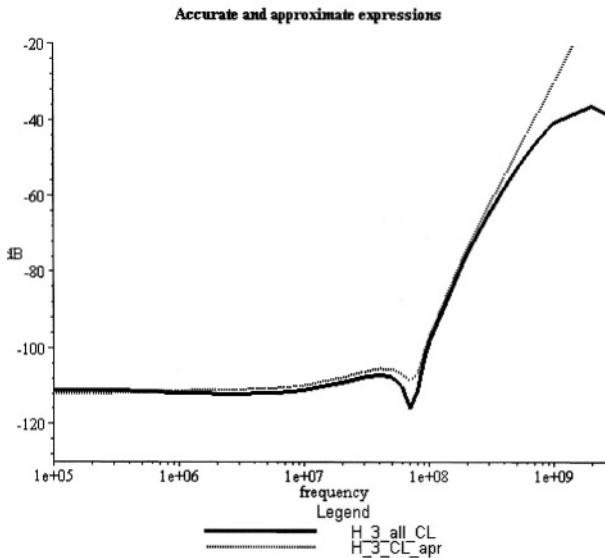


Figure 5-6. 3<sup>rd</sup> order response, accurate expression (“H\_3\_all\_CL”) and approximated expression (“H\_3\_CL\_apr”) for the 1.8V opamp.

### 5.2.3 Measurement Results

All measurement results presented in this section are done with the measurement system and procedures described in section 5.1. First,  $HD_2$  and  $HD_3$  are presented as a function of frequency and compared to the simulations carried out in Maple and Eldo. Further, to illustrate the robustness of the design,  $HD_2$ ,  $HD_3$  and  $THD$  are presented as a function of output signal swing, input CM-voltage, supply voltage and bias current.

$HD_2$  and  $HD_3$  were measured at certain input frequencies in the range from 100kHz to 200MHz. For frequencies below 20MHz the measurement system contributions are at the same level as the circuit, as shown in Figure 5-2. Measured values in this frequency range are not reliable. Thus, only measurements done in the 20-200MHz range will be considered here.

The measured values for  $HD_2$  and  $HD_3$  from three different samples of the circuit are shown in Figure 5-7 and Figure 5-8, respectively. The measurements are carried out with the output voltage swing of the opamp equal to  $0.75V_{p-p}$ .  $HD_2$  and  $HD_3$  are both less than  $-90.5\text{dB}$  at 20MHz, less than  $-77.5\text{dB}$  at 80MHz and less than  $-62.5\text{dB}$  at 150MHz. The figures also show that there are only small variations between the three samples. The variations are less than 1.2dB. In Table 5-3  $HD_2$  and  $HD_3$  are listed for some test frequencies.

The resistor at the output of the opamp (see Figure 5-1) together with the capacitive load due to pad, package and PCB, makes a LP-filter. Using the values extracted from layout, the specific pin of the package and off-chip PCB, the  $-3\text{dB}$  frequency is located at 660MHz and shall have minor effect on the measurements. However, the plot for  $HD_3$  shows lower 3<sup>rd</sup> harmonic at 200MHz input frequency than at 150MHz. When applying a 200MHz signal at the input the 3<sup>rd</sup> harmonic at the output is at 600MHz. A possible explanation of the decrease in  $HD_3$  can be that package and PCB effects cause a notch in the 3<sup>rd</sup> order response. This notch is not visible in the simulations, which can be due to the simplified model used.

The simulation results of  $HD_2$  and  $HD_3$  from Maple and Eldo are also plotted in Figure 5-7 and Figure 5-8. The Eldo simulation is carried out including the folded cascode and a model for the load seen by the output of the opamp. First, a transient analysis at each test frequency is done. Further, Fast Fourier Transform (FFT) is performed on the output voltage of the opamp. To get reliable estimate of the nonlinear distortion it is important to use high accuracy and correct settings for Eldo. For both  $HD_2$  and  $HD_3$  there is a gap between Eldo and Maple simulations. As shown later, the error due to large-signal behavior of the opamp is small, only a few dB. Thus, the folded cascode is suspected to be the major reason for the difference between Maple and Eldo.

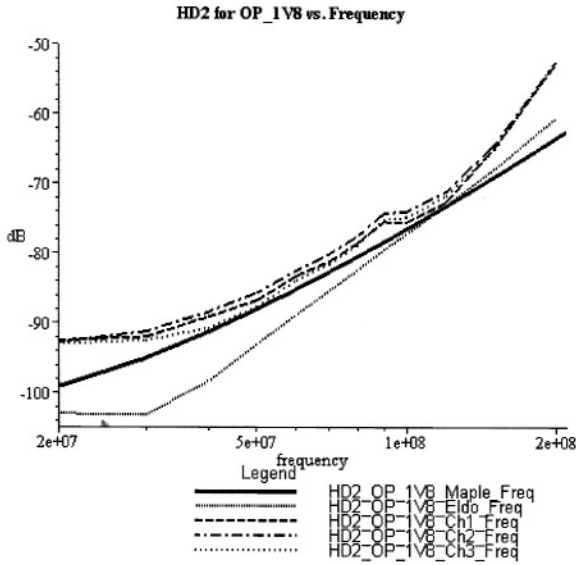


Figure 5-7. HD2 of the 1.8V opamp. The curves marked “Ch1” to “Ch3” are the measured results of three different circuit samples. The curves marked “Maple” and “Eldo” are the simulation results from Maple and Eldo, respectively.

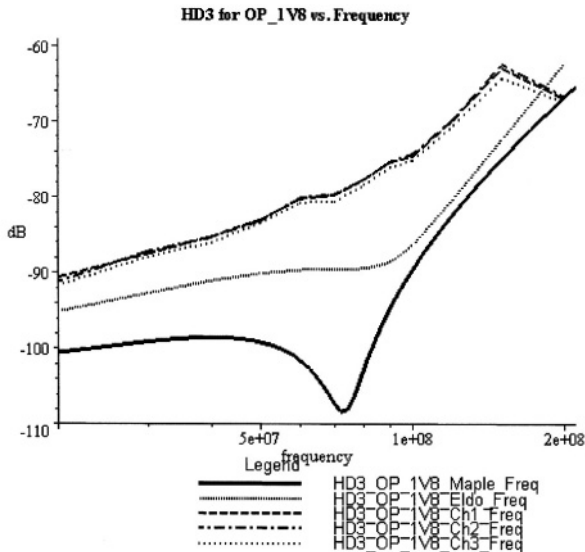


Figure 5-8. HD3 of the 1.8V opamp. The naming of the curves follows the same “convention” as used in Figure 5-7.

Figure 5-7 shows that the curve from the Eldo simulation has a minimum at 20MHz and a larger inclination above 20MHz than both the Maple simulation and measurement results. The reason for this can be cancellations between nonlinear coefficients in the cascode and the output transistors. Since the opamp is optimized for low  $HD2$  (in addition to low  $HD3$ ) in Eldo, it is possible that such effects have been utilized. On the other hand, the simulation carried out by Maple shows the same inclination as the measurements in the frequency range from 20MHz to 120MHz. The measured  $HD2$  is a little bit higher.

For  $HD3$  the gaps between Maple and Eldo are larger than for  $HD2$ . Both curves have the same shape, with the same inclination at low and high frequencies. However, the curve estimated by Eldo shows a larger  $HD3$  than the simulation from Maple. Because of the low supply voltage, the transistors in the folded cascode had to be biased with low DS-voltages. To keep the saturation voltage small enough, it was necessary to keep the GS-voltage low. As shown in section 3.1 such biasing leads to large nonlinear coefficients. Thus, it is expected that the folded cascode have strong contribution to  $HD3$  for this opamp. The “notch” in the Maple simulation, due to canceling effects, is not as distinct in the Eldo simulation, but this is reasonable since also the cascode contributes here.

Further, there is a large difference between simulations and measurements for  $HD3$ . At low and high frequencies the same inclination is observed in all curves, indicating the two zeros at  $f_6$  and  $f_7$  (see Table 5-1) in the 3<sup>rd</sup> order responses. However, the minimum in the simulated curves does not appear in the measurement results. Additionally, the absolute value is larger. An important reason for this can be the models and parameter sets from the fabrications technology used for transistors. Models in conjunction with the parameter set are often optimized to give accurate values for currents and their 1<sup>st</sup> order derivatives. The higher order derivatives are not necessarily very accurate and tend to be less accurate for higher order. Thus, it is reasonable that there is larger gap between simulations and measurements of  $HD3$  than  $HD2$ . This problem is described in [1] and [12], which show that especially the output conductance of the transistor suffers from large errors in its higher order derivatives. These errors will of course influence the accuracy of the Eldo simulation.

Measurements on 1.8V CMOS Opamp		
$V_{out}=0.75V_{p-p}$ , $AVDD=1.8V$ , $I_{BIAS}=250\mu A$ , $V_{CM}=0.9V$ (input CM-voltage)		
Parameter	Values (“worst” case of 3 samples)	Unit
<b>HD2:</b> $f_{in}=20\text{MHz}$ $f_{in}=50\text{MHz}$ $f_{in}=80\text{MHz}$ $f_{in}=100\text{MHz}$ $f_{in}=150\text{MHz}$	-92.5	dB
	-86.0	dB
	-77.5	dB
	-75.0	dB
	-64.5	dB
<b>HD3:</b> $f_{in}=20\text{MHz}$ $f_{in}=50\text{MHz}$ $f_{in}=80\text{MHz}$ $f_{in}=100\text{MHz}$ $f_{in}=150\text{MHz}$	-90.5	dB
	-83.0	dB
	-77.5	dB
	-74.5	dB
	-62.5	dB

Table 5-3. Worst case *HD2* and *HD3* of three measured samples at some test frequencies.

The measured *HD2* and *HD3* as function of the output amplitude of the opamp are plotted in Figure 5-9. In the same figure, also the weakly nonlinear versions of *HD2* and *HD3* are shown, given by (5-1) and (5-2), respectively. Here,  $HD2_N$  and  $HD3_N$  are normalized values of *HD2* and *HD3*. The normalized values are obtained from *HD2* and *HD3* measured when the output signal swing is equal to  $0.35V_{p-p}$ . The assumption made is that the circuit has weakly nonlinear behavior at this signal level. Because of the biasing guidelines, described in section 3.1, the nonlinear coefficients of the transistors are relative constants in a large part of the opamp voltage range. As Figure 5-9 shows, the opamp has nearly weakly nonlinear behavior when its output swing is  $0.75V_{p-p}$ , which is used for the measurements and simulations plotted in Figure 5-7 and Figure 5-8. The error is a few dB and the large-signal effect is thus a minor reason for the gap between the simulations from Maple and Eldo. For higher output levels the large-signal effects become considerable, especially when the output level approach the supply voltage.

$$HD2 \approx HD2_N \cdot V_{out,p} \quad (5-1)$$

$$HD3 \approx HD3_N \cdot V_{out,p}^2 \quad (5-2)$$

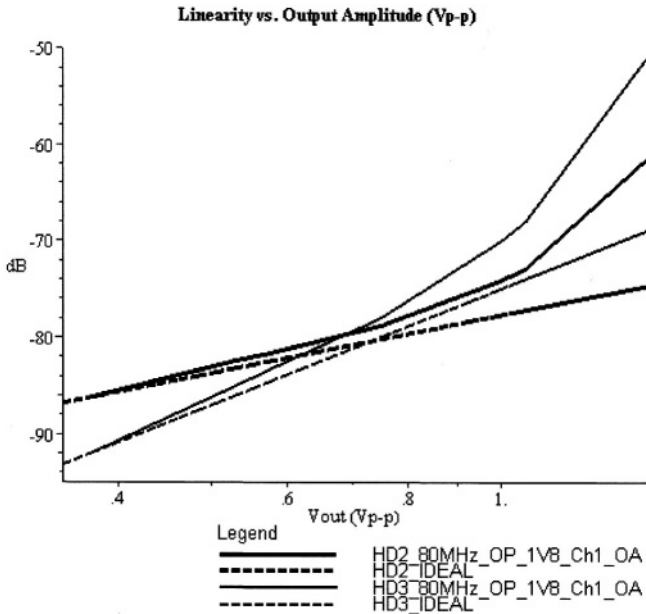


Figure 5-9.  $HD2$  and  $HD3$  versus output amplitude at 80MHz. The two curves named “\_IDEAL” are the weakly nonlinear values of  $HD2$  and  $HD3$ . The assumption made is that the circuit has weakly nonlinear behavior at  $0.35V_{p-p}$  output swing.

The next three figures are included to show the robustness of the linearity performance against variations in certain circuit conditions. All measurements are carried out at 80MHz input frequency and the nominal circuit conditions are the same as in Table 5-3.

In Figure 5-10 the measured values of  $HD2$ ,  $HD3$  and  $THD$  is plotted versus the input CM-voltage of the opamp.  $THD$  is computed from the first five harmonics. The figure shows that the optimum CM-voltage is between 0.8V and 0.9V. Outside this range, the harmonics increases, but are lower than  $-64\text{dB}$  in the range  $0.9V \pm 0.2V$  at 80MHz signal frequency.

Figure 5-11 shows the linearity performance versus the supply voltage. The CM-voltage is scaled with the supply voltage and the bias current is kept constant. When the supply voltage is increased to 1.9V,  $HD2$  and  $HD3$  both decreases below  $-80\text{dB}$ .  $THD$  is  $-78.7\text{dB}$  at 1.9V and less than  $-80\text{dB}$  at 2.0V supply voltage. At 1.6V  $HD2$  and  $HD3$  are still below  $-67\text{dB}$  and  $THD$  is below  $-63\text{dB}$ .

Figure 5-12 shows that changing the bias current ( $I_{BIAS}$  in Figure 5-1), around the typical value of  $250\mu\text{A}$ , a small variation in  $HD3$  (1.2dB) and a slightly larger variation in  $HD2$  (6dB) occur. Both  $HD2$  and  $HD3$  are lower at smaller bias currents.

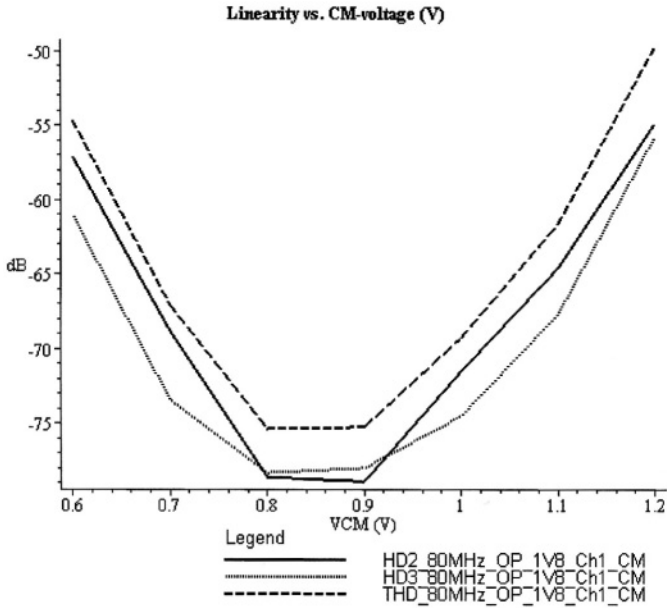


Figure 5-10. Linearity versus CM-voltage at 80MHz.

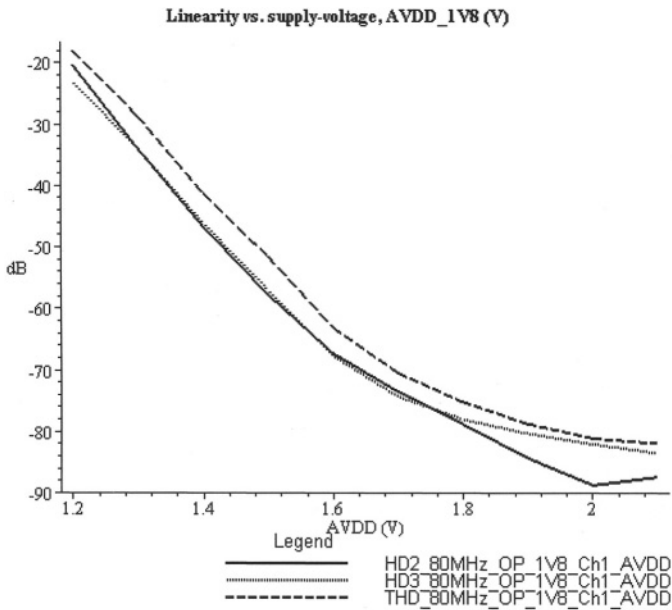


Figure 5-11. Linearity versus supply voltage at 80MHz.

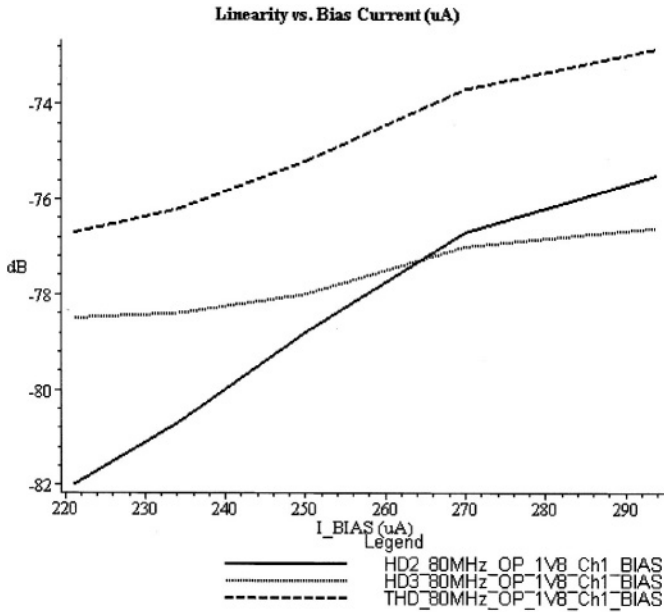


Figure 5-12. Linearity versus input bias current at 80MHz.

### 5.3 A 3.3V CMOS Opamp with $-80\text{dB}$ $HD_3$ at 80 MHz

In this section a CMOS opamp fabricated in a  $0.18\mu\text{m}$  process is presented. The opamp uses thick oxide transistors and has  $3.3\text{V}$  power-supply voltage. The OL-gain is  $79.6\text{dB}$  (typ.) and when connected in inverting configuration with CL-gain equal to  $-1$ , the bandwidth is  $1.99\text{GHz}$  (typ.). The opamp is optimized for low nonlinear distortion, especially low  $HD_3$ , using the design criteria described in Chapter 3 and Chapter 4. Measurements show  $HD_3$  less than  $-92\text{dB}$  at  $20\text{MHz}$  and less than  $-80\text{dB}$  at  $80\text{MHz}$  with  $1\text{Vp-p}$  signal swing at the output of the opamp.

#### 5.3.1 Design Considerations

The design considerations described for the  $1.8\text{V}$  opamp in section 5.2 are also used for the  $3.3\text{V}$  opamp. The folded cascode Miller opamp is shown in Figure 5-13. For Eldo simulations the test-bench of the  $1.8\text{V}$  opamp is used, adjusted for slightly different load. The reason for the adjustment is that another output pin on the package was used. The key computed and simulated results are shown in Table 5-4. The DC OL-gain is larger than for the  $1.8\text{V}$  opamp. However, the unity gain frequency, of the loop formed by the opamp and feedback network, is smaller. In addition, the FPBW is larger ensuring that the opamp is far from slewing in any of its nodes.

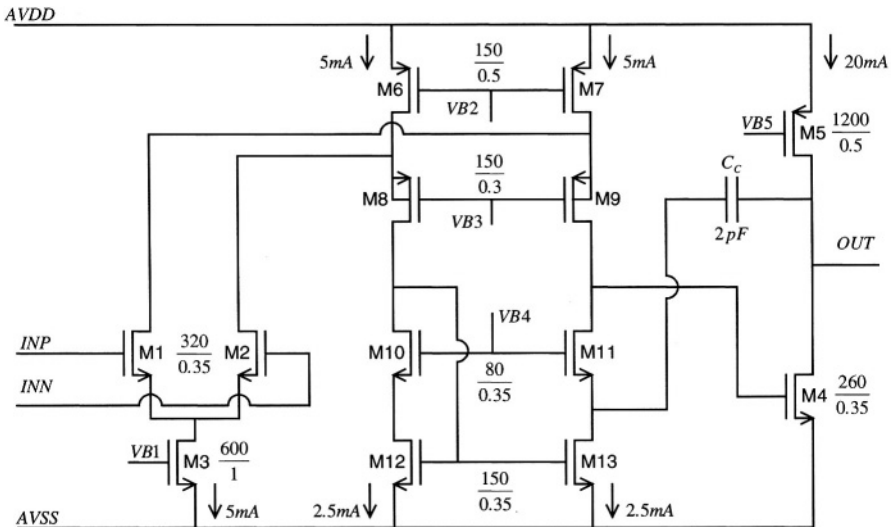


Figure 5-13. The  $3.3\text{V}$  opamp in  $0.18\mu\text{m}$  fabrication technology.

<b>3.3V CMOS Opamp</b>		
$AV_{DD}=3.3V, I_{BIAS}=250\mu A, V_{CM}=1.65V$ (input CM-voltage)		
Parameter	Values (typ.)	Unit
$A_0$ DC OL-Gain	79.6*	dB
$A_1$ ((3-13) on p. 48) DC-gain in 1 <sup>st</sup> stage	1201**	V/V
$A_2$ ((3-14) on p. 49) DC-gain in 2 <sup>nd</sup> stage	7.9**	V/V
$f_1$ Dominant pole	202*	kHz
$f_6$ ((4-24) on p. 74)	6.4**	MHz
$f_7$ ((4-25) on p. 74)	103**	MHz
$f_T$ Unity gain bandwidth of the opamp + feedback network	799*	MHz
$PM$ Phase Margin for opamp + feedback network	60.4*	degrees
$GM$ Gain Margin for opamp + feedback network	14.3*	dB
$f_{-3dB,CL}$ -3 dB bandwidth of the CL circuit, at the output of the opamp	1.99*	GHz
$f_{FPBW} = SR/(2\pi V_{peak}), V_{peak} = 0.5V$ Full Power Bandwidth	590*	MHz

Table 5-4. Estimated result for the 3.3V opamp. The estimated values are from simulations carried out in Eldo (\*) and equation given in previous chapters (\*\*). The simulations include the effects from the output pad, package and external load (see Figure 5-1). Additionally, parasitic capacitances are extracted from layout.

### 5.3.2 Contributions to Nonlinear Distortion

As for the 1.8V opamp the small-signal parameters and nonlinear coefficients are extracted for each of the transistors M1 to M5 in Figure 5-13 at their bias point. The values are given in Table 5-5, where  $g_{ol}$  and  $C_C$  are adjusted such that the DC-gain and the dominant pole of the opamp are equal in Maple and Eldo simulations. The accurate and approximated equations for 2<sup>nd</sup> and 3<sup>rd</sup> order responses are plotted in Figure 5-14 and Figure 5-15, respectively. The figures show that (4-23), (4-26) and (4-27) are describing the nonlinear behavior well.

M1 and M2 (W/L=320/0.35 (μm))					
1 <sup>st</sup> order		2 <sup>nd</sup> order		3 <sup>rd</sup> order	
$g_m$	29.3mS	$K2_{gm}$	104m	$K3_{gm}$	-68.9m
$g_d$	0.490mS	$K2_{gd}$	5.91μ	$K3_{gd}$	12.7μ
$g_{mb}$	8.15mS	$K2_{gmb}$	10.5m	$K3_{gmb}$	4.21m
$C_{GS}$	0.101pF	$K2_{gm\_gd}$	3.73m	$K3_{2gm\_gd}$	0.666m
$d_{gm}$	0.6%	$K2_{gmb\_gm}$	58.2m	$K3_{gm\_2gd}$	-0.25m
		$K2_{gmb\_gd}$	0.76m	$K3_{2gmb\_gm}$	5.39m
				$K3_{gmb\_2gm}$	-50.8m
				$K3_{2gmb\_gd}$	-0.175m
				$K3_{gmb\_2gd}$	-0.103m
				$K3_{gm\_gmb\_gd}$	-0.100m
M3 (W/L=600/1 (μm))					
1 <sup>st</sup> order		2 <sup>nd</sup> order		3 <sup>rd</sup> order	
$gd_3$	0.217mS	$K2_{gd3}$	-0.412m	$K3_{gd3}$	0.966m
$C_S$	0.820pF	$K2_{CS}$	-79.0f	$K3_{CS}$	27.5f
M4 (W/L=260/0.35 (μm))					
1 <sup>st</sup> order		2 <sup>nd</sup> order		3 <sup>rd</sup> order	
$gm_4$	57.2mS	$K2_{gm4}$	17.5m	$K3_{gm4}$	-20.1m
$gd_4$	0.975mS	$K2_{gd4}$	-0.185m	$K3_{gd4}$	0.130m
		$K2_{gm\_gd4}$	1.71m	$K3_{2gm\_gd4}$	-0.0944m
		$K2_{CDB4}$	-7.29f	$K3_{gm\_2gd4}$	-0.732m
				$K3_{CDB4}$	1.36f
M5 (W/L=1200/0.5 (μm))					
1 <sup>st</sup> order		2 <sup>nd</sup> order		3 <sup>rd</sup> order	
$gd_5$	0.444mS	$K2_{gd5}$	0.210m	$K3_{gd5}$	0.119m
		$K2_{CDB5}$	32.0f	$K3_{CDB5}$	5.86f
Other parameters					
$g_{ol}$	1/41.0kΩ	$C_6$	0.605pF	$R_L$	173Ω
$C_L$	8.8pF	$C_C$	2.35pF	$\beta$	½
$V_{OUT}$	1V <sub>P-P</sub>				

Table 5-5. Extracted parameters from the transistor models for the 3.3V opamp for use in Maple simulations of nonlinear distortion.

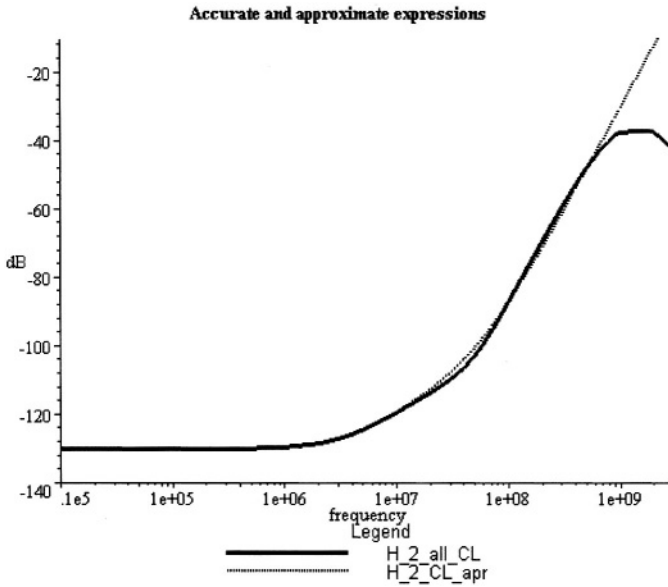


Figure 5-14. 2<sup>nd</sup> order response, accurate expression (“H\_2\_all\_CL”) and approximated expression (“H\_2\_CL\_apr”) for the 3.3V opamp.

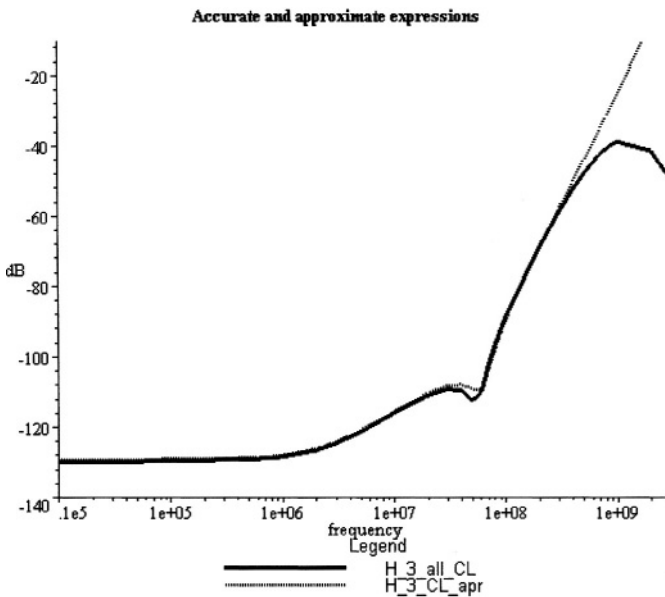


Figure 5-15. 3<sup>rd</sup> order response, accurate expression (“H\_3\_all\_CL”) and approximated expression (“H\_3\_CL\_apr”) for the 3.3V opamp.

It should be no surprise that  $H_{2V_{e\_CL}}(j\omega)$  and  $H_{3V_{e\_CL}}(j\omega)$  are the strongest contributions to 2<sup>nd</sup> and 3<sup>rd</sup> harmonic, respectively. The strongest contributions to  $H_{2V_{e\_CL}}(j\omega)$  are  $K_{2_{gm4}}$ ,  $K_{2_{gm\_gd4}}$ ,  $K_{2_{gd5}}$  and  $K_{2_{gd4}}$  at low frequency and  $K_{2_{gm4}}$  at high frequency. For  $H_{3V_{e\_CL}}(j\omega)$   $K_{3_{gd4}}$ ,  $K_{3_{gd5}}$ , and  $K_{3_{gm\_2gd4}}$  are the strongest contributions for low frequencies. For high frequencies,  $K_{2_{gm}}$  has a larger part of the total 3<sup>rd</sup> order distortion than was the case for the 1.8V opamp. At the frequency where  $K_{2_{gm}}$  becomes dominant, there is an optimum in the 3<sup>rd</sup> order response. As Figure 5-15 shows, this optimum is at approximately 50MHz.

Table 5-6 shows a comparison of the 3.3V opamp and 1.8V opamp of section 5.2. The design equations (4-28) to (4-30), given in section 4.2, describe the attenuation of the 2<sup>nd</sup> and 3<sup>rd</sup> order responses due to the Miller stage at frequencies below  $f_6$ , between  $f_6$  and  $f_7$  and above  $f_7$ , respectively. Equation (4-31) describes the asymptote for the nonlinear responses due to the input stage. The equations are quoted in Table 5-6. The frequencies  $f_1$ ,  $f_6$  and  $f_7$  ((3-15) p. 49, (4-24) and (4-25) p. 74, respectively) are zeros in the nonlinear responses. Their values for the 1.8V and 3.3V opamps are given in Table 5-1 and Table 5-4, respectively. Table 5-6 shows that at low frequency the 3.3V opamp has larger attenuation, and thus lower  $HD2$  and  $HD3$ , than the 1.8V opamp. At frequencies above  $f_6$  (of the 1.8V opamp) the 1.8V opamp suppress the harmonics more than the 3.3V opamp. However, because of smaller nonlinear coefficients the 3.3V opamp shows better linearity performance even at larger output voltage swing. The ratio between the supply voltage and threshold voltage is larger for the 3.3V transistors than for the 1.8V transistors. Thus, for the 1.8V opamp it was necessary to bias the transistors with lower GS overdrive. The nonlinear coefficients became higher as shown when comparing Table 5-2 and Table 5-5. This is also shown by the simulations. When comparing Figure 5-5 and Figure 5-6 with Figure 5-14 and Figure 5-15 the 3.3V opamp has better linearity performance even at higher output swing. This will also be shown by the measurement results presented in the next section.

Equation	1.8V opamp	3.3V opamp
$A_1 \cdot \beta \cdot gm_4, \quad f < f_6 \quad (4-28)$	9.83	34.4
$\beta \cdot \frac{gm \cdot gm_4}{C_6}, \quad f_6 < f < f_7 \quad (4-29)$	$3.24 \cdot 10^9$	$1.39 \cdot 10^9$
$\beta \cdot \frac{gm \cdot gm_4^2}{C_6 \cdot (C_C + C_L)}, \quad f > f_7 \quad (4-30)$	$32 \cdot 10^{18}$	$7.1 \cdot 10^{18}$
$\beta \cdot gm^2 \cdot \omega_{GBW}^3, \quad f > f_1 \quad (4-31)$	$3.1 \cdot 10^{27}$	$0.75 \cdot 10^{27}$

Table 5-6. Comparison of the attenuation of nonlinear responses between the 1.8V and 3.3V opamps. The equations are quoted from section 4.2.

### 5.3.3 Measurement Results

The measurements done on the 3.3V opamp are carried out by the same measurement system and the same procedures as for the 1.8V opamp. The results will be presented in the same order.

The measured values of  $HD2$  and  $HD3$  as a function of frequency are shown in Figure 5-16 and Figure 5-17, respectively, and tabulated for some test frequencies in Table 5-7. The opamp was optimized for low 3<sup>rd</sup> harmonic and the measurements shows that  $HD3$  is less than  $-92.7\text{dB}$  at 20MHz, less than  $-80.4\text{dB}$  at 80MHz and less than  $-64.8\text{dB}$  at 150MHz. The measurement was done with  $1V_{p-p}$  voltage swing at the output of the opamp. As for the 1.8V opamp the resistor between the output and the pad will perform filtering on the signal. The  $-3\text{dB}$  frequency is lower for the 3.3V opamp because of its output pin is worst-case regarding capacitive and inductive load. This effect is viewable in Figure 5-17. For frequencies above 120MHz the inclination in  $HD3$  falls off and is smaller than the Eldo simulation show. In addition,  $HD3$  is lower at 200MHz input frequency than at 150MHz. As for the 1.8V opamp, package and PCB effects is suspected to be the reason.

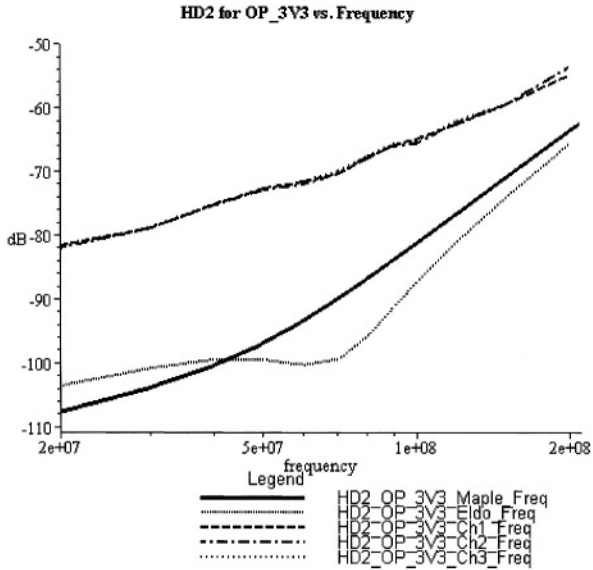


Figure 5-16. HD2 of the 3.3V opamp. The curves marked “Ch1” to “Ch3” are the measured results of three different circuit samples. The curves marked “Maple” and “Eldo” are the simulation results from Maple and Eldo, respectively.

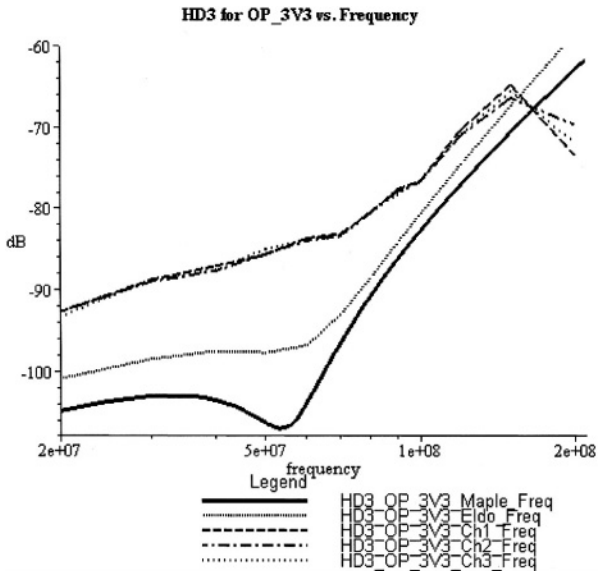


Figure 5-17. HD3 of the 3.3V opamp.

Measurements on 3.3V CMOS Opamp			
$V_{out} = 1.0V_{p-p}$ , $AVDD = 3.3V$ , $I_{BIAS} = 250\mu A$ , $V_{CM} = 1.65V$ (input CM-voltage)			
Parameter	Values (“worst” case of 3 samples)	Unit	
<b>HD2:</b> $f_{in} = 20MHz$	-81.6	dB	
	$f_{in} = 50MHz$	-72.7	dB
	$f_{in} = 80MHz$	-67.5	dB
	$f_{in} = 100MHz$	-64.9	dB
	$f_{in} = 150MHz$	-59.5	dB
<b>HD3:</b> $f_{in} = 20MHz$	-92.7	dB	
	$f_{in} = 50MHz$	-85.0	dB
	$f_{in} = 80MHz$	-80.4	dB
	$f_{in} = 100MHz$	-76.5	dB
	$f_{in} = 150MHz$	-64.8	dB

Table 5-7. Worst case *HD2* and *HD3* of three measured samples at some test frequencies.

For *HD2* the match between Eldo and Maple are better than for the 1.8V opamp. The inclination in the two curves are the same at low and high frequencies, but the Eldo simulations shows a minimum at 60MHz, which is not visible in the Maple simulation or the measurements. This is probably because of cancellations between different nonlinear coefficients of the cascode and the output transistors, as was the case for the 1.8V opamp.

The simulations carried out for *HD3* shows that both curves have the same inclination at low and high frequencies. Further, an optimum is located at approximately 55MHz. Additionally, the difference between the curves is smaller than for the 1.8V opamp. The reason is expected to be lower contributions from the folded cascode due to higher GS-overdrive that used for the 1.8V opamp.

The difference between simulated and measured *HD2* and *HD3* is larger than for the 1.8V opamp. The reason for this is suspected to be the transistor models and the belonging parameter sets, as was explained in section 5.2.3. The thick oxide transistors have other parameter sets than the thin oxide transistors. It seems that the parameter sets for the thick oxide transistors are less accurate regarding higher order derivatives and thus gives a poorer estimate of the nonlinear distortion.

The measurement results presented below are all carried out at 80MHz input frequency and at the circuit condition listed in Table 5-7. *THD* is computed from the first five harmonics.

In Figure 5-18 *HD2* and *HD3* are plotted versus the output amplitude. In addition, the weakly nonlinear versions of *HD2* and *HD3* are plotted (named “\_IDEAL”) using (5-1) and (5-2) and assuming that the opamp is acting as a

weakly nonlinear circuit at  $V_{out}=0.5V_{p-p}$ . This assumption was verified by simulations, where the opamp was simulated with an output voltage swing equal to  $100mV_{p-p}$ . When the simulation result was corrected for lower swing, it showed the same results as for  $1V_{p-p}$ . The measured results in Figure 5-18 shows that the opamp has weakly nonlinear behavior for output voltage swing lower than  $1.4V_{p-p}$ . This shows that the biasing guidelines of section 3.1 cause stable nonlinear coefficients in the entire range of the output voltage.

Figure 5-19 shows  $HD2$ ,  $HD3$  and  $THD$  as a function of the input CM-voltage at 80MHz input frequency. The figure shows that  $HD3$  has an optimum at the nominal value and is very stable over variations in the CM-voltage. On the other hand,  $HD2$  has a large decrease with increasing CM-voltage. The reason for this can be the trade-off made when optimizing for low  $HD3$ .

In Figure 5-20  $HD2$ ,  $HD3$  and  $THD$  are plotted versus the power supply voltage. In these measurements, the bias current was scaled down with the supply voltage. The measurements show that  $HD3$  is less than  $-60dB$  at 2V supply voltage, less than  $-70dB$  at 2.4V and less than  $-82dB$  at 3.5V at 80MHz signal frequency.

The nonlinear distortion versus the bias current ( $I_{BIAS}$  in Figure 5-1) is shown in Figure 5-21. Both  $HD2$  and  $HD3$  show only small variations over the range of the bias current, and  $HD3$  has a minimum for the nominal value of  $250\mu A$ .

The results described above show robust linearity performance against variations in circuit conditions. This is achieved by biasing the transistors that contribute most to distortion such that the nonlinear coefficients are relatively constant over variations in terminal voltages. The robustness for the 3.3V opamp is even better than for the 1.8V opamp because of the ratio between the supply and the threshold voltage is larger.

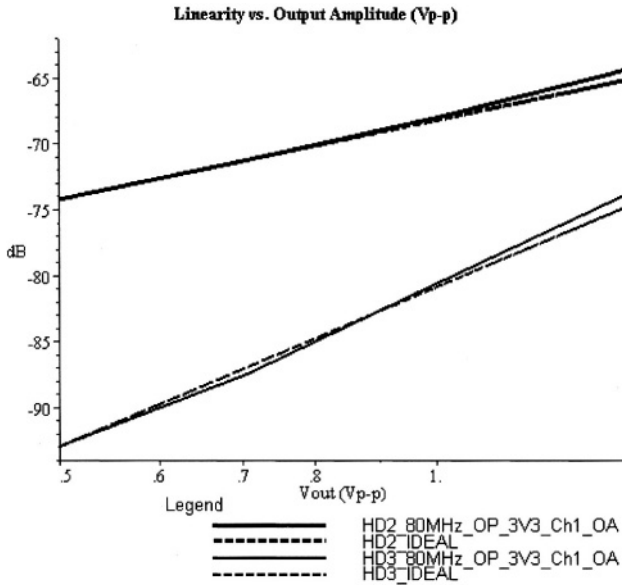


Figure 5-18. HD2 and HD3 versus output amplitude at 80MHz. The two curves named “\_IDEAL” are the weakly nonlinear values of HD2 and HD3. The assumption made is that the circuit has weakly nonlinear behavior at 0.5V<sub>p-p</sub> output swing.

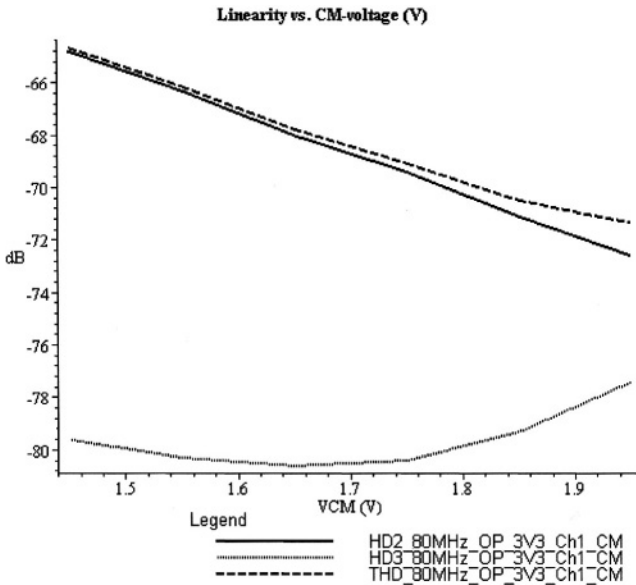


Figure 5-19. Linearity versus CM-voltage at 80MHz.

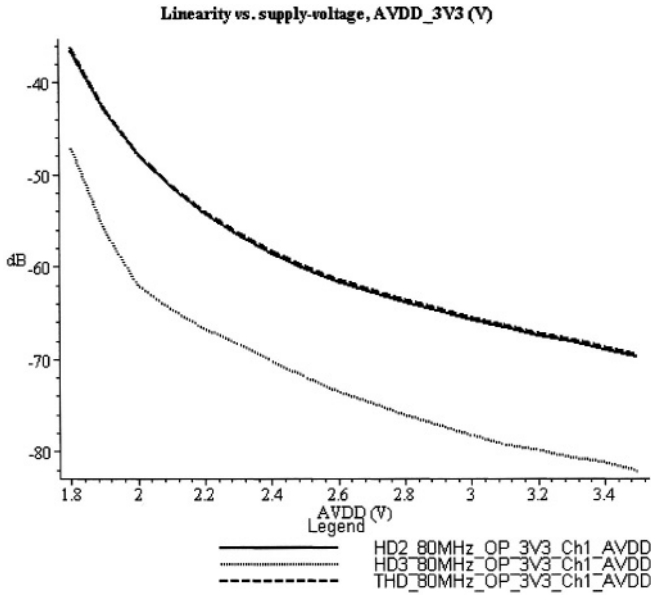


Figure 5-20. Linearity versus power-supply voltage at 80MHz. Here, the bias current is scaled with the power-supply voltage.

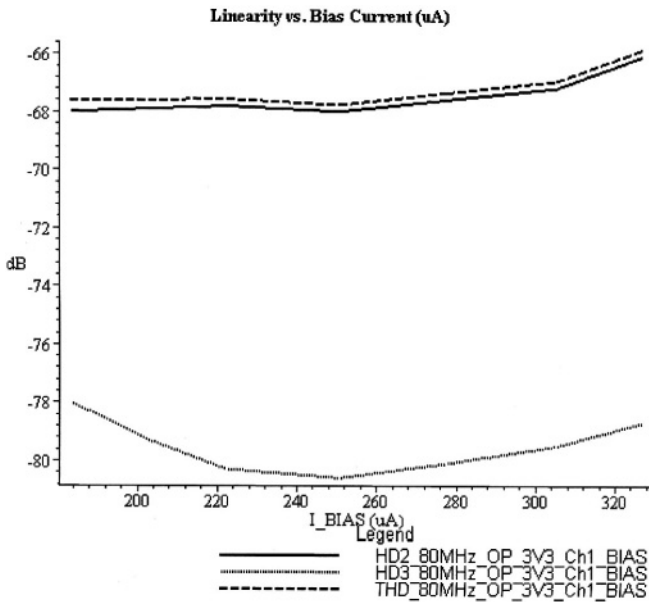


Figure 5-21. Linearity versus bias current at 80MHz.

## 5.4 A 3.3V CMOS Current Opamp with $-63\text{dB HD3}$ at 100MHz

A CMOS COA fabricated in a  $0.18\mu\text{m}$  process is presented in this section. The opamp uses thick oxide transistors and has 3.3V supply voltage. When the inverting opamp configuration is used, with CL gain equal to  $-1$ , the OL-gain of the opamp and feedback circuit is  $64.7\text{dB}$  (typ.) and the CL bandwidth equals  $724\text{MHz}$  (typ.). The opamp is optimized for low nonlinear distortion, especially low  $HD3$ , using the design criteria described in Chapter 4. Measurements show  $HD3$  less than  $-79\text{dB}$  at  $20\text{MHz}$  and less than  $-63\text{dB}$  at  $100\text{MHz}$  with  $1\text{Vp-p}$  signal swing at the output of the opamp.

### 5.4.1 Design Considerations

A COA is a device with one high impedance input node, one low impedance input node and a voltage or current output. The high impedance input node, which is the non-inverting input, has a voltage gain equal to 1 to the low impedance input node and sets the voltage on the inverting input. The main advantages of COA's are high SR (and FPBW) and constant CL bandwidth when altering the CL gain with  $R_f$  in Figure 5-1. When using the opamp with resistive feedback in switched systems the parasitic capacitance on the inverting input can be large due to switches. By using a COA the resistance level in the inverting node will be lowered and the parasitic pole will be at a frequency which is well above the GBW of the opamp. This is an additional advantage of the COA and was the main reason for doing this design.

COA are discussed in many scientific papers, e.g. in [13] to [16]. In [16], a low voltage COA is described and the idea for the circuit shown in Figure 5-22 was taken from this paper. The transistors M1 to M3 makes a one-stage "opamp" connected in unity gain. This "opamp" has the non-inverting terminal of the COA as the input and the inverting terminal as the output. This ensures relatively low resistance in the inverting input terminal of the COA and the voltage here is set by the non-inverting input. The current that flows into the inverting input goes through M2 and M1, into the folded cascode M7 and M9 and is converted to a voltage at the output of the cascode. The second stage, M4 and M5, is an ordinary Miller stage.

The COA in Figure 5-22 can be viewed as a Miller opamp with the differential input transistors replaced with a "current" input stage. Replacing  $A_I$  in  $H_{Ve}(j\omega)$  ((3-10), p. 48) with (5-4) the voltage transfer function from the inverting input terminal to the output of the opamp is obtained (5-3). Here,  $G_{im}$  in (5-4) is given by (5-6). The feedback factor for the COA with resistive feedback is given in (5-5). This is the same expression as for the

voltage opamp except for  $G_{inn}$  in the denominator. This causes the feedback factor for the COA to be lower than for the voltage opamp.

$$H_{ve,COA}(j\omega) \approx \frac{A_{1,COA} \cdot A_2}{\left(1 + j \frac{\omega}{\omega_1}\right)} \quad (5-3)$$

$$A_{1,COA} \approx \frac{G_{inn}}{g_{o1}} \quad (5-4)$$

$$\beta_{COA} = \frac{G_2}{G_1 + G_2 + G_{inn}} \quad (5-5)$$

$$G_{inn} \approx \frac{gm_2 + gd_2}{2} \quad (5-6)$$

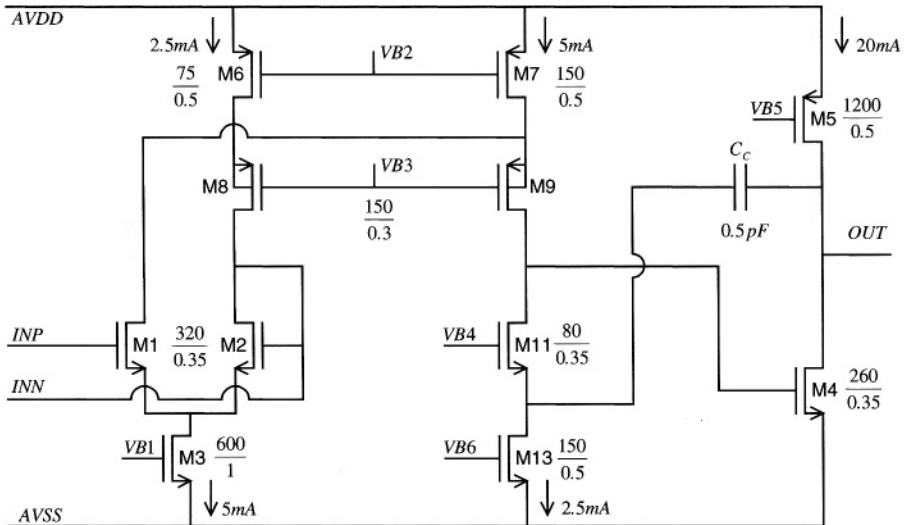


Figure 5-22. The 3.3V COA in 0.18 $\mu$ m fabrication technology.

The resulting opamp with transistor sizes and bias currents is shown in Figure 5-22 and its essential parameters are listed in Table 5-8. To show the difference in the harmonic linearity performance between COA and the voltage opamp, all transistors and bias currents are the same as for the 3.3V opamp, described in section 5.3. Because of the smaller feedback factor, the Miller capacitance  $C_C$  is set to 0.5pF. Table 5-8 shows an OL gain, for COA and the feedback circuit together, equal to 64.7dB(typ.). This is 12.5dB less than for the 3.3V opamp because of reduced  $\beta$ -factor and transconductance in the input stage. The FPBW is larger, as expected for COA.

<b>3.3V CMOS Current Opamp</b>		
$AVDD=3.3V, I_{BIAS}=250\mu A, V_{CM}=1.65V$ (input CM-voltage)		
Parameter	Values (typ.)	Unit
$A\beta_0$ DC OL Gain of the opamp + feedback network	64.7*	dB
$A_{1,COA}$ (5-4) DC-gain in 1 <sup>st</sup> stage	1090**	V/V
$A_2$ ((3-14) on p. 49) DC-gain in 2 <sup>nd</sup> stage	7.9**	V/V
$f_l$ Dominant pole	374*	kHz
$f_6$ ((4-24) on p. 74)	3.7**	MHz
$f_7$ ((4-25) on p. 74)	119**	MHz
$f_T$ Unity gain bandwidth of the opamp + feedback network	494*	MHz
$PM$ Phase Margin for opamp + feedback network	64.5*	degrees
$GM$ Gain Margin for opamp + feedback network	15.1*	dB
$f_{-3dB,CL}$ -3 dB bandwidth of the CL circuit, at the output of the opamp	724*	MHz
$f_{FPBW} = SR/(2\pi V_{peak}), V_{peak} = 0.5V$ Full Power Bandwidth	759*	MHz

Table 5-8. Estimated results for the 3.3V COA. The estimated values are from simulations carried out in Eldo (\*) and equations given above, and in previous chapters (\*\*). The simulations include the effects from the output pad, package and external load (see Figure 5-1). Additionally, parasitic capacitances are extracted from layout.

### 5.4.2 Contributions to Nonlinear Distortion

For simulation in Maple the same small-signal parameters and nonlinear coefficients were used as for the 3.3V opamp in section 5.3. The output conductance of the folded cascode  $g_{ol}$  and  $C_C$  were adjusted such that the OL gain and the dominant pole obtained in Maple and Eldo were equal. The capacitive load is also different because the COA uses another output pin on the package and has another PCB loading. All parameters are given in Table 5-9 (p. 119).

The model of the circuit implemented in Maple is shown in Figure 5-23. Here, the COA and the feedback network are modeled together and solved as one set of equations. Thus, the CL transfer functions are found directly, and not by finding the OL responses first as were done for the voltage opamps. The drawback is the increased difficulties obtaining simplified symbolic expressions for the nonlinear responses. However, since the voltage opamps and COA are similar circuits, symbolic expressions for the CL transfer functions for COA can be obtained from the equations for the voltage opamp given in section 4.2. This is done by replacing  $A_1$  and  $\beta$  in (4-23), (4-26) and (4-27) with  $A_{1,COA}$  and  $\beta_{COA}$  given by (5-4) and (5-5), respectively. Additionally, the term due to  $K2_{gm}$  must be multiplied with  $\frac{1}{2}$  since the output from the first stage of the COA is not differential. The accurate and simplified 2<sup>nd</sup> and 3<sup>rd</sup> order responses are plotted together in Figure 5-24 and Figure 5-25, respectively (p. 120). The plots show close match, indicating the correctness of the simplified equations.

The contributions to the 2<sup>nd</sup> order response are  $K2_{gm4}$ ,  $K2_{gm\_gd4}$ ,  $K2_{gd5}$  and  $K2_{gd4}$  at low frequency and  $K2_{gm4}$  at high frequency, which is the same as for the 3.3V opamp. For the 3<sup>rd</sup> order response  $K3_{gd4}$ ,  $K3_{gd5}$ , and  $K3_{gm\_2gd4}$  are the strongest contribution at low frequencies and  $K3_{gm4}$ ,  $K2_{gm4}$  and  $K2_{gm}$  at high frequencies. Near the frequency where the high-frequency contributions take over, an optimum occurs due to canceling of effects. This optimum is located at a higher frequency than for the 3.3V opamp, because of weaker contribution from  $K2_{gm}$ .

In Table 5-10 (p. 121) the design equations (4-28) to (4-31) for the voltage opamp are compared to (5-7) to (5-10) below. The equations below are achieved by replacing  $\beta$  and  $A_1$  with  $\beta_{COA}$  and  $A_{1,COA}$ , respectively. Because of the reduced feedback factor and the reduced voltage gain in the input stage, the COA has lower attenuation of the nonlinear responses. Especially in the frequency range between  $f_6$  and  $f_7$ , COA has poor linearity performance. This will also be shown when comparing the measurement results from the circuits.

$$A_{1,COA} \cdot \beta_{COA} \cdot gm_4, \quad f < f_6 \tag{5-7}$$

$$\beta_{COA} \cdot A_{1,COA} \cdot gm_4 \cdot \omega_6 \approx \beta_{COA} \cdot \frac{1}{2} \cdot \frac{gm \cdot gm_4}{C_6}, \quad f_6 < f < f_7 \tag{5-8}$$

$$\beta_{COA} \cdot A_{1,COA} \cdot gm_4 \cdot \omega_6 \cdot A_2 \cdot \omega_7 \approx \frac{1}{2} \cdot \beta_{COA} \cdot \frac{gm \cdot gm_4^2}{C_6 \cdot (C_C + C_L)}, \quad f > f_7 \tag{5-9}$$

$$\frac{gm^2}{2} \cdot \beta_{COA} \cdot \omega_{GBW}^3, \quad f > f_1 \tag{5-10}$$

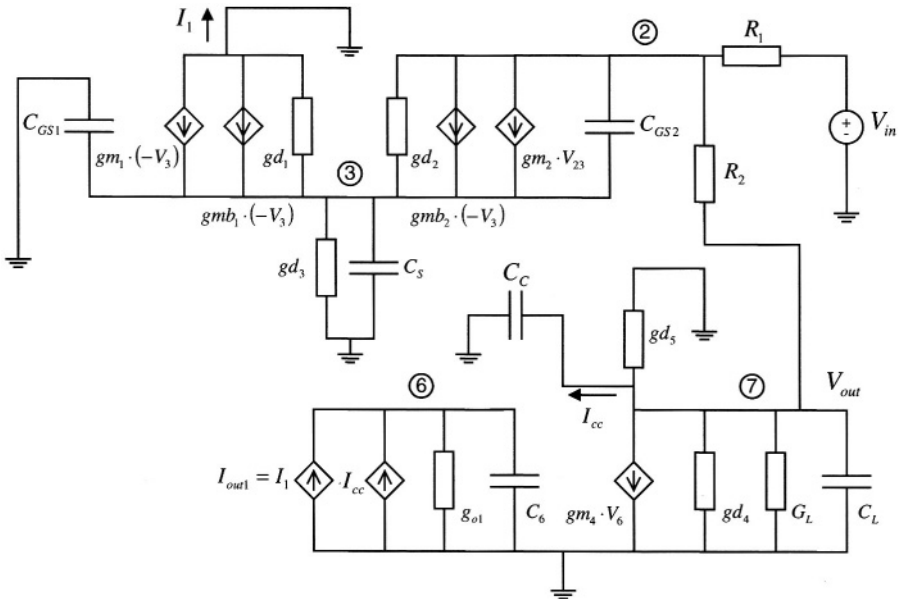


Figure 5-23. Model of the COA used for simulations of nonlinear responses in Maple.

<b>M1 and M2 (W/L=320/0.35 (μm))</b>					
1 <sup>st</sup> order		2 <sup>nd</sup> order		3 <sup>rd</sup> order	
$g_m$	29.3mS	$K2_{gm}$	104m	$K3_{gm}$	-68.9m
$g_d$	0.490mS	$K2_{gd}$	5.91μ	$K3_{gd}$	12.7μ
$g_{mb}$	8.15mS	$K2_{gmb}$	10.5m	$K3_{gmb}$	4.21m
$C_{GS}$	0.101pF	$K2_{gm\_gd}$	3.73m	$K3_{2gm\_gd}$	0.666m
$d_{gm}$	0.6%	$K2_{gmb\_gm}$	58.2m	$K3_{gm\_2gd}$	-0.247m
		$K2_{gmb\_gd}$	0.76m	$K3_{2gmb\_gm}$	5.39m
				$K3_{gmb\_2gm}$	-50.8m
				$K3_{2gmb\_gd}$	-0.175m
				$K3_{gmb\_2gd}$	-0.103m
				$K3_{gm\_gmb\_gd}$	-0.100m
<b>M3 (W/L=600/1 (μm))</b>					
1 <sup>st</sup> order		2 <sup>nd</sup> order		3 <sup>rd</sup> order	
$g_{d3}$	0.217mS	$K2_{gd3}$	-0.412m	$K3_{gd3}$	0.966m
$C_S$	0.820pF	$K2_{CS}$	-79.0f	$K3_{CS}$	27.5f
<b>M4 (W/L=260/0.35 (μm))</b>					
1 <sup>st</sup> order		2 <sup>nd</sup> order		3 <sup>rd</sup> order	
$g_{m4}$	57.2mS	$K2_{gm4}$	17.5m	$K3_{gm4}$	-20.1m
$g_{d4}$	0.975mS	$K2_{gd4}$	-0.185m	$K3_{gd4}$	0.130m
		$K2_{gm\_gd4}$	1.71m	$K3_{2gm\_gd4}$	-0.0944m
		$K2_{CDB4}$	-7.29f	$K3_{gm\_2gd4}$	-0.732m
				$K3_{CDB4}$	1.36f
<b>M5 (W/L=1200/0.5 (μm))</b>					
1 <sup>st</sup> order		2 <sup>nd</sup> order		3 <sup>rd</sup> order	
$g_{d5}$	0.444mS	$K2_{gd5}$	0.210m	$K3_{gd5}$	0.119m
		$K2_{CDB5}$	32.0f	$K3_{CDB5}$	5.86f
<b>Other parameters</b>					
$g_{ol}$	1/71.75k	$C_6$	0.605pF	$R_L$	1276Ω
$C_L$	9.0pF	$C_C$	0.687pF	$\beta_{COA}$	0.2
$V_{OUT}$	1V <sub>pp</sub>				

Table 5-9. Extracted parameters from the transistor models for the 3.3V opamp for use in Maple simulations of nonlinear distortion.

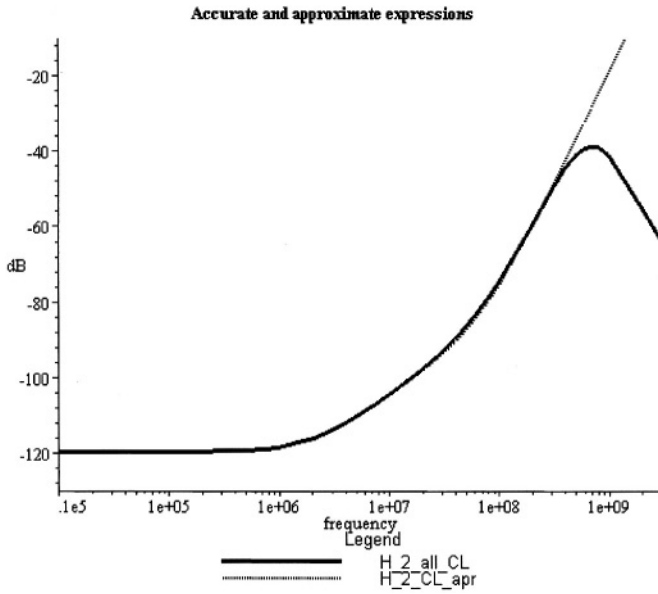


Figure 5-24. 2<sup>nd</sup> order response, accurate expression (“H\_2\_all\_CL”) and approximated expression (“H\_2\_CL\_apr”) for the 3.3V COA.

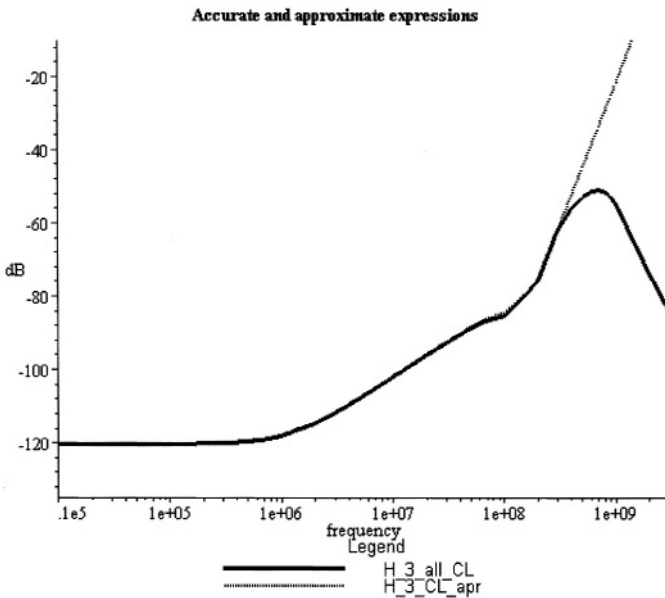


Figure 5-25. 3<sup>rd</sup> order response, accurate expression (“H\_3\_all\_CL”) and approximated expression (“H\_3\_CL\_apr”) for the 3.3V COA.

Equations	3.3V Opamp	3.3V COA	Difference
(4-28) and (5-7), $f < f_6$	34.4	12.4	8.9dB
(4-29) and (5-8), $f_6 < f < f_7$	$1.39 \cdot 10^9$	$0.29 \cdot 10^9$	13.6dB
(4-30) and (5-9), $f > f_7$	$7.1 \cdot 10^{18}$	$1.6 \cdot 10^{18}$	13dB
(4-31) and (5-10), $f > f_1$	$0.75 \cdot 10^{27}$	$0.71 \cdot 10^{27}$	0.5dB

Table 5-10. Comparison of the attenuation of nonlinear responses between the COA and the 3.3V opamps.

### 5.4.3 Measurement Results

The measurements for the COA are carried out on three samples of the circuit using the same procedure as for the opamps described previously. The results will be presented in the same way and compared to the results of the 3.3V opamp.

The measured  $HD2$  and  $HD3$  are shown in Figure 5-26 and Figure 5-27, respectively, and the worst case sample is tabulated in Table 5-11 for some test frequencies. Measurements show that  $HD2$  is less than  $-69.0$ dB at 20MHz,  $-56.4$ dB at 80MHz and  $-53.7$ dB at 100MHz.  $HD3$  is less than  $-79.3$ dB,  $-65.9$ dB and  $-62.9$ dB at the same frequencies, respectively.

At 20MHz signal frequency the difference between COA and the 3.3V opamp is 12.6dB and 13.4dB for  $HD2$  and  $HD3$ , respectively. This corresponds to the second row of Table 5-10, which gives 13.6dB. At 150MHz, which is above  $f_7$  but below where the input differential pair becomes dominant, the difference between COA and the voltage opamp should be 13dB according to the 3<sup>rd</sup> row of the table. The measurements show 10.3dB and 9.2dB difference in  $HD2$  and  $HD3$ , respectively. This shows that a voltage opamp has better performance regarding nonlinear distortion than COA. This is also predicted accurately by the design equations compared in Table 5-10.

The difference between the simulations carried out in Maple and Eldo are smaller than for the voltage opamp for both  $HD2$  and  $HD3$ . However, the gap from simulations to measurements is about the same as for the voltage opamp. This is no surprise since the same transistor models and parameters are used.

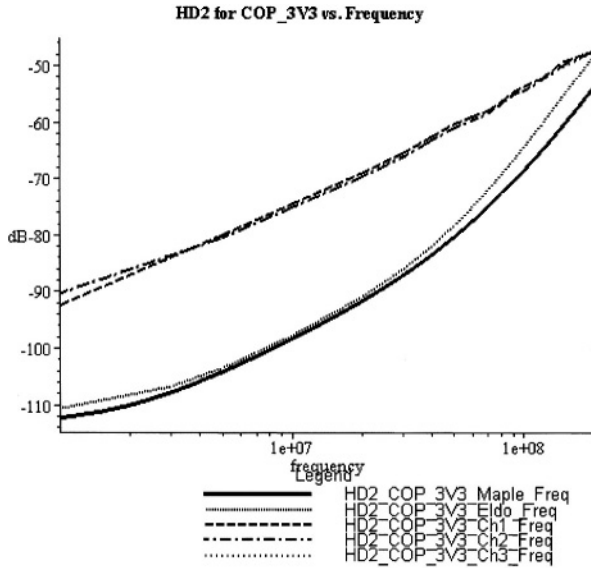


Figure 5-26. HD2 of the 3.3V COA. The curves marked “Ch1” to “Ch3” are the measured results of three different circuit samples. The curves marked “Maple” and “Eldo” are the simulation results from Maple and Eldo, respectively.

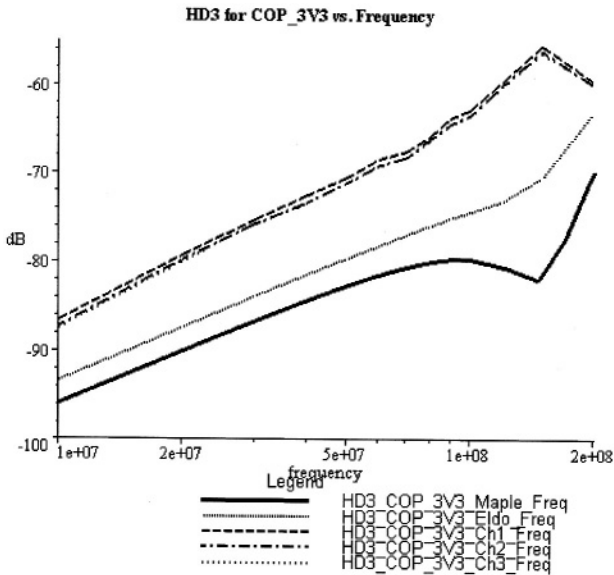


Figure 5-27. HD3 of the 3.3V COA.

Measurements on 3.3V CMOS Current Opamp		
$V_{out}=1.0V_{p-p}$ , $AVDD=3.3V$ , $I_{BIAS}=250\mu A$ , $V_{CM}=1.65V$ (input CM-voltage)		
Parameter	Values ("worst" case of 3 samples)	Unit
<b>HD2:</b> $f_{in}=20MHz$	-69.0	dB
$f_{in}=50MHz$	-60.3	dB
$f_{in}=80MHz$	-56.4	dB
$f_{in}=100MHz$	-53.7	dB
$f_{in}=150MHz$	-49.2	dB
<b>HD3:</b> $f_{in}=20MHz$	-79.3	dB
$f_{in}=50MHz$	-70.6	dB
$f_{in}=80MHz$	-65.9	dB
$f_{in}=100MHz$	-62.9	dB
$f_{in}=150MHz$	-55.6	dB

Table 5-11. Worst case *HD2* and *HD3* of three measured samples at some test frequencies.

In Figure 5-28 the measured and ideal *HD2* and *HD3* are plotted as a function of the COA output amplitude. As for the voltage opamps (5-1) and (5-2) are used as the ideal curves, assuming that the opamp is acting as a weakly nonlinear circuit at  $V_{out}=0.35V_{p-p}$ . The deviation from the weakly nonlinear behavior is small for signal amplitude below  $1.4V_{p-p}$ . This indicates that the transistors in the circuit are biased such that the nonlinear coefficients are nearly constant in this voltage range.

In Figure 5-29, Figure 5-30 and Figure 5-31 *HD2*, *HD3* and *THD* are plotted against CM-voltage, supply voltage and bias current ( $I_{BIAS}$  in Figure 5-1), respectively. All measurements are carried out with the signal frequency equal to 80MHz. All these plots show lower performance than the 3.3V opamp. However, the shapes are mainly the same.

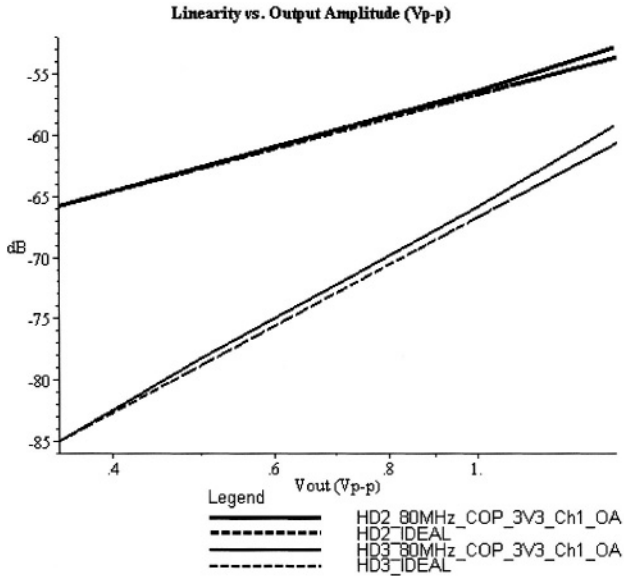


Figure 5-28. *HD2* and *HD3* versus output amplitude at 80MHz. The two curves named “\_IDEAL” are the weakly nonlinear values of *HD2* and *HD3*. The assumption made is that the circuit has weakly nonlinear behavior at 0.35V<sub>p-p</sub> output swing.

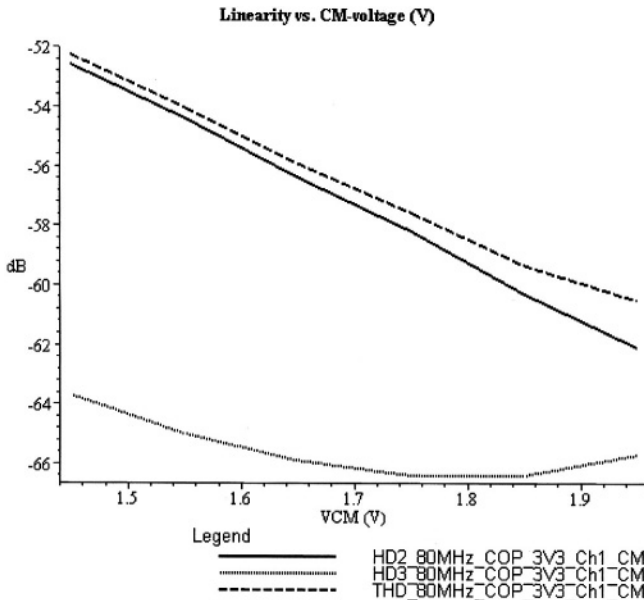


Figure 5-29. Linearity versus CM-voltage at 80MHz.

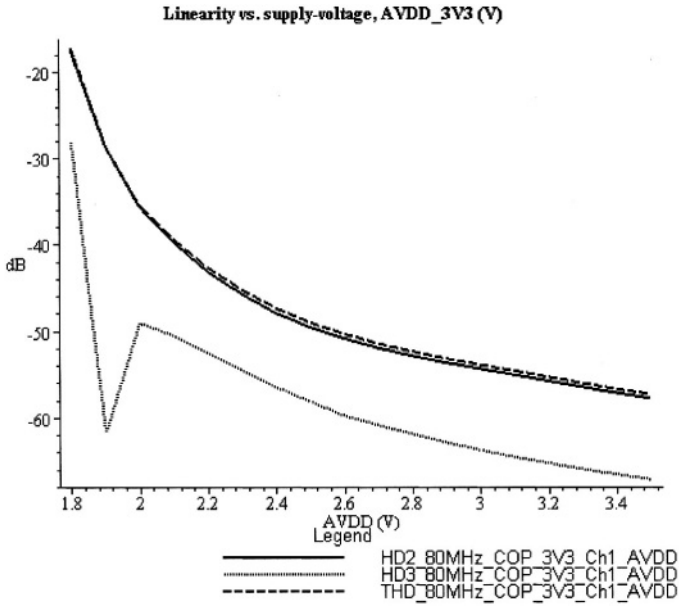


Figure 5-30. Linearity versus power-supply voltage at 80MHz. The bias current is scaled with the power-supply voltage.

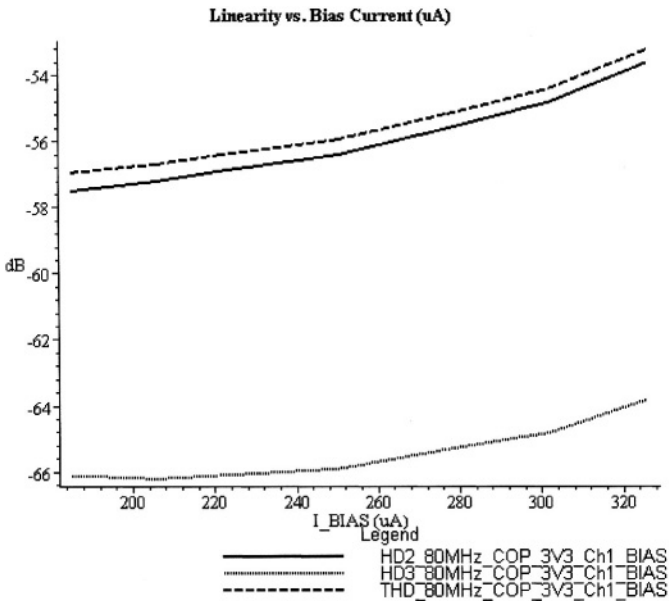


Figure 5-31. Linearity versus bias current at 80MHz.

### 5.5 A 3.3V CMOS Unity-Gain Opamp with $-80\text{dB HD}_3$ at 10MHz

A unity-gain CMOS opamp with high linearity performance is presented [1]. The opamp is fabricated in a  $0.35\mu\text{m}$  process and has 3.3V supply voltage. The OL-gain of the one-stage opamp is 51.9dB (typ.) and the CL bandwidth equals 624MHz (typ.). The opamp uses a tail current compensation circuit to increase the resistance of the tail current source of the input differential pair. As shown in section 4.1 this resistance has to be high to keep the CM-gain low and thus to achieve low distortion at low frequencies. Additionally, the shape of the tail current was optimized for low  $HD_3$  at high frequencies, compensating for non-linearities in the differential input stage together with the folded cascode, which makes the output stage of the opamp. The simulated characteristics of the opamp are shown in Table 5-12. The measurements show  $HD_3$  less than  $-80\text{dB}$  at 10MHz and less than  $-60\text{dB}$  up to 80MHz with 1Vp-p signal swing at the output of the opamp. The circuit and measurement system is thoroughly explained in the paper.

3.3V CMOS Unity-Gain Opamp		
$AVDD=3.3\text{V}$ , $I_{BIAS}=250\mu\text{A}$ , $V_{CM}=1.65\text{V}$ (input CM-voltage), $C_L=9\text{pF}$		
Parameter	Values (typ.)	Unit
$A_0$ DC OL Gain of the opamp	51.9	dB
$f_l$ Dominant pole	1.94	MHz
$f_T$ Unity gain bandwidth of the opamp	675	MHz
$PM$ Phase Margin for opamp	54.0	degrees
$GM$ Gain Margin for opamp	21.5	dB
$f_{-3\text{dB},CL}$ -3 dB bandwidth of the CL circuit	1.0	GHz
$f_{FPBW} = SR/(2\pi V_{peak})$ , $V_{peak} = 0.5\text{V}$ Full Power Bandwidth	211	MHz

Table 5-12. Estimated result for the 3.3V unity-gain opamp. The values are from Eldo simulations, which are done with parasitic capacitances extracted from layout.

The opamp is made for on-chip applications and therefore has a well-defined capacitive load. Thus, it was necessary to design a voltage buffer to bring the signal off-chip. To avoid affecting the measurements of the

harmonics from the opamp, the buffer must have linearity performance far beyond the opamp. The buffer is shown in Figure 5-32. The transistor M3 makes a source follower with M1 and M2 as the cascoded current source. To make the DS-voltage of M3 relatively constant, and thus enhance the linearity performance, M4 and M5 are added. M4 is a source follower with M5 as the current source, ensuring that the voltage on the drain of M3 follows the input signal. Since this circuit was designed for test purposes only, high bias currents and supply voltage could be used. Thus,  $AVDD\_2$  was set to 6.5V and the transistors were biased such that non of them had terminal voltages larger than 3V, even in the start up of the circuit. According to simulation results the 3<sup>rd</sup> harmonic was below -100dB up to 120MHz and was thus well below what was expected for the opamp. However, the measurement results showed that the linearity performance of the buffer was far lower than estimated by simulation and on the same level as the opamp. Thus, it was necessary to estimate the  $HD_3$  of the opamp. This is explained in [1]. Some simulated parameters for the voltage buffer are shown in Table 5-13.

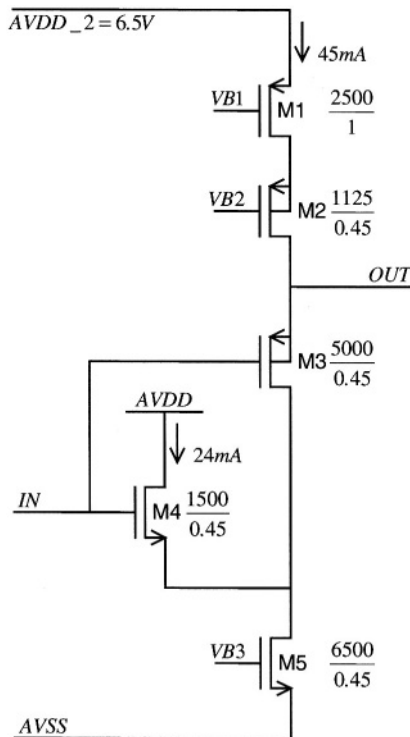


Figure 5-32. Voltage buffer, to buffer the signal from the opamp to the off-chip load.

<b>6.5V CMOS Voltage Buffer</b>		
<i>AVDD</i> =3.3V, <i>AVDD_2</i> =6.5V, <i>I<sub>BIAS</sub></i> =350μA, <i>V<sub>CM</sub></i> =2.0V (input CM-voltage)		
Parameter	Values (typ.)	Unit
DC output voltage	3.0	V
DC Gain	0.0	dB
<i>f<sub>-3dB,CL</sub></i> -3 dB bandwidth	677	MHz
<i>f<sub>FPBW</sub></i> = <i>SR</i> /(2π <i>V<sub>peak</sub></i> ), <i>V<sub>peak</sub></i> = 0.225V Full Power Bandwidth	1.8	GHz

Table 5-13. Simulated result for the 6.5V voltage buffer. The simulations are carried out in Eldo with the effects from the output pad, external load and parasitic capacitances extracted from layout.

## 5.6 Concluding Remarks

In this chapter, four opamps have been presented, all designed to have low distortion. Three were connected in inverting opamp configuration and one in unity gain, which is a special case of the non-inverting configuration.

The opamps in inverting configuration were designed and optimized using the biasing guidelines described in section 3.1 and the design equations of 4.2. All show high linearity performance and robustness against variations in circuit conditions. Further, the difference between the voltage opamp and COA was shown. Because of lower feedback factor, due to low input resistance, COA has less attenuation of the nonlinear responses and thus lower linearity performance than the voltage opamp.

As described in Chapter 4, the non-inverting configuration has a drawback due to high CM-voltage swing on the input terminals of the opamp. This causes the input differential pair to contribute significantly to nonlinear distortion. The presented unity-gain opamp utilizes a tail current compensation circuit to increase the output resistance of the tail current source. Additionally, the tail current was shaped such that some of the distortion from the rest of the opamp was canceled out. The opamp shows low *HD3* with an optimum at 70MHz. However, the distortion figures were poorer than for all the opamps designed for the inverting configuration. Thus, for superior linearity performance at low supply voltages the inverting opamp configurations should be preferred.

A problem in the design of circuits with high linearity is to make reliable estimates of the distortion. As shown in this chapter, the gaps between simulations and measured results are large. The reason for this is suspected to be inaccurate modeling of higher order derivatives of the transistor current. It is possible to optimize the parameter set, used for the transistor

model, to achieve better accuracy in higher order derivatives. More reliable simulation results give improved optimization. Further, it gives the opportunity to exploit canceling between nonlinear coefficients with different sign. Thus, opamps with even lower distortion can be achieved.

Design of low distortion opamps in modern CMOS technologies is difficult because of the low supply voltage. Thus, it is of major importance to have large insight and understanding of the nonlinear behavior of opamp circuits. By using the biasing guidelines of section 3.1 and the CL equations for the harmonic responses of Chapter 4, it was possible to obtain opamp circuits with high linearity even at low supply voltage. To visualize the value of the biasing guidelines and the design equations, a comparison between the 1.8V opamp and previous work is carried out below.

It was difficult to find scientific papers that report opamps with low distortion at frequencies from 10MHz to 100MHz. However, [17] and [18] describes similar circuits. In [17] a differential IF amplifier in 0.8 $\mu$ m CMOS technology and 3.3V supply voltage was described. For a differential output voltage at 1V<sub>p-p</sub> (which is 0.5V<sub>p-p</sub> single ended) it was reported *THD* equal to 0.006%, or -84.4dB, at 20MHz signal frequency. In [18] a bipolar IF amplifier was described with 5V supply voltage. At 20MHz and 5V<sub>p-p</sub> differential output voltage, 0.068% *THD* was reported, which is -63.4dB. In both papers, the measurements were done with 1KOhm load. Since these circuits are differential, the odd harmonics are the strongest contributions to *THD*. *THD* for the 1.8V opamp was -88.5dB at 20MHz including odd and even harmonics up to 5<sup>th</sup> harmonic, where the 2<sup>nd</sup> and 3<sup>rd</sup> harmonics were the strongest contributions.

The opamps presented in section 5.2 to 5.4 and some commercial available opamps, AD8037 and AD8009 [19], are compared in Figure 5-33 and Figure 5-34. The commercial available opamps are intended for applications that require low distortion and are the opamps with the highest linearity performance found (October 2001). The comparison criteria are the 2<sup>nd</sup> and 3<sup>rd</sup> order harmonic intercept point, *IP*2<sub>h</sub> and *IP*3<sub>h</sub>, defined in section 2.1. For each opamp, the intercept points are obtained by using (5-11) and (5-12) below, and further inserting the output amplitude, *HD*2 and *HD*3 of the opamp. The assumption is that, at the signal swing that they were tested, the opamps are acting weakly nonlinear. For the 3.3V opamp and the 3.3V COA, this is a good approximation. For the 1.8V opamp, the assumption is pessimistic. The commercial available opamps are tested with a signal swing equal to 1/5 of the supply voltage, which is far lower than for the opamps presented in this chapter. Thus, AD8037 and AD8009 should also be acting weakly nonlinear.

$$IP2_h = 20 \cdot \log_{10}(V_{peak}) - HD2 \quad (5-11)$$

$$IP3_h = 20 \cdot \log_{10}(V_{peak}) - \frac{1}{2} \cdot HD3 \quad (5-12)$$

As explained in section 2.1, the harmonic intercept points,  $IP2_h$  and  $IP3_h$ , describe the nonlinear coefficients of 2<sup>nd</sup> and 3<sup>rd</sup> order, respectively. These coefficients are frequency dependent. Thus, in Figure 5-33 and Figure 5-34 the intercept points are found for four different frequencies. Further, for all opamps the intercept points are referred to the signal amplitude at the output of the opamp.

For  $IP2_h$ , Figure 5-33 shows that the 1.8V opamp is far better than the other opamps. Further, both the 1.8V and the 3.3V opamps show higher  $IP2_h$  than AD8037 and AD8009.

A comparison of  $IP3_h$  in Figure 5-34 shows that the 3.3V opamp has the best performance and thus the lowest 3<sup>rd</sup> order nonlinear coefficient.  $IP3_h$  for AD8037 and AD8009 are closer to the 1.8V and 3.3V opamps than was the case for  $IP2_h$ . The reason can be that they are optimized for low 3<sup>rd</sup> order nonlinear coefficient. The 3<sup>rd</sup> order coefficient is the reason for the 3<sup>rd</sup> order intermodulation product. In a multi-channel communication system it is important that the 3<sup>rd</sup> order intermodulation product is small. This is because of the 3<sup>rd</sup> order mixing of two relatively close frequency components will cause distortion components in the same frequency band.

The comparison in Figure 5-33 and Figure 5-34 shows that it is possible to obtain highly linear opamps in deep sub-micron CMOS technologies by using the design method and design equations presented in this book.

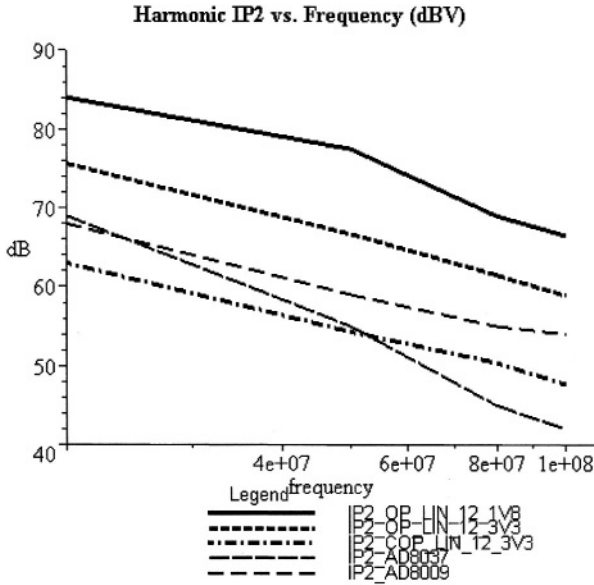


Figure 5-33. Comparison of harmonic IP2.

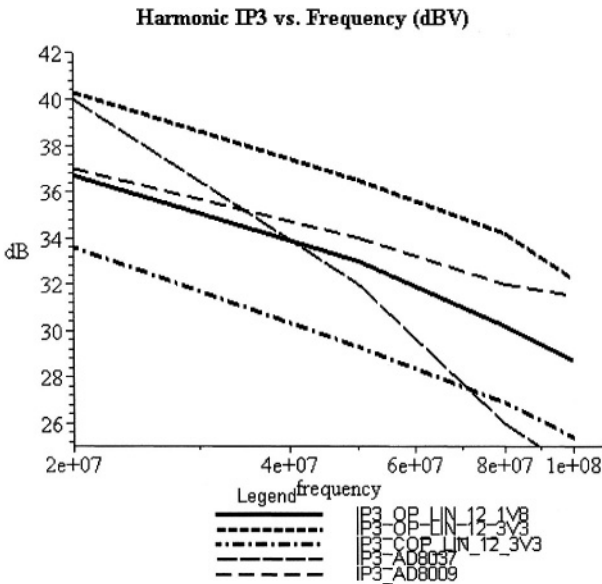


Figure 5-34. Comparison of harmonic IP3.

## REFERENCES

- [1] B. Hernes, Ø. Moldsvor, T. Sæther, "A -80dB HD3 Opamp in 3.3V CMOS Technology using Tail Current Compensation," *IEEE International Symposium on Circuits and Systems 2001*, vol. 1, 2001, pp. 216-219.
- [2] Rohde & Schwarz SML 03, see <http://www.rohde-schwarz.com/Homepage>
- [3] TTE, KC4 bandpass filter, see <http://www.tte.com/>
- [4] Hewlett-Packard Company, "HP89440A/HP89441A Operator's Guide", HP part number 89441-90053, Nov. 1996
- [5] Hewlett-Packard Company, "HP89410A Operator's Guide", HP part number 89410-90079, Nov. 1996
- [6] nAD1080-18, see <http://www.nvlsi.no>
- [7] nAD 1280-18T, see <http://www.nvlsi.no>
- [8] R. Hogervorst, J. H. Huijsing, "Design of Low-Voltage, Low-Power Operational Amplifier Cells," Norwell, MA: Kluwer Academic Publishers, 1996.
- [9] Eldo, See <http://www.mentorg.com/eldo/overview.html>
- [10] Maple 6, See <http://www.maplesoft.com/>
- [11] Y. Cheng, M. Chan, K. Hui, M. Jeng, Z. Liu, J. Huang, K. Chen, J. Chen, R. Tu, P. K. To, C. Hu, "BSIM3v3 Manual (final version)," Dep. of Electrical Engineering and Computer Sciences, University of California, Berkeley, 1995.
- [12] P. Wambacq, G. G. E. Gielen, P. R. Kinget, W. Sansen, "High-Frequency Distortion Analysis of Analog Integrated Circuits," *IEEE Tr. on Circuits and Systems—II: Analog and Digital Signal Processing*, vol. 46, no. 3, pp. 335-345, Mar. 1999.
- [13] E. Abou-Allam, E. I. El-Masry, "Design of Wideband CMOS Current-Mode Operational Amplifiers," *IEEE International Symposium on Circuits and Systems 1995*, vol. 3, pp. 1556-1559, 1995.
- [14] E. Abou-Allam, E. I. El-Masry, "A 200MHz Steered Current Operational Amplifier in 1.2 $\mu$ m CMOS Technology," *IEEE Journal of Solid-State Circuits*, vol. 32, no. 2, pp. 245-249, Feb. 1997.
- [15] D. Smith, M. Koen, A. F. Witulski, "Evolution of High-Speed Operational Amplifier Architectures," *IEEE Journal of Solid-State Circuits*, vol. 29, no. 10, pp. 1166-1179, Oct. 1994.
- [16] G. Ferri, S. Pennisi, "A 1.5-V Current-Mode Capacitance Multiplier", *Proceedings of the Tenth International Conference on Microelectronics 1998*, p. 9-12, 1998.
- [17] H. Sjöland, S. Mattisson, "A 100MHz CMOS Wide-Band IF Amplifier," *IEEE Journal of Solid-State Circuits*, vol. 33, no. 4, pp. 631-634, Apr. 1998.
- [18] H. Sjöland, S. Mattisson, "A 160MHz Bipolar Wide-Band IF Amplifier," *IEEE Journal of Solid-State Circuits*, vol. 33, no. 10, pp. 1555-1558, Oct. 1998.
- [19] Analog devices, AD8009, AD8036/37, see [http://products.analog.com/products\\_html/list\\_gen\\_3\\_2\\_1.html](http://products.analog.com/products_html/list_gen_3_2_1.html)

## Chapter 6

### Conclusions and Discussions

In this book the issue has been achievement of highly linear opamps in deep sub-micron CMOS technologies. To make this possible, design procedures and design equations for minimization of the nonlinear distortion in feedback opamp circuits have been developed. The design procedure can be summarized as follows:

1. Biasing for low distortion:
  - a) Choose the bias current for the transistors to be well above the associate signal current in the specified frequency range. For low frequencies, the resistive load decides the bias currents. For high frequencies, the bias currents must be chosen such that the circuit is far from slewing at the highest signal frequency. In other words, FPBW of the CL circuit has to be well above the highest signal frequency.
  - b) Use the bias current in a) and set the voltage bias point for each transistor such that the nonlinear coefficients are small and stable in the entire range of the terminal voltages. This is done by proper dimensioning of the transistors. The result of the biasing is used as a starting point for the optimization, which will be carried out in point 3 below.
2. Find the strongest contributions to nonlinear distortion for the CL circuit and derive symbolic expressions for these. From the symbolic expressions, design equations can be obtained. The small-signal parameters and nonlinear coefficients, required for this analysis, are extracted from the circuit obtained in point 1.
3. Use the biasing of point 1 as the starting point for the optimization of the CL circuit for low nonlinear distortion. The optimization is carried out in

a circuit simulator and the design equations obtained in point 2 are used to see what parameters to alter to minimize the distortion.

The biasing of the circuit is the foundation of high linearity performance. First, the bias current of each transistor in the circuit is set. This is done by choosing the drain current of the transistors to be well above the associated signal current in the specified frequency range. Thus, the circuit is far from both clipping and slewing due to limited available current. Second, small nonlinear coefficients are generally obtained by using large overhead for the terminal voltages of the transistor. This means large GS-overdrive and a DS-voltage well above the saturation voltage. Each transistor in the circuit is dimensioned under these constraints. Especially in deep sub-micron CMOS technologies, the velocity saturation of the transistor can be utilized for achieving small and stable nonlinear coefficients.

To develop symbolical expressions for the nonlinear responses, a tool that describes nonlinear behavior as a function of frequency is required. The phasor method has been used in this work, which leads to a subset of the Volterra series [1]. The assumption made is that the circuit behaves weakly nonlinear, which is true for well-designed CL opamp circuits with excitation levels well below the supply voltage. The phasor method has been implemented in Maple6 and applied on a model of the folded cascode Miller opamp, which has been the example opamp throughout this book.

To include the effect that the CM-voltage swing has on the linearity performance, a two-input model of the opamp was developed. This model was further used to explore the non-inverting and inverting opamp configurations regarding nonlinear behavior. For each of them, the strongest contributions to nonlinear distortion were found, and simplified symbolical expressions including the strongest contributions were developed. From the simplified expressions, design equations were extracted. These have further been used to optimize the circuit for high linearity performance.

The simplified expressions were obtained by splitting the accurate but rather complex equations for the CL nonlinear responses in different factors. This was done by exploiting the iterative nature of the phasor method, and further, the two-input model of the opamp. Because of the split-up, it was possible to do simplifications on each factor, obtaining simple and informative equations for the CL nonlinear transfer functions. The simplified equations show close match to the accurate nonlinear transfer functions.

For low CL-gain, the non-inverting configuration has large swing in the CM-voltage. This swing is damaging for the linearity performance. Thus, the requirements to the input stage of the opamp become tough. It is especially important to have low CM-gain. Further, even with low CM-gain, the input stage is the main contribution to the nonlinear distortion in the entire

frequency range. For high CL-gain, the CM-voltage swing becomes smaller and the non-inverting opamp configuration is approaching the inverting configuration regarding nonlinear behavior.

The inverting configuration does not have large swing in the CM-voltage. Thus, the output stage of the opamp has the largest contribution to nonlinear distortion, which is smaller than for the non-inverting configuration. Because of this, the inverting configuration should be the preferred choice when low nonlinear distortion is a requirement.

The optimization of the CL circuit is done in a circuit simulator. Using the biasing as a starting point, the design equations show what parameters to use to suppress the nonlinear distortion. Generally, increasing the transconductance of the amplifying transistors suppress the nonlinear transfer functions. At the same time the nonlinear coefficients increase and will counteract the decrease in distortion.

Three opamps, connected in inverting opamp configuration, have been design and fabricated as a result of the design procedure. Additionally, a unity-gain opamp was made using a new approach to minimize the effect of the large swing in the input CM-voltage. This approach is called “tail current compensation circuit” and is described in [2].

Throughout this book just one opamp topology is used, the folded cascode Miller opamp. In the next sub-sections some comments are made for other opamp topologies and it will be discussed why the folded cascode Miller opamp is a good choice for obtaining high linearity for frequencies up to approximately 1/10 of the GBW of the opamp.

## 6.1 Opamp Topologies Versus Linearity

The biasing guidelines in Chapter 3 stated that each transistor connected to the signal path should be biased with high GS-overdrive and further, such that the DS saturation voltage is well below the lowest DS-voltage. In other words, to obtain high linearity performance for the overall circuit the transistors need some voltage headroom. The necessary voltage headroom is easier to gain in some opamp topologies than others. Thus, the choice of opamp topology should be done with this in mind. Chapter 4 shows that the linearity performance is strongly related to the OL-gain and high frequency capabilities of the opamp. This is also a key issue when choosing what opamp to use. In the following only fully differential opamps are discussed. A fully differential circuit will suppress the even order harmonics strongly such that the odd order harmonics will be the largest contributions to nonlinear distortion. Further, a fully differential opamp in inverting configuration will have zero input CM-voltage swing. The only contribution to 3<sup>rd</sup> harmonic is thus from  $H_{3ve\_CL}(j\omega)$  (see Chapter 4). Thus, only the 3<sup>rd</sup>

harmonic due to  $H_{3ve\_cl}(j\omega)$  will be considered in the following. The opamp topologies are compared with the 1.8V opamp presented in section 5.2. They will be discussed and compared to the folded cascode Miller opamp in three frequency ranges:

1. Low frequencies:  $DC < f < 1\text{MHz}$ 
  - below the dominant pole of the 1.8V opamp
2. High frequencies:  $1\text{MHz} < f < 200\text{MHz}$ 
  - all zeroes in the nonlinear transfer function given by (4-26) are located in this range for the 1.8V opamp
3. Very high frequencies:  $f > 200\text{MHz}$ 
  - 3<sup>rd</sup> harmonic totally decided by the contribution from the input transistors (equation (4-27))

### 6.1.1 One-Stage Opamp

The simplest one-stage opamp consist of five transistors. Two make the differential pair, two the active load to the differential pair and one the tail current source. The largest GBW possible in the given fabrication technology is obtained with this opamp. A major drawback when it comes to linearity performance is the limited voltage swing at the opamp outputs. From the output node to one of the supply rails there are two DS-voltages, and each shall be well above the saturation voltage. To satisfy this requirement the signal swing must be limited. This problem is solved by choosing the opamp in Figure 6-1. Here, there is only one DS-voltage from the output node to each of the power supply rails. This means that the signal swing can be large and the DS-voltages are well above the saturation voltage in the entire output voltage range.

The circuit works as follows: the current from the differential pair M1 and M2 is mirrored from M6P/N to M4P/N and injected in the output nodes. The dominant pole of the opamp is made at the output node. By varying the load capacitance the dominant pole changes and further the GBW. This is called load compensation, which is common for all one-stage topologies. Further, the opamp has one non-dominant pole located at the node on the gate on M4P/N. To obtain safe phase- and gain margins for the CL-circuit the non-dominant pole has to be well above the GBW of the loop formed by the opamp and feedback circuit. The CM-feedback circuit to control the CM-voltage on the opamp output is not shown in Figure 6-1. This opamp topology is described in more detail in [3] (Chapter 6).

The contributors to distortion are the same as for the folded cascode Miller opamp. At low and high frequencies the output transistors are the strongest contributors. Because of the low OL-gain the distortion is far larger

than for the folded cascode Miller opamp. The gain from the input terminals of the single-stage opamp to the gate of M4P/N can replace  $A_1$  in equation (4-26). For the one-stage opamp  $A_1$  is low and most likely from 1 to 4 if the saturation voltage of M4P/N shall be low enough. Compared to the 1.8V folded cascode Miller opamp presented in section 5.2,  $A_1$  is roughly 40dB lower for the one stage opamp. The 3<sup>rd</sup> harmonic will then be 40dB higher for low frequencies and well above the 3<sup>rd</sup> harmonic of the 1.8V opamp in the whole high-frequency range. This is under the assumption that all other parameters are the same for the two opamps. Thus, at both low and high frequencies the distortion is less suppressed than for the folded cascode Miller opamp.

At very high frequencies the nonlinear contribution from the input differential pair takes over. The suppression of this contribution depends on the GBW of the opamp. Thus, since the GBW of a one-stage opamp can be larger than for a two-stage opamp, the linearity performance can potentially be better in this frequency range.

The opamp in Figure 6-1 is a good choice among one-stage opamps. The complexity is low and it is easy to design. If the linearity specification for the circuit is not too demanding this could be the best choice.

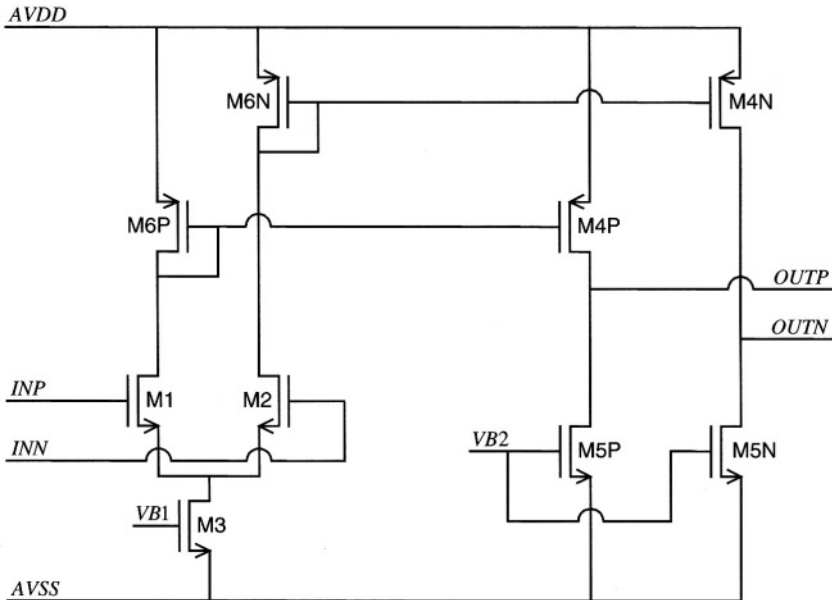


Figure 6-1. One-stage opamp capable to handle large output voltage swing.

### 6.1.2 Two-Stage Opamp

Figure 6-2 shows a Miller compensated two-stage opamp. M1, M2, M3 and M6 make the input stage and M4 and M5 are the common source output stage. The opamp is compensated by the capacitor  $C_C$ . Due to the feed-forward path through the compensation capacitor, a zero in the right half of the  $s$ -plane occurs in the OL transfer function. This zero contributes negatively to the phase margin. The resistor  $R_C$  moves this zero to the left half of the  $s$ -plane and the phase margin becomes larger. This makes it possible to make the GBW of the opamp larger. The opamp is described further in [4].

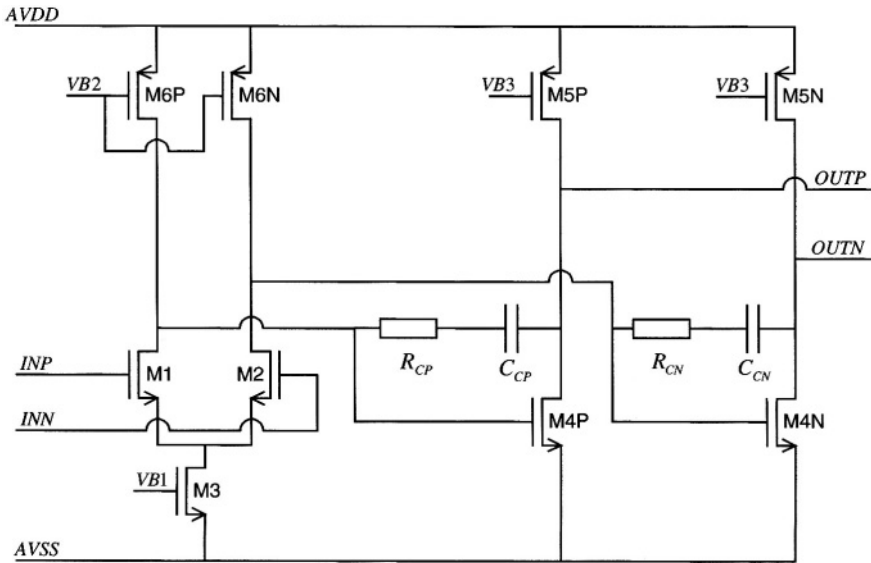


Figure 6-2. Two-stage Miller opamp.

$$\omega_{6,M} = \frac{gd_{1/2} + gd_{6P/N}}{C_C + C_{6,M}} \quad (6-1)$$

As for the one-stage opamp in Figure 6-1 the high-swing node, the output node, sees only one DS-voltage to each of the supply rails. This means that the output is well suited for obtaining low distortion. The contributors to distortion are the same as for the folded cascode Miller opamp and the equations (4-26) and (4-27) can be used when replacing  $g_{O1}$  with  $g_{O1,M} = gd_{1/2} + gd_{6P/N}$  and  $\omega_b$  with  $\omega_{b,M}$  given by (6-1). This means that the gain  $A_1$  of

the Miller opamp first stage is lower than for the folded cascode Miller opamp. Equation (4-26) shows that all distortion contributions from the output transistors are increased with the same amount at low frequencies. In addition, because  $\omega_b$  goes to  $\omega_{b,M}$ , suppression of distortion above  $\omega_{b,M}$  is lower. This is shown by design equations (4-29) and (4-30), where  $C_6$  is replaced with  $C_C + C_{6,M}$ .  $C_{6,M}$  will be larger than  $C_6$  because that the cascode transistors (M9 and M11 in Figure 3-10) can be made smaller such that their drain capacitances are smaller than for M1/2 and M6P/N. Thus, the Miller opamp has poorer linearity performance for low and high frequencies compared to the folded cascode Miller opamp.

For very high frequencies the contribution from the input differential pair is dominant. The GBW decides the suppression of the distortion. According to [4] the GBW for the Miller opamp is half the GBW of the folded cascode Miller opamp. This means that also at very high frequencies the cascoded Miller opamp has higher linearity performance.

### 6.1.3 Three-Stage Opamp

Before compensation a three-stage opamp has three dominant poles in the OL transfer function. Thus, a three-stage opamp needs one additional Miller feedback loop compared to the two-stage opamp. A three-stage opamp has thus larger OL DC gain, but more non-dominant poles, which results in lower obtainable GBW. Various topologies for three-stage opamps are discussed in [4]. In this section the nested Miller compensation is considered.

As for the one- and two-stage opamps the output node should see only one DS-voltage to each of the power supply rails. Thus, the output stage should be of the common-source type as it is in the two-stage Miller opamp in Figure 6-2. When using a common-source output stage, equation (4-26) can be used to describe the contributions to 3<sup>rd</sup> harmonic from the output transistors. Because of one more stage compared to the two-stage opamp,  $A_I$  shall now be replaced with the gain of the two first stages of the three-stage opamp. Further, because of the additional Miller feedback loop  $\omega_b$  in (4-26) will be replaced with two zeroes. Above these zeroes the incline of the 3<sup>rd</sup> order response is 20dB/dec larger than for the two-stage opamp. Nevertheless, the contributions from the output transistors will be lower for the three-stage opamp than for the two-stage folded cascode Miller opamp at low and high frequency.

The contributions from the input transistors are suppressed by the cubic GBW for frequencies above the dominant pole. This is shown by the design equation (4-31). Thus, since the highest obtainable GBW of the three-stage opamp is smaller than for a two-stage opamp, the distortion due to the input

transistors is larger. Since the contributions from the output transistors are smaller for a three-stage opamp the input transistors becomes dominant at much lower frequency than for the two-stage opamps. So, at high and very high frequency the three-stage opamp has poorer linearity performance than the two-stage cascoded Miller opamp.

#### 6.1.4 Concluding Remarks

The last subsections show that a one-stage opamp has the lowest linearity performance in the low and high frequency ranges, but potentially the best performance at very high frequency due to high GBW. The three-stage opamp is probably the best choice for high linearity for low frequencies, especially if the linearity requirement is high. The two-stage opamp, especially the folded cascode Miller opamp, is a good choice for combining high linearity for low and high frequencies and low complexity and power consumption.

Compare the 1.8V folded cascode Miller opamp presented in section 5.2 with a three-stage nested Miller compensated opamp. Assume that the input stages are equal. According to [4] the GBW of the three-stage opamp is 3 to 4 times lower than the GBW of the folded cascode Miller opamp. For the 1.8V opamp the distortion from the input differential pair becomes dominant at 100MHz (see Figure 5-6). If the GBW of the three-stage opamp is 3 times lower, the 3<sup>rd</sup> harmonic produced by this opamp will be larger than for the two-stage cascoded Miller opamp for frequencies above 20MHz. Thus, the three-stage opamp has lower 3<sup>rd</sup> harmonic for frequencies below 20MHz and higher for frequencies above.

## REFERENCES

- [1] P. Wambacq, W. Sansen, "Distortion Analysis of Analog Integrated Circuits," Norwell, MA: Kluwer Academic Publishers, 1998.
- [2] B. Hernes, Ø. Moldsvor, T. Sasther, "A -80dB HD3 Opamp in 3.3V CMOS Technology using Tail Current Compensation," *IEEE International Symposium on Circuits and Systems 2001*, vol. 1, 2001, pp. 216-219.
- [3] K. R. Laker, W. Sansen, "Design of Analog Integrated Circuits and Systems", McGraw-Hill, Inc., 1994.
- [4] R. Hogervorst, J. H. Huijsing, "Design of Low-Voltage, Low-Power Operational Amplifier Cells," Norwell, MA: Kluwer Academic Publishers, 1996.

## Appendix A

### Transistor Model

The three-dimensional drain current  $i_d$  is given in (A-1). The equation is a Taylor expansion to 3<sup>rd</sup> order with  $v_{gs}$ ,  $v_{ds}$  and  $v_{bs}$  as the signal terminal voltages. The explanations of the coefficients are given in (A-3) to (A-8). When the transistor is in saturation it is assumed that all transistor capacitances are linear, except for the DB and SB diffusion capacitances. The current for the nonlinear capacitance is given in (A-2), and the coefficients in (A-9).

$$\begin{aligned} i_d &= f(v_{gs}, v_{ds}, v_{bs}) \\ &\approx gm \cdot v_{gs} + gd \cdot v_{ds} + gmb \cdot v_{bs} \\ &\quad + K2_{gm} \cdot v_{gs}^2 + K2_{gd} \cdot v_{ds}^2 + K2_{gmb} \cdot v_{bs}^2 \\ &\quad + K2_{gm\_gd} \cdot v_{gs} \cdot v_{ds} + K2_{gmb\_gm} \cdot v_{bs} \cdot v_{gs} \\ &\quad + K2_{gmb\_gd} \cdot v_{bs} \cdot v_{ds} \\ &\quad + K3_{gm} \cdot v_{gs}^3 + K3_{gd} \cdot v_{ds}^3 + K3_{gmb} \cdot v_{bs}^3 \\ &\quad + K3_{2gm\_gd} \cdot v_{gs}^2 \cdot v_{ds} + K3_{gm\_2gd} \cdot v_{gs} \cdot v_{ds}^2 \\ &\quad + K3_{2gmb\_gm} \cdot v_{bs}^2 \cdot v_{gs} + K3_{gmb\_2gm} \cdot v_{bs} \cdot v_{gs}^2 \\ &\quad + K3_{2gmb\_gd} \cdot v_{bs}^2 \cdot v_{ds} + K3_{gmb\_2gd} \cdot v_{bs} \cdot v_{ds}^2 \\ &\quad + K3_{gm\_gmb\_gd} \cdot v_{gs} \cdot v_{ds} \cdot v_{bs} \end{aligned} \tag{A-1}$$

$$\begin{aligned}
 i_{C_{XB}} &= C_{XB} \cdot \frac{dv_{XB}}{dt} + i_{NL,C_{XB}} \\
 &\approx C_{XB} \cdot \frac{dv_{XB}}{dt} + K2_{C_{XB}} \cdot v_{XB} \cdot \frac{dv_{XB}}{dt} + K3_{C_{XB}} \cdot v_{XB}^2 \cdot \frac{dv_{XB}}{dt}
 \end{aligned} \tag{A-2}$$

$$\begin{aligned}
 gm &= \frac{\partial f(v_{gs}, v_{ds}, v_{bs})}{\partial v_{gs}} \\
 gd &= \frac{\partial f(v_{gs}, v_{ds}, v_{bs})}{\partial v_{ds}} \\
 gmb &= \frac{\partial f(v_{gs}, v_{ds}, v_{bs})}{\partial v_{bs}}
 \end{aligned} \tag{A-3}$$

$$\begin{aligned}
 Kn_{gm} &= \frac{1}{n!} \cdot \frac{\partial^n f(v_{gs}, v_{ds}, v_{bs})}{\partial v_{gs}^n}, \quad n \in \{2,3\} \\
 Kn_{gd} &= \frac{1}{n!} \cdot \frac{\partial^n f(v_{gs}, v_{ds}, v_{bs})}{\partial v_{ds}^n}, \quad n \in \{2,3\} \\
 Kn_{gmb} &= \frac{1}{n!} \cdot \frac{\partial^n f(v_{gs}, v_{ds}, v_{bs})}{\partial v_{bs}^n}, \quad n \in \{2,3\}
 \end{aligned} \tag{A-4}$$

$$\begin{aligned}
 Kn_{j \cdot gm \cdot (n-j) \cdot gd} &= \frac{1}{j!} \cdot \frac{1}{(n-j)!} \cdot \frac{\partial^n f(v_{gs}, v_{ds}, v_{bs})}{\partial v_{gs}^j \cdot \partial v_{ds}^{(n-j)}}, \\
 n &= \begin{cases} 2 & \Rightarrow j = 1 \\ 3 & \Rightarrow j \in \{1,2\} \end{cases}
 \end{aligned} \tag{A-5}$$

$$Kn_{j, gm_{(n-j)}, gmb} = \frac{1}{j!} \cdot \frac{1}{(n-j)!} \cdot \frac{\partial^n f(v_{gs}, v_{ds}, v_{bs})}{\partial v_{gs}^j \cdot \partial v_{bs}^{(n-j)}}, \quad (\text{A-6})$$

$$n = \begin{cases} 2 & \Rightarrow j = 1 \\ 3 & \Rightarrow j \in \{1, 2\} \end{cases}$$

$$Kn_{j, gmb_{(n-j)}, gd} = \frac{1}{j!} \cdot \frac{1}{(n-j)!} \cdot \frac{\partial^n f(v_{gs}, v_{ds}, v_{bs})}{\partial v_{bs}^j \cdot \partial v_{ds}^{(n-j)}}, \quad (\text{A-7})$$

$$n = \begin{cases} 2 & \Rightarrow j = 1 \\ 3 & \Rightarrow j \in \{1, 2\} \end{cases}$$

$$K3_{gm_{gd}, gmb} = \frac{\partial^3 f(v_{gs}, v_{ds}, v_{bs})}{\partial v_{gs} \cdot \partial v_{ds} \cdot \partial v_{ds}} \quad (\text{A-8})$$

$$Kn_{c_{xb}} = \frac{1}{n!} \cdot \frac{\partial^n i_{c_{xb}}}{\partial v_{xb}^n} \quad (\text{A-9})$$

*This page intentionally left blank*

## Appendix B

### Closed Loop Opamp Transfer Functions

In section 3.2.1, p. 42, the opamp was described as a two-input device whose OL output responses, truncated to 3<sup>rd</sup> order, can be expressed as (3-7) to (3-9). In this appendix, the CL responses for non-inverting and inverting opamp configurations will be derived as a function of the OL transfer functions given in (3-7) to (3-9).

Because of large complexity in the derivations, it is necessary to do some simplifications. It is assumed that the feedback network is resistive and linear. This is a good approximation when using metal resistors in the implementation. The loading effects on the feedback network due to the inverting input terminal are disregarded, and likewise the parasitic pole in the same node. Loading on the output terminal due to the feedback network is included in the load. For frequencies below GBW of the opamp these simplifications give accurate modeling of the CL circuit.

All voltages and currents are on phasor representations in this section. The method is similar to the method used in Appendix C. The only difference is that the nonlinear coefficients are replaced with the 2<sup>nd</sup> and 3<sup>rd</sup> order OL transfer functions of the opamp.

#### B.1 Non-Inverting Opamp Configuration

The non-inverting opamp configuration is shown in Figure B-1 (a) and its 1<sup>st</sup> order model in Figure B-1(b). The models for deriving 2<sup>nd</sup> and 3<sup>rd</sup> order CL transfer functions are shown in Figure B-2.  $H_1(\cdot)$ ,  $H_2(\cdot)$  and  $H_3(\cdot)$  are given by (3-7), (3-8) and (3-9) on p. 44.

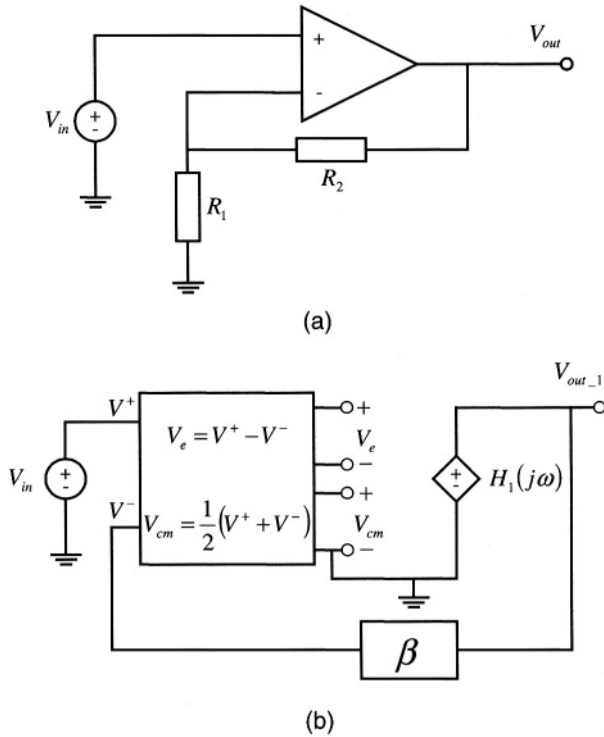


Figure B-1. Non-inverting opamp configuration (a) and its 1<sup>st</sup> order model (b).

### B.1.1 First Order CL Response

From Figure B-1(b) it is possible to see that  $V_e = V_{e\_1} = (V_{in} - \beta \cdot V_{out\_1})$  and  $V_{cm} = V_{cm\_1} = (1/2) \cdot (V_{in} + \beta \cdot V_{out\_1})$ . When inserting these equations in (3-7) the following equation is obtained:

$$V_{out\_1} = H_{V_e}(j\omega) \cdot (V_{in} - \beta \cdot V_{out\_1}) + \frac{1}{2} H_{V_{cm}}(j\omega) \cdot (V_{in} + \beta \cdot V_{out\_1}) \quad (\text{B-1})$$

where

$$\beta = \frac{R_1}{R_1 + R_2}$$

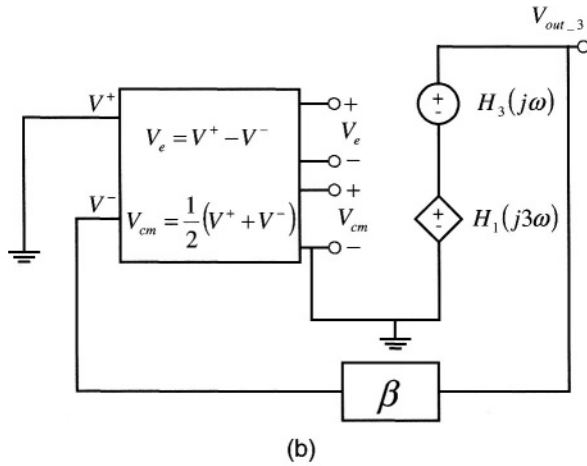
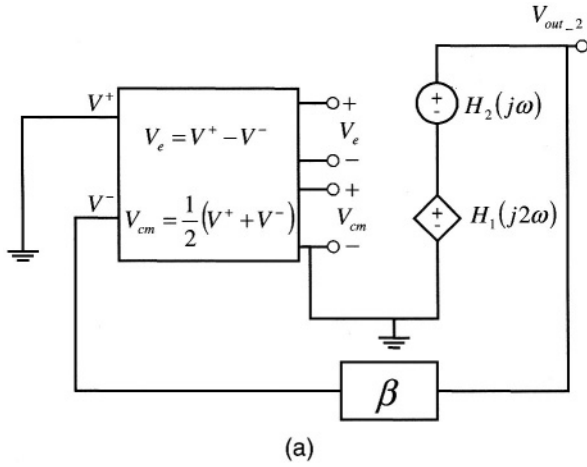


Figure B-2. Models for derivation of CL transfer functions, 2<sup>nd</sup> order (a) and 3<sup>rd</sup> order (b).

Solving (B-1) for  $V_{out\_1}$  gives (B-2):

$$\begin{aligned}
 V_{out\_1} &= \frac{H_{ve}(j\omega) + \frac{1}{2}H_{vcm}(j\omega)}{1 + \beta \cdot \left( H_{ve}(j\omega) - \frac{1}{2}H_{vcm}(j\omega) \right)} \cdot V_{in} \\
 &\approx \frac{H_{ve}(j\omega)}{1 + \beta \cdot H_{ve}(j\omega)} \cdot V_{in}
 \end{aligned}
 \tag{B-2}$$

1<sup>st</sup> order differential and CM-voltages then become:

$$V_{e-1} = \frac{1 - \beta \cdot H_{vcm}(j\omega)}{1 + \beta \cdot \left( H_{ve}(j\omega) - \frac{1}{2} \cdot H_{vcm}(j\omega) \right)} \cdot V_{in}$$

$$\approx \frac{1 - \beta \cdot H_{vcm}(j\omega)}{1 + \beta \cdot H_{ve}(j\omega)} \cdot V_{in} \quad (\text{B-3})$$

$$V_{cm-1} \approx \frac{\frac{1}{2} + \beta \cdot H_{ve}(j\omega)}{1 + \beta \cdot \left( H_{ve}(j\omega) - \frac{1}{2} \cdot H_{vcm}(j\omega) \right)} \cdot V_{in} \approx V_{in} \quad (\text{B-4})$$

### B.1.2 Second Order CL Response

The CL 2<sup>nd</sup> order output voltage can easily be found by using the model of Figure B-2(a), where  $H_1(\cdot)$  and  $H_2(\cdot)$  are given by (3-7) and (3-8), respectively. Here,  $H_2(\cdot)$  is the circuit excitation indicated by an independent voltage source.  $H_1(\cdot)$  applies feedback in the system. The model is running at the frequency  $2 \cdot \omega$ . When inserting (3-7) for  $H_1(\cdot)$  with  $V_e = V_{e-2} = -\beta \cdot V_{out-2}$  and  $V_{cm} = V_{cm-2} = (1/2) \cdot \beta \cdot V_{out-2}$  (B-5) is obtained. When solving this for  $V_{out-2}$  (B-6) results, which is the 2<sup>nd</sup> order output CL response for the non-inverting opamp configuration.

$$V_{out-2} = H_{ve}(j2\omega) \cdot (-\beta \cdot V_{out-2}) + \frac{1}{2} H_{vcm}(j2\omega) \cdot \beta \cdot V_{out-2}$$

$$+ H_2(V_{e-1}, V_{cm-1}, j\omega, j\omega) \quad (\text{B-5})$$

$$V_{out\_2} \approx \frac{1}{1 + \beta \cdot H_{Ve}(j2\omega)} \cdot \left\{ \begin{array}{l} \left[ \frac{[1 - \beta \cdot H_{Vcm}(j\omega)]^2}{[1 + \beta \cdot H_{Ve}(j\omega)]^2} \cdot H_{2Ve}(j\omega) + \right. \\ \left. \frac{1 - \beta \cdot H_{Vcm}(j\omega)}{1 + \beta \cdot H_{Ve}(j\omega)} \cdot H_{Ve\_Vcm}(j\omega) + \right. \\ \left. H_{2Vcm}(j\omega) \right] \cdot V_{in}^2 \end{array} \right. \quad (\text{B-6})$$

### B.1.3 Third Order CL Response

The 3<sup>rd</sup> order response is obtained in the same way as the 2<sup>nd</sup> order response, replacing  $H_2(\cdot)$  with  $H_3(\cdot)$ , given by (3-9). The model (Figure B-2(b)) is running at the frequency  $3 \cdot \omega$ . Solving (B-7) for  $V_{out\_3}$ , the 3<sup>rd</sup> order response is given by (B-8). Because of the global feedback loop represented by the  $\beta$ -network, the 2<sup>nd</sup> harmonic will be present at the input terminals of the opamp. Because of the 2<sup>nd</sup> order nonlinearity this frequency will be mixed with the fundamental frequency and thus contributes to 3<sup>rd</sup> order response. This is covered by  $H_{3\_2}(\cdot)$ .

$$\begin{aligned} V_{out\_3} = & H_{Ve}(j3\omega) \cdot (-\beta \cdot V_{out\_3}) + \frac{1}{2} H_{Vcm}(j3\omega) \cdot \beta \cdot V_{out\_3} \\ & + H_3(V_{e\_1}, V_{cm\_1}, j\omega, j\omega) \\ & + H_{3\_2}(V_{e\_1}, V_{e\_2}, V_{cm\_1}, V_{cm\_2}, j\omega, j2\omega) \end{aligned} \quad (\text{B-7})$$

$$V_{out\_3} \approx \frac{1}{1 + \beta \cdot H_{V_e}(j3\omega)} \left\{ \begin{array}{l} \frac{[1 - \beta \cdot H_{V_{cm}}(j\omega)]^3}{[1 + \beta \cdot H_{V_e}(j\omega)]^3} \cdot H_{3V_e}(j\omega) + \\ \frac{[1 - \beta \cdot H_{V_{cm}}(j\omega)]^2}{[1 + \beta \cdot H_{V_e}(j\omega)]^2} \cdot H_{2V_e\_V_{cm}}(j\omega) + \\ \frac{1 - \beta \cdot H_{V_{cm}}(j\omega)}{1 + \beta \cdot H_{V_e}(j\omega)} \cdot H_{V_e\_2V_{cm}}(j\omega) + \\ H_{3V_{cm}}(j\omega) + \\ H_{3\_2}(V_{e\_1}, V_{e\_2}, V_{cm\_1}, V_{cm\_2}, j\omega, j2\omega) \end{array} \right\} \cdot V_{in}^3 \quad (\text{B-8})$$

## B.2 Inverting Opamp Configuration

The inverting opamp configuration is shown in Figure B-3(a), and the 1<sup>st</sup> order model in Figure B-3(b). To derive 2<sup>nd</sup> and 3<sup>rd</sup> order CL responses, the models used for the non-inverting configurations, shown in Figure B-2(a) and (b), can also be applied on the inverting configuration. The OL transfer functions of the opamp are given by (3-7), (3-8) and (3-9) on p. 44.

### B.2.1 First, Second and Third Order CL Responses

For the inverting opamp configuration the 1<sup>st</sup> order  $V_e$  can be expressed as (B-9):

$$\begin{aligned} V_{e\_1} &= \left( -\frac{R_2}{R_1} \right) \cdot \frac{R_1}{R_1 + R_2} \cdot V_{in} - \frac{R_1}{R_1 + R_2} \cdot V_{out\_1} \\ &= A_{CL} \cdot \beta \cdot V_{in} - \beta \cdot V_{out\_1} \end{aligned} \quad (\text{B-9})$$

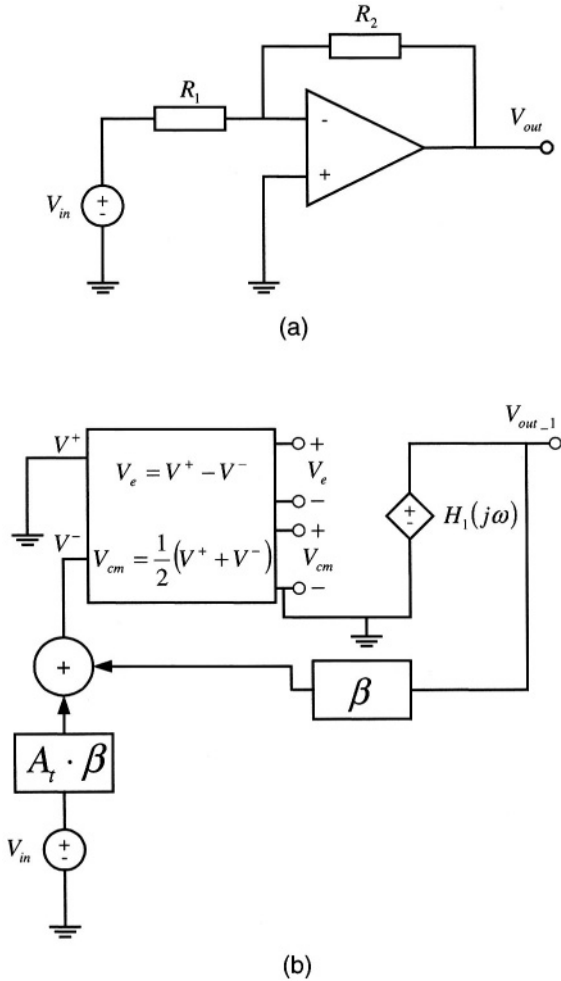


Figure B-3. Inverting opamp configuration (a), and its 1<sup>st</sup> order model (b).

where

$$\beta = \frac{R_1}{R_1 + R_2}, \quad A_{CL} = -\frac{R_2}{R_1}$$

When inserting for  $V_{e-1}$  and  $V_{cm-1} = (-1/2) \cdot V_{e-1}$  in (3-7), (B-10) is obtained. Solving this with respect to  $V_{out-1}$  gives (B-11). Note that the differential voltage  $V_{e-1}$  (B-12) and CM-voltage  $V_{cm-1}$  (B-13) are different from the voltages for the non-inverting configuration, which are given by (B-3) and

(B-4), respectively. Inserting (B-12) and (B-13) in (B-5) and (B-7) (instead of the differential and CM-voltage of the non-inverting configuration), and solving for  $V_{out\_2}$  and  $V_{out\_3}$  gives 2<sup>nd</sup> and 3<sup>rd</sup> order CL responses, respectively, for the inverting configuration. These are given in (B-14) and (B-15).

$$V_{out\_1} = H_{ve}(j\omega) \cdot (A_{CL} \cdot \beta \cdot V_{in} - \beta \cdot V_{out\_1}) - \frac{1}{2} H_{vcm}(j\omega) \cdot (A_{CL} \cdot \beta \cdot V_{in} - \beta \cdot V_{out\_1}) \quad (\text{B-10})$$

$$V_{out\_1} = A_{CL} \cdot \frac{\beta \cdot \left( H_{ve}(j\omega) - \frac{1}{2} H_{vcm}(j\omega) \right)}{1 + \beta \cdot \left( H_{ve}(j\omega) - \frac{1}{2} H_{vcm}(j\omega) \right)} \cdot V_{in} \quad (\text{B-11})$$

$$\approx A_{CL} \cdot \frac{\beta \cdot H_{ve}(j\omega)}{1 + \beta \cdot H_{ve}(j\omega)} \cdot V_{in}$$

$$V_{e-1} \approx \frac{A_{CL} \cdot \beta}{1 + \beta \cdot H_{ve}(j\omega)} \cdot V_{in} \quad (\text{B-12})$$

$$V_{cm-1} \approx -\frac{1}{2} \cdot V_{e-1} \quad (\text{B-13})$$

$$V_{out\_2} \approx A_{CL}^2 \cdot \frac{\beta^2}{[1 + \beta \cdot H_{ve}(j2\omega)] \cdot [1 + \beta \cdot H_{ve}(j\omega)]^2} \cdot \left\{ H_{2ve}(j\omega) - \frac{1}{2} H_{ve\_vcm}(j\omega) + \frac{1}{4} H_{2vcm}(j\omega) \right\} \cdot V_{in}^2 \quad (\text{B-14})$$

$$\begin{aligned}
 V_{out\_3} \approx & A_{CL}^3 \cdot \frac{\beta^3}{[1 + \beta \cdot H_{Ve}(j3\omega)] \cdot [1 + \beta \cdot H_{Ve}(j\omega)]^3} \\
 & \cdot \left\{ \begin{aligned} & H_{3Ve}(j\omega) - \frac{1}{2} H_{2Ve\_Vcm}(j\omega) + \\ & \frac{1}{4} H_{Ve\_2Vcm}(j\omega) - \frac{1}{8} H_{3Vcm}(j\omega) \end{aligned} \right\} \cdot V_{in}^3 \\
 & + \frac{H_{3\_2}(V_{e\_1}, V_{e\_2}, V_{cm\_1}, V_{cm\_2}, j\omega, j2\omega)}{[1 + \beta \cdot H_{Ve}(j3\omega)]} \cdot V_{in}^3
 \end{aligned} \tag{B-15}$$

*This page intentionally left blank*

## Appendix C

### Open Loop Opamp Transfer Functions

In this appendix a procedure for finding the 1<sup>st</sup> to 3<sup>rd</sup> orders OL transfer functions for the cascoded Miller opamp is described. The opamp is shown in Figure 3-10 in section 3.2.3. The opamp is considered as a two-input device with the differential and CM voltages as the input variables. The procedure implements the phasor method carried out on a two-input system. Nonlinear analysis of two-input systems is described in [1], [2] and [3]. Because of the complexity of the higher order transfer functions, only the 1<sup>st</sup> order responses are given here. For 2<sup>nd</sup> and 3<sup>rd</sup> order transfer functions the procedure is implemented in Maple6 [4].

The small-signal circuit in Figure 3-11 (p. 47) will be used as the model for the opamp. The circuit equations, using Kirchhoff's current law and phasor representation of current and voltages, can be expressed as (C-1). Here, the equations are arranged such that the circuit excitations are on the right-hand side, and the node voltages are on the left-hand side. The admittance matrix is shown in (C-2) and the elements in this matrix in (C-5) to (C-9). The circuit parameters are related to Figure 3-11. The voltage and current vectors are shown in (C-3) and (C-4), respectively, where the indexes  $n$  and  $m$  are the exponent of the input voltages  $V_e$  and  $V_{cm}$ , respectively. For instance, when  $n=0$ ,  $V_e$  is equal to zero and when  $n>0 \Rightarrow V_e^n$ . The current vector represents the circuit excitations and are the currents entering the indexed node, for example  $I_{3,n,m}$  is the excitation current entering node 3 in Figure 3-11. The frequency that this excitation runs at is  $(n+m) \cdot \omega$ .

$$\bar{Y}(j(n+m) \cdot \omega) \cdot \bar{V}_{n,m} = \bar{I}_{n,m} \quad (\text{C-1})$$

$$\bar{Y}(j\omega) = \begin{bmatrix} y_{33}(j\omega) & 0 & 0 \\ 0 & y_{66}(j\omega) & y_{67}(j\omega) \\ 0 & y_{76}(j\omega) & y_{77}(j\omega) \end{bmatrix} \quad (\text{C-2})$$

$$\bar{V}_{n,m} = \begin{bmatrix} V_{3\_n,m} \\ V_{6\_n,m} \\ V_{7\_n,m} \end{bmatrix} \quad (\text{C-3})$$

$$\bar{I}_{n,m} = \begin{bmatrix} I_{3\_n,m} \\ I_{6\_n,m} \\ I_{7\_n,m} \end{bmatrix} \quad (\text{C-4})$$

$$y_{33}(j\omega) = gm_1 + gmb_1 + gd_1 + gm_2 + gmb_2 + gd_2 + gd_3 + j\omega \cdot (C_s + C_{GS1} + C_{GS2}) \quad (\text{C-5})$$

$$y_{66}(j\omega) = g_{o1} + j\omega \cdot C_6 \quad (\text{C-6})$$

$$y_{67}(j\omega) = -j\omega \cdot C_C \quad (\text{C-7})$$

$$y_{76}(j\omega) = gm_4 \quad (\text{C-8})$$

$$y_{77}(j\omega) = gd_4 + gd_5 + G_L + j\omega \cdot (C_C + C_L) \quad (\text{C-9})$$

The various OL transfer functions for the opamp can be found using the following procedure:

1. Solve the equation-set (C-1) and find the node voltages  $V_{i\_n,m}$  as a function of the excitation currents  $I_{i\_n,m}$ .

2. Find the excitation currents  $I_{i_{n,m}}$  for the circuit. These currents are for 1<sup>st</sup> order ( $n+m=1$ ) a direct function of the input voltages. For higher order ( $n+m>1$ ) these currents are functions of lower order controlling voltages of nonlinear elements, which further depends on the input voltages.
3. Find the output voltage and insert for  $I_{i_{n,m}}$  found in 2.
4. Find the voltages that control the nonlinear elements and insert for  $I_{i_{n,m}}$  found in 2. These voltages will be used to derive excitation currents of higher order.

This procedure has to be repeated for all combination of  $n$  and  $m$ .

## C.1 First Order Responses

The first order response  $H_i(\cdot)$  ((3-7) on p. 44) consist of two transfer functions,  $H_{V_e}(j\omega)$  and  $H_{V_{cm}}(j\omega)$ .  $H_{V_e}(j\omega)$  is due to the differential input voltage  $V_e$ , and  $H_{V_{cm}}(j\omega)$  is due to CM input voltage  $V_{cm}$ .

### C.1.1 $H_{V_e}(j\omega)$

Here,  $V_{cm}$  is set to zero and  $V_e$  is applied to the circuit at the frequency  $\omega$ . The circuit equations can be expressed as (C-10), with the current excitations shown in (C-11) and (C-12).  $H_{V_e}(j\omega)$  (C-13) is obtained by taking the ratio of  $V_7$  and  $V_e$  and setting  $gm_1 = gm_2 = gm$ . The controlling voltages for the nonlinear elements are also computed and are denoted  $V_{i_{j,0}}$ , and will be used for computing higher order transfer functions. The gain factors  $A_1$  and  $A_2$ , which are the gain magnitudes of the input- and output stage, respectively, are given in (C-14) and (C-15). The dominant and non-dominant poles are shown in (C-16) and (C-17), respectively.

$$\bar{Y}(j\omega) \cdot \bar{V}_{1,0} = \bar{I}_{1,0} \quad (C-10)$$

$$\bar{I}_{1,0} = \begin{bmatrix} I_{3_{-1,0}} \\ I_{6_{-1,0}} \\ I_{7_{-1,0}} \end{bmatrix} = \begin{bmatrix} 0 \\ I_{out1_{-1,0}} \\ 0 \end{bmatrix} \quad (C-11)$$

$$I_{out1_{-1,0}} = -\frac{1}{2} \cdot (gm_1 + gm_2) \cdot V_e \quad (C-12)$$

$$H_{V_e}(j\omega) = \frac{A_1 \cdot A_2}{\left(1 + j \frac{\omega}{\omega_1}\right) \cdot \left(1 + j \frac{\omega}{\omega_2}\right)} \quad (\text{C-13})$$

$$A_1 = \frac{gm}{g_{o1}} \quad (\text{C-14})$$

$$A_2 = \frac{gm_4}{gd_4 + gd_5 + G_L} \quad (\text{C-15})$$

$$\omega_1 = \frac{g_{o1} \cdot (gd_4 + gd_5 + G_L)}{C_6 G_L + C_C gm_4} \quad (\text{C-16})$$

$$\omega_2 = \frac{C_6 G_L + C_C gm_4}{C_6 (C_C + C_L)} \quad (\text{C-17})$$

### C.1.2 $H_{V_{cm}}(j\omega)$

Now,  $V_e$  is set to zero and  $V_{cm}$  is applied to the circuit at the frequency  $\omega$ . As for  $H_{V_e}(j\omega)$  the node voltages are computed by solving a similar set of equations, the equation-set in (C-18). The excitation currents are expressed in (C-19) and (C-20).  $H_{V_{cm}}(j\omega)$  is shown in (C-21), where  $D$  is given in (C-22). In  $D$ ,  $d_{gm}$ ,  $d_{gmb}$  and  $d_{gd}$  are the mismatch in the small-signal parameters  $gm$ ,  $gmb$  and  $gd$ , respectively, of M1 and M2. The small-signal parameters without indexes are due to the differential pair. The zero and pole that the CM-voltage experiences is shown in (C-23) and (C-24), respectively. The controlling voltages  $V_{i_{0,l}}$  for the nonlinear elements can be computed from the node voltages found when solving (C-18).

$$\bar{Y}(j\omega) \cdot \bar{V}_{0,l} = \bar{I}_{0,l} \quad (\text{C-18})$$

$$\bar{I}_{0,1} = \begin{bmatrix} I_{3,0,1} \\ I_{6,0,1} \\ I_{7,0,1} \end{bmatrix} = \begin{bmatrix} 2 \cdot (gm + j\omega \cdot C_{GS}) \cdot V_{cm} \\ I_{out1,0,1} \\ 0 \end{bmatrix} \quad (C-19)$$

$$I_{out1,0,1} = \frac{d_{gm} \cdot gd_3 \cdot gm}{gd_3 + 2gm + 2gd + 2gmb} \cdot \frac{\left(1 + j \frac{\omega}{\omega_{z,cm}}\right)}{\left(1 + j \frac{\omega}{\omega_{p,cm}}\right)} V_{cm} \quad (C-20)$$

$$H_{V_{cm}}(j\omega) = \frac{-D \cdot A_1 \cdot A_2}{gd_3 + 2gm + 2gd + 2gmb} \cdot \frac{\left(1 + j \frac{\omega}{\omega_{z,cm}}\right)}{\left(1 + j \frac{\omega}{\omega_1}\right) \cdot \left(1 + j \frac{\omega}{\omega_2}\right) \cdot \left(1 + j \frac{\omega}{\omega_{p,cm}}\right)} \quad (C-21)$$

$$D = 2 \cdot gmb \cdot (d_{gm} - d_{gmb}) + 2 \cdot gd \cdot (d_{gm} - d_{gd}) + gd_3 \cdot d_{gm} \quad (C-22)$$

$$\omega_{z,cm} = \frac{gd_3}{C_S - 2 \cdot \left(\frac{gd + gmb}{gm}\right) \cdot C_{GS}} \quad (C-23)$$

$$\omega_{p,cm} = \frac{2(gm + gd + gmb) + gd_3}{C_S + 2C_{GS}} \approx \frac{2gm}{C_S + 2C_{GS}} \quad (C-24)$$

The 2<sup>nd</sup> and 3<sup>rd</sup> order responses, given in (3-8) and (3-9) (p. 44), can be found using the same procedure as above. The circuit excitations are then nonlinear currents of order 2 and 3, respectively.

**REFERENCES**

- [1] P. Wambacq, W. Sansen, “Distortion Analysis of Analog Integrated Circuits,” Norwell, MA: Kluwer Academic Publishers, 1998.
- [2] P. Wambacq, G. G. E. Gielen, P. R. Kinget, W. Sansen, “High-Frequency Distortion Analysis of Analog Integrated Circuits,” *IEEE Tr. on Circuits and Systems—II: Analog and Digital Signal Processing*, vol. 46, no. 3, pp. 335–345, Mar. 1999.
- [3] P. Wambacq, J. Vanthienen, G. Gielen, W. Sansen, “A Design Tool for Weakly Nonlinear Analog Integrated Circuits With Multiple Inputs (Mixers, Multipliers),” *Proceedings of the IEEE 1991 Custom Integrated Circuit Conference*, 1991, pp. 5.1/1-5.1/4.
- [4] Maple 6, See <http://www.maplesoft.com/>